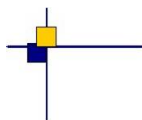


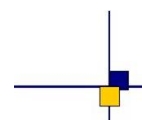


CalVal Jason-3



Jason-3 validation and cross calibration activities (Annual report 2021)

Contract No 160182-14026 Lot 1.8.1



Nomenclature : SALP-RP-MA-EA-23528-CLS

Issue : 1.3

Date : August 25, 2022

Chronology Issues:

Issue:	Date:	Reason for change:
0.0	2021-12-15	Creation
1.0	2022-31-01	Version delivered to CNES for reviewing
1.1	2022-03-20	taking into account CNES review add of investigation on model dry tropospheric corrections
1.2	2022-06-20	Modifications of the Executive Summary
1.3	2022-08-25	Adding comparisons with Sentinel-6

People involved in this issue :

	AUTHORS	COMPANY	DATE	INITIALS
Written by:	B. Flamant H. Roinard A. Guerou	CLS CLS CLS		
Checked by:		CLS		
Approved by:		CLS CLS		
Application autho- rised by:	F. Bignalet-Cazalet	CNES		

Index Sheet :

Context:	
Keywords:	
Hyperlink:	

Distribution:

Company	Means of distribution	Names
CLS/DOS	electronic copy	V.ROSMORDUC
CNES	electronic copy	thierry.guinle@cnes.fr nicolas.picot@cnes.fr francois.bignalet-cazalet@cnes.fr gerald.dibarboure@cnes.fr aqgp_rs@cnes.fr dominique.chermain@cnes.fr delphine.vergnoux@cnes.fr

List of tables and figures

List of Tables

1	<i>Events on Jason-3 mission</i>	19
2	<i>Acquisition mode</i>	20
3	<i>List of GDR version "D" standard (version "F" for O/IGDR from cycle 174 onwards and for all GDR)</i>	25
4	<i>List of missing Jason-3 passes</i>	36
5	<i>Editing criteria over cycles 1 to 208</i>	43
6	<i>Seasonal variations of Jason SLA (cm) for years 2016 to 2021</i>	84
7	<i>Seasonal variations of Jason SLA standard deviation (cm) for years 2016 to 2021</i>	86

List of Figures

1	<i>Acquisition mode for cycle 060 (identical to acquisition mode automatic switch for cycles 6, 9, 11-19, 21-56, 58-167). 8 = autonomous acquisition / tracking, 9 = autonomous DIODE acquisition / tracking, 10 = DIODE + Digital Elevation Model tracking</i>	21
2	<i>Acquisition mode for cycle 170 (identical to acquisition mode automatic switch for cycles 169-214). Left: 9 = autonomous DIODE acquisition / tracking. Right: 10 = DIODE + Digital Elevation Model tracking</i>	22
3	<i>Global GDRs data availability per cycle</i>	27
4	<i>Map of percentage of available measurements over land for Jason-3 (left) and for Jason-2 (right). Top: Jason-3 cycle 039 in DEM mode and Jason-2 cycle 320 in median mode. Bottom: Jason-3 cycle 031 in DEM mode and Jason-2 cycle 311 in DEM mode</i>	37
5	<i>Jason-2 and Jason-3 GDR data availability over ocean (per cycle)</i>	38
6	<i>Jason-3 data editing average by cycle.</i>	39
7	<i>Cycle per cycle monitoring of the percentage of edited measurements by ice flag criterion.</i>	40
8	<i>Top: Percentage of edited measurements by altimeter rain flag criterion. Bottom left: Map of global edited measurements without considering the rain flag. Bottom right: Map of global edited measurements using all criteria and considering the rain flag. All figures are computed over ocean and from cycle 171 to 208.</i>	41
9	<i>Jason-3 data editing by thresholds average by cycle.</i>	43
10	<i>Percentage of edited measurements by 20Hz range measurements threshold criterion (top) and by 20Hz range measurements standard deviation threshold criteria (bottom). Cycle per cycle monitoring compared with Jason-2 (left) and Jason-3 averaged map from cycle 171 to 208 (right).</i>	44
11	<i>Percentage of edited measurements by SWH threshold criterion. Left: Cycle per cycle monitoring compared with Jason-2 (Jason-2 DEM cycle in cyan. Jason-3 median tracker cycles in purple.) Right: Jason-3 averaged map from cycle 171 to 208.</i>	45
12	<i>Percentage of edited measurements by backscatter coefficient threshold criterion (top) and by 20Hz backscatter coefficient standard deviation threshold criteria (bottom). Cycle per cycle monitoring compared with Jason-2 (left, Jason-2 DEM cycle in cyan. Jason-3 median tracker cycles in purple) and Jason-3 averaged map from cycle 171 to 208 (right).</i>	46
13	<i>Percentage of edited measurements by radiometer wet troposphere correction threshold criterion. Left: Cycle per cycle monitoring compared with Jason-2. Right: Jason-3 averaged map from cycle 171 to 208.</i>	47
14	<i>Percentage of edited measurements by ionospheric correction threshold criterion. Left: Cycle per cycle monitoring compared with Jason-2. Right: Jason-3 averaged map from cycle 171 to 208.</i>	48

15	Percentage of edited measurements by wind speed threshold criterion. Left: Cycle per cycle monitoring compared with Jason-2. Right: Jason-3 averaged map from cycle 171 to 208.	49
16	Percentage of edited measurements by sea state bias threshold criterion. Left: Cycle per cycle monitoring compared with Jason-2. Right: Jason-3 averaged map from cycle 171 to 208.	50
17	Percentage of edited measurements by ocean tide threshold criterion. Cycle per cycle monitoring compared with Jason-2.	51
18	Percentage of edited measurements by square off nadir angle threshold criterion. Left: Cycle per cycle monitoring compared with Jason-2. Right: Jason-3 averaged map from cycle 171 to 208.	51
19	Percentage of edited measurements by sea surface height threshold criterion. Left: Cycle per cycle monitoring compared with Jason-2. Right: Jason-3 averaged map from cycle 171 to 208.	52
20	Percentage of edited measurements by sea level anomaly threshold criterion. Left: Cycle per cycle monitoring compared with Jason-2. Right: Jason-3 averaged map from cycle 171 to 208.	53
21	Top: Cyclic monitoring of number of elementary 20 Hz range measurements for Jason-2 and Jason-2 for Ku-band and C-band. Bottom: Jason-2 - Jason-3 difference daily monitoring of elementary 20 Hz range measurements number (until september 2017). Note that the bottom figure was computed using GDR-D data for both Jason-3 and Jason-2.	55
22	Map of number of 20 Hz range measurements for Jason-3 averaged over cycles 171 to 208, in Ku-band (left) and in C-band (right).	56
23	Top: Cyclic monitoring of elementary 20 Hz range measurements standard deviation for Jason-2 and Jason-3 for Ku-band and C-band. Bottom: Jason-2 - Jason-3 difference daily monitoring of elementary 20 Hz range measurements standard deviation. Note that the bottom figure was computed using GDR-D data for both Jason-3 and Jason-2.	57
24	Map of 20 Hz range measurements standard deviation for Jason-3 averaged over cycles 171 to 208, in Ku-band (left) and in C-band (right).	57
25	Left: Cyclic monitoring of the square off-nadir angle for Jason-2 and Jason-3 for GDRs (blue and red curves) and Jason-3 IGDRs (product IGDR for cycles 1 to 41, and IGDR L2P from cycle 25 to 132 in green). Right: Jason-2 - Jason-3 difference daily monitoring of the square off-nadir angle (Note that the figure on right panel was computed using GDR-D data for both Jason-3 and Jason-2.).	58
26	Map of the square off-nadir angle for Jason-3 averaged over cycles 171 to 208.	59
27	Left: Mean per day of mispointing for Jason-3 from cycle 4. Right: Square off nadir angle against swl.	59
28	Top: Cyclic monitoring of backscatter coefficient for Jason-3 (Ku-band) OGDR/IGDR/GDR. Bottom: difference of atmospheric attenuation applied to sigma0 between IGDR and GDR products.	60
29	Top: Cyclic monitoring of backscatter coefficient for Jason-2 and Jason-3 for Ku-band (left) C-band (right). Bottom: daily monitoring of Jason-2 - Jason-3 GDR difference of the backscatter coefficient. Note that the bottom figure was computed using GDR-D data for both Jason-3 and Jason-2.	61
30	Map of backscatter coefficient for Jason-3 averaged over cycles 171 to 208, in Ku-band (left) and in C-band (right).	61
31	Cyclic monitoring of significant wave height for Jason-3 (Ku-band) OGDR/IGDR/GDR.	62
32	Cyclic monitoring of significant wave height for Jason-2 and Jason-3 for Ku-band (left) and for C-band (right). Jason-2 - Jason-3 difference daily monitoring of significant wave height (bottom). Note that the bottom figure was computed using GDR-D data for both Jason-3 and Jason-2.	62
33	Map of significant wave height for Jason-3 averaged over cycles 171 to 208, in Ku-band (left) and in C-band (right).	63

34	Cyclic monitoring of ionospheric correction for Jason-2 and Jason-3. (left) . Cyclic monitoring of Jason-3 ionospheric correction for IGDR and GDR data (right) . Jason-2 - Jason-3 difference daily monitoring of ionospheric correction (bottom) . Note that the bottom figure was computed using GDR-D data for both Jason-3 and Jason-2.	64
35	Left: Map of ionospheric correction for Jason-3 averaged over cycles 171 to 208. Right: Map of dual-frequency minus GIM ionospheric correction solutions.	64
36	Cyclic monitoring of GIM ionosphere correction minus filtered altimeter ionosphere correction for Jason-2 and Jason-3. Left: mean, right: standard deviation.	65
37	Global difference in number of valid points (i.e. within thresholds) between ionospheric correction solutions. MLE4 retracking (left) or adaptive retracking (right). Statistics are computed over cycles 001 (17/02/2016) to 184 (14/02/2021)	66
38	Difference in number of valid points (i.e. within thresholds) between ionospheric correction solutions wrt distance to coast. MLE4 retracking (left) or adaptive retracking (right). Statistics are computed over cycles 001 (17/02/2016) to 184 (14/02/2021)	66
39	Difference in number of valid points (i.e. within thresholds) between ionospheric correction solutions. Statistics are computed over cycles 001 (17/02/2016) to 184 (14/02/2021)	67
40	Difference in number of valid points (i.e. within thresholds) between ionospheric correction solutions. Statistics are computed over cycles 001 (17/02/2016) to 184 (14/02/2021)	67
41	Map of Jason-3 brightness temperatures averaged over cycles 171 to 208: 18.7 Ghz channel (top left), 23.8 Ghz channel (top right) and 34.0 Ghz channel (bottom left). Map of AMR wet troposphere correction for Jason-3 averaged over cycles 171 to 208 (bottom right)	68
42	Daily monitoring of AMR minus ECMWF model wet tropospheric correction over one year.	69
43	Daily monitoring of AMR minus ECMWF model wet tropospheric correction. mean (left) and standard deviation (right)	70
44	Jason-3 evolution of both WTC models over 2021. Left: mean per day. Right: mean per day of difference.	70
45	Jason-3 difference WTC model - rad over 2021. Left: mean per day. Right: std per day.	71
46	Wet tropospheric correction : left compared to other missions and right using the two available correction models.	71
47	Cyclic monitoring of altimeter wind speed mean (left) and standard deviation (right). Top: for Jason-2 and Jason-3. Bottom: for Jason-3 GDR, IGDR and OGDR data.	72
48	Jason-2 - Jason-3 difference daily monitoring of altimeter wind speed mean (left) and standard deviation (right). Both were computed using GDRD data. Note that the bottom figure was computed using GDR-D data for both Jason-3 and Jason-2.	72
49	Wind speed comparison product and ERA5 model	73
50	Cyclic monitoring of the sea state bias mean and standard deviation for Jason-3 IGDR/GDR	74
51	Cyclic monitoring of the sea state bias mean and standard deviation for Jason-2 and Jason-3	74
52	Jason-2 - Jason-3 difference daily monitoring of the sea state bias mean (left) and standard deviation (right). Note that the figures were computed using GDR-D data for both Jason-3 and Jason-2.. . . .	74
53	Monitoring of mean of Jason-3 SSH crossover differences for OGDRs, IGDRs and GDRs. Only data with $ \text{latitude} < 50^\circ$, bathymetry $< -1000\text{m}$ and low oceanic variability were selected. (ocean_tide_fes = FES14B is used in SSH computation)	76
54	Map of SSH crossovers differences mean for Jason-3 cycle 0 to 208 (left) and for Jason-2 cycle 281 to 506 (right)	76
55	Cyclic monitoring of Jason-2 - Jason-3 SSH crossover differences mean (left) and map over cycle 1 to 58 (right). Only data with $ \text{latitude} < 50^\circ$, bathymetry $< -1000\text{m}$ and low oceanic variability were selected (for both missions, GDR-D data are used for these figures).	77

56	Cycle by cycle standard deviation of SSH crossover differences for Jason-2 and Jason-3 (left), and for Jason-3 using OGDs, IGDRs and GDRs (right). Only data with $ \text{latitude} < 50^\circ$, bathymetry $< -1000\text{m}$ and low oceanic variability were selected.	77
57	Monitoring (left) and periodogram (right) of pseudo time-tag bias estimated cycle by cycle from GDR products for Jason-2 and Jason-3	78
58	Daily monitoring of SSH bias between Jason-2 and Jason-3 before Jason-2 moved to interleaved ground-track in October 2016 (using GDRD data for both missions) : SSH bias without applying geophysical corrections (black) and with corrections using radiometer wet troposphere correction (blue) or using ECMWF model wet troposphere correction (cyan).	79
59	GDR data. Caution: color map ranges are different between the two figures. Left: Map of SLA difference between Jason-2 and Jason-3 over tandem phase Right: Map of Jason-2 and Jason-3 SLA differences for Jason-3 cycles 025 to 058 (using Jason-3 GDR-F data and updated to GDR-F like Jason-2 data).	80
60	Cyclic monitoring of along-track SLA standard deviation. Jason-3 OGDs, IGDRs and GDRs (left). Jason-2 and Jason-3 GDRs residuals (=interpolated over theoretical ground track)(right) .	81
61	Global (right) and regional (left) MSL trends from 1993 onwards.	87
62	J3 GMSL difference between GDR-F adaptive and MLE4 with (left) and without removal of cycles 057 to 085 (right). Figures extracted from the [19]	88
63	range_{std} and SWH for both retrackings over cycle 177 and pass 199. The SLA measurements are rejected with the SWH threshold for the MLE4 and the range_{std} threshold for the ADAPTIVE. . .	90
64	Reprocessing of all class 13 waveforms using the best fitting configuration.	91
65	Difference of classification between the 1Hz class and the most frequent class of the 20Hz measures	92
66	Difference of classification between the 1Hz class and the most frequent class of the 20Hz measures, zoomed over low latitudes (On the right figure, the orange points correspond to a difference of classification).	93
67	GDR data. Map of Sentinel-6 and Jason-3 SLA differences for Jason-3 cycles 220 to 221	94
68	GDR data. Plot of Sentinel-6 and Jason-3 noise level with regard to LRM SWH.	95
69	GDR data. Map of Sentinel-6 and Jason-3 SWH differences for Jason-3 cycles 220 to 221	95
70	GDR data. Plot of Sentinel-6 and Jason-3 SSH differences at crossover points.	96
71	Top left: Jason-3 net_instr_corr_sig0_C flag. Top right: Jason-3 net_instr_corr_sig0_Ku flag. Bottom: Evolution of PTR power.	97
72	Jason-3 net_instr_corr_sig0_C flag over ocean. Left: Jason-3 cycle 205. Right: Jason-3 cycle 208. .	98
73	Dry tropospheric correction over ocean for Jason-3 cycle 150. model_dry_tropo_cor_zero_altitude (top left), model_dry_tropo_cor_measurement_altitude (top right), and model_dry_tropo_cor_measurement_altitude minus model_dry_tropo_cor_zero_altitude point to point difference (bottom)	99
74	Dry tropospheric correction over ocean for Jason-3 cycle 150. Dry tropospheric correction from ERA5 pressures at sea level (top), model_dry_tropo_cor_zero_altitude minus $DTC_{fromERA5}$ point to point difference (bottom left), and model_dry_tropo_cor_measurement_altitude minus $DTC_{fromERA5}$ point to point difference (bottom right)	100
75	Dry tropospheric correction over ocean for Jason-3 cycle 150. Contribution of sea level pressure, S1S2 pressures climatology and atmospheric tide (top) with regard to model_dry_tropo_cor_measurement_altitude minus model_dry_tropo_cor_zero_altitude point to point difference (bottom left) model_dry_tropo_cor_zero_altitude minus $DTC_{fromERA5}$ point to point difference (bottom middle), and model_dry_tropo_cor_measurement_altitude minus $DTC_{fromERA5}$ point to point difference (bottom right)	101

List of items to be defined or to be confirmed

Applicable documents / reference documents

Contents

1. Introduction	2
2. Processing status	12
2.1. Data Used	12
2.2. List of events	12
2.3. Tracking and acquisition mode	19
2.4. Models and standards	22
2.5. Processing versions	25
2.6. Cautions	26
3. Data coverage and edited measurements	27
3.1. Missing measurements	27
3.1.1. Over land and ocean	27
3.1.2. Over ocean	36
3.2. Edited measurements	39
3.2.1. Global editing	39
3.2.2. Flagging quality criterion: Ice flag	40
3.2.3. Flagging quality criterion: Rain flag	41
3.2.4. Editing on thresholds criteria	42
3.2.4.1. Threshold criteria: 20-Hz range measurements number and standard deviation	44
3.2.4.2. Threshold criteria: Significant wave height (swh)	45
3.2.4.3. Threshold criteria: Backscatter coefficient (sigma0)	46
3.2.4.4. Threshold criteria: Radiometer wet troposphere correction	47
3.2.4.5. Threshold criteria: Ionospheric correction	48
3.2.4.6. Threshold criteria: Altimeter wind speed	49
3.2.4.7. Threshold criteria: Sea State Bias	50
3.2.4.8. Threshold criteria: Ocean tide	51
3.2.4.9. Threshold criteria: Square off nadir angle	51
3.2.4.10. Threshold criteria: Sea surface height	52
3.2.4.11. Threshold criteria: Sea Level Anomaly	52
4. Monitoring of altimeter and radiometer parameters	54
4.1. Methodology	54
4.2. 20 Hz range measurements	54
4.2.1. 20 Hz range measurements number in Ku-Band and C-Band	55
4.2.2. 20 Hz range measurements standard deviation in Ku-Band and C-Band	56
4.3. Off-Nadir Angle from waveforms	58
4.4. Backscatter coefficient	60
4.5. Significant wave height	62
4.6. Dual-frequency ionosphere correction	63
4.7. AMR Wet Troposphere Correction	68
4.7.1. Overview	68
4.7.2. Comparison with the ECMWF model	69
4.7.3. Wet Tropospheric Correction model comparison	70
4.7.4. Drift of the Jason-3 Radiometer	71
4.8. Altimeter wind speed	72
4.9. Sea state bias	74

5. SSH crossover analysis	75
5.1. Overview	75
5.2. Mean of SSH crossover differences	76
5.3. Standard deviation of SSH crossover differences	77
5.4. Estimation of pseudo time-tag bias	78
6. Sea Level Anomalies (SLA) Along-track analysis	79
6.1. Overview	79
6.2. Mean of SLA differences between Jason-3 and Jason-2	79
6.3. Standard deviation of SLA differences between Jason-3 and Jason-2	80
6.4. Sea level seasonal variations	82
7. Mean Sea Level (MSL) trends	87
7.1. Computation of the Mean Sea Level	87
7.2. Comparison of the MLE4 & the ADAPTIVE GDRF solutions for the GMSL computation	88
8. Particular points and investigations	89
8.1. Investigations surrounding the retracking ADAPTIVE	90
8.2. Waveform classification	92
8.3. Tandem Phase with Sentinel-6	94
8.3.1. Range Differences	94
8.3.1.1. Sea Level Anomalies	94
8.3.1.2. Equatorial Band	94
8.3.1.3. Noise Level	94
8.3.2. SWH Differences	95
8.3.3. Crossover differences	96
8.4. Caution about qual_inst_corr_1hz_sig0_ku	97
8.5. Dry tropospheric correction solutions	99
9. Conclusion	102
10. References	103

Glossary

AMR Advanced Microwave Radiometer

CLS Collecte Localisation Satellites

CNES Centre National d'Etudes Spatiales

CNG Consigne Numerique de Gain (= Automatic Gain Control)

DEM Digital Elevation Model

DIODE Détermination Immédiate d'Orbite par Doris Embarqué

ECMWF European Centre for Medium-range Weather Forecasting

GDR Geophysical Data Record

GIM Global Ionosphere Maps

GOT Global Ocean Tide

IGDR Interim Geophysical Data Record

JPL Jet Propulsion Laboratory (Nasa)

MLE Maximum Likelihood Estimator

MOE Medium Orbit Ephemeris

MQE Mean Quadratic Error

MSS Mean Sea Surface

PLTM PayLoad TeleMetry

POE Precise Orbit Ephemeris

OGDR Operational Geophysical Data Record

SALP Service d'Altimétrie et de Localisation Précise

SSH Sea Surface Height

SLA Sea Level Anomaly

SLR Satellite Laser Ranging

SSB Sea State Bias

SWH Significant Wave Height

TM TeleMetry

1. Introduction

This document presents the synthesis report concerning validation activities of Jason-3 data (Geophysical Data Records (GDRs), as well as Interim and Operational Data Records (I/OGDR)) under SALP contract (N° 160182/Lot 1.8.1) supported by CNES at the CLS Environment & Climate Business Unit.

History

Jason-3 satellite was successfully launched on the 17th of January 2016. Since February 12th, Jason-3 is on its operational orbit to continue the long term climate data record on the primary TOPEX, Jason-1, and OSTM/Jason-2 ground track. Until October 2nd, 2016, Jason-3 and Jason-2 were in tandem flight, with only 80 seconds delay, before Jason-2 was moved to the same interleaved orbit that was used by TOPEX from 2002 to 2005 and Jason-1 from 2009 to 2012. Jason-2 was on its repetitive interleaved position until May 17th 2017, then was moved on a first Long Repeat Orbit from July 11th 2017 to July 18th 2017, and finally was on a second interleaved long repeat orbit from July 25th 2018 to the end of the mission on October 1st 2019. After tandem phase with Jason-2, Jason-3 has become the reference mission in DUACS system from mid-september 2016 onwards. On February 24th 2019 at 09:57:16, Jason-3 entered in Safe Hold Mode (SHM). This SHM ended 10 days after on March 6th 2019 at 08:44:21. On April 6th 2019 at 23:17:22, another SHM occurred. This SHM lasted for around 7 days and ended on April 12th 2019 at 02:20:01. Over 2020, Jason-3 has triggered a SHM 3 times : on January 31st 2020 at 04:51:17 for 6 days until February 5th 2020 at 09:37:14 and on the same day at 21:00:53 for 8 other days until February 13th 2020 at 08:42:44. The last Safe Hold Mode of the year occurred on June 15th 2020 at 21:50:42 and lasted for around 4 days until June 15th 2020 at 21:50:42. In addition, due to a DORIS anomaly, Jason-3 data are unavailable between October 27th 2020 at 13:23:01 and October 29th 2020 at 11:36:00. Jason-3 was also used as a reference to perform the tandem phase with Sentinel-6 / Michael Freilich. During the year 2022, the success of this tandem phase will lead to Jason-3 orbit change to leave the place to Sentinel-6.

Over 2021, specific events observed for Jason-3 are :

- A radiometer anomaly on pass 191 which set the wet tropospheric correction to DV from 24/04/2021 17:18:33 to 25/04/2021 01:21:54;
- A routine calibration anomaly between cycle 202 and cycle 205 which led to missing points over ocean;
- A DEM patch upload over cycle 190 (from 07/04/2021 13:27:46 to 07/04/2021 13:27:59);
- A DEM patch upload over cycle 193 (from 05/05/2021 13:54:41 to 05/05/2021 13:54:55);

Also during this year, the entire mission was reprocessed with standard "F".

CalVal activities

Since the beginning of the mission, Jason-3 data have been analyzed and monitored in order to assess the quality of Jason-3 products. Cycle per cycle reports summarizing mission performance are generated and made available through the AVISO web page ¹. Please note that analyses are done **over ocean** only, no assessment is done over hydrological targets. This encompasses several points, which are either part of Cal/Val routine activities or following mission events:

- mono-mission validation and monitoring,
- Jason-3/Jason-2 cross-calibration,

¹<http://www.aviso.altimetry.fr/en/data/calval/systematic-calval/validation-reports.html>

-
- accuracy and stability of SLA measurements check,
 - specific studies and investigations.

Overview

The present document assesses Jason-3 data quality and mission performance **over ocean**. After an executive summary in the following pages, dedicated sections of this report deal with:

- description of data processing,
- data coverage / availability,
- monitoring of rejected spurious data,
- analysis of relevant parameters derived from instrumental measurements and geophysical corrections.
- system performance via analyses at crossover points,
- system performance via along-track Sea Level Anomalies monitoring,
- long-term monitoring and contribution to climate surveys.

Over all these parts, the document also focuses on Jason-3/Jason-2 cross-calibration:

- During the tandem flight (February, 12th to October 2nd 2016) both satellites were on the same ground track, which is a unique opportunity to precisely assess parameter discrepancies between both missions and detect geographically correlated biases, jumps or drifts.
- But even after Jason-2 moved to interleaved orbit (formation flight phase, after the end of the tandem phase and until move to LRO) and also during Jason-2 flight on LRO, comparisons were still possible while Jason-2 data were available.

The difference at crossovers, SLA performances and consistency with Jason-2 are described. *Please note that in this document, only Jason-2 cycles 281 to 506 - corresponding to February 2016 to mid September 2017 - are used to compute Jason-2 GDR statistics.*

By succeeding to TOPEX/Poseidon, Jason-1 and Jason-2 on their primary ground track, Jason-3 has extended the high-precision ocean altimetry data record ^[1]. It was launched on January 17th 2016.

During Jason-3 tandem phase with Jason-2 (February 12th to October 2nd 2016), both satellites were on the same ground-track (with only 80 seconds delay), which is a unique opportunity to precisely assess parameter discrepancies between both missions and detect geographically correlated biases, jumps or drifts. OGDR and IGDR products have been publicly available since June 30th 2016. OGDRs were generated in version “T” until cycle 18/pass 137, and then turned into “D” version. Concerning IGDRs, they turned from “T” to “D” version at cycle 14/pass 143 on June 27th. GDR products have been available in version “T” since early October 2016 (more details on products versions on Jason-3 handbook ^[2]). **From cycle 174 onwards (29/10/2020), IGDR and OGDR have been produced in standard F. The complete reprocessing to standard “F” of the GDR data was achieved during 2021.** [see OSTST2020 dedicated presentation³]. GDR data have been distributed in standard F from cycle 171 onwards (16/12/2020).

In order to insure the extension of the legacy of sea-surface height measurements, Sentinel-6 / Michael Freilich satellite was launched on November 21st 2020: it reached Jason-3 orbit at end of december. From cycle 179 onwards (18/12/2020), Jason-3 is used as a reference for Sentinel-6 tandem phase.

During each cycle, missing measurements were monitored, spurious data were edited and relevant parameters derived from instrumental measurements and geophysical corrections were analysed for OGDR, IGDR and GDR. Please note that analysis are done **over ocean** only, no assessment is done over hydrological targets.

Jason-3 can use two on-board tracking modes: Diode/DEM (open loop) and median tracker (more details in complete annual report). In addition, a tracking automatic transition is possible, which means that when authorized: acquisition mode switches automatically from autonomous DIODE acquisition mode over land to Diode/DEM over ocean and referenced inland water. In September 2020, an update of DEM (Digital Elevation Model) was uploaded during cycle 168. 21038 lakes, 4236 rivers and 1478 reservoirs have been added. As a result, hydrological targets increased from 4721 up to 31473 (+566% : 26752 new virtual stations).

Please note the change in orbit standard solution available in the products:

- GDR-F data orbit solution is POE-F ;
- until Jason-3 cycle 094, MOE-E orbit standard is available in IGDR products (MOE-F from cycle 095 onwards) ;
- from Jason-3 cycle 113 onwards, MOE orbit standard uses both DORIS and GPS data.

¹<https://www.aviso.altimetry.fr/?id=601&L=0>

²https://www.aviso.altimetry.fr/fileadmin/documents/data/tools/hdbk_j3.pdf

³https://meetings.aviso.altimetry.fr/fileadmin/user_upload/tx_ausyclsseminar/files/CVL_J3_GDRF_ready_v02_ostst2020_02.pdf

Data availability

Data availability is excellent for Jason-3. Jason-3 presents 99.89% of data availability over ocean after removing specific events (99.98% for Jason-2, see figure 1). Such events occurred only a few times over Jason-3 full period, but four times only during 2020. **No important event occurred over 2021:**

- during cycle 3, where 21.02% of measurements are missing due to the GPS platform upload,
- during cycle 57, where 1.76% of measurements are missing due to the DEM-onboard upload.
- during cycles 112/113, where 79.89% (for cycle 112) and 24.21% (for cycle 113) of measurements are missing due to SHM from 24/02/2019 09:57:16 until 06/03/2019 08:44:21.
- during cycle 116, where 53.19% of measurements are missing due to SHM from 06/04/2019 23:17:22 until 12/04/2019 02:20:01.
- during cycles 146/147, SHM occurred from 31/01/2020 04:51:17 until 05/02/2020 09:37:14, and another time from 05/02/2020 21:00:53 until 13/02/2020 08:42:44. Due to those SHM events, missing data rate is 38.94% for cycle 146 and 88.81% for cycle 147.
- during cycle 160, SHM occurred from 15/06/2020 21:50:42 until 19/06/2020 07:32:46. Due to this SHM event, missing data rate is 33.58% for cycle 160.
- during cycles 173/174, there is a DORIS anomaly from 27/10/2020 13:23:01 until 29/10/2020 11:36:00. Due to this event, missing data rate is 12.80% for cycle 173 and 6.66% for cycle 174.

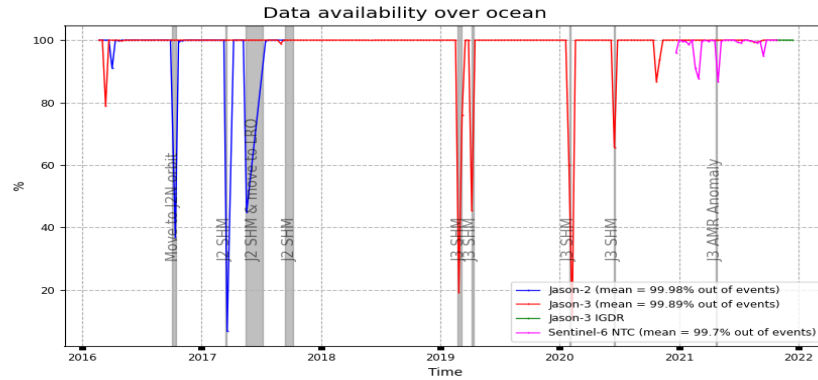


Figure 1 – Sentinel-6, Jason-2 and Jason-3 GDR data availability over ocean (per cycle)

Sea Level Anomalies

Over the tandem phase, the mean SLA differences between Jason-2 and Jason-3 data is stable in time with variations close to 1 mm rms (left of figure 2) and shows no drift. It presents only a weak hemispheric bias as both satellites measure the same oceanic features only 1'20" apart (figure 2) that corresponds to orbital signatures observed on sea surface height. The global average SSH bias is close to 2.6 cm using SSH corrections.

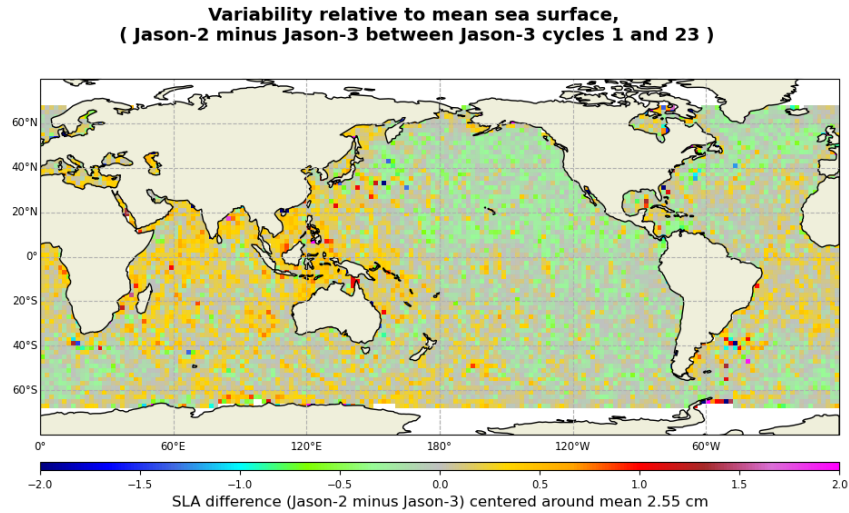


Figure 2 – Jason-3/Jason-2 tandem phase: until 02-10-2016. Map of SLA difference between Jason-2 and Jason-3 over tandem phase.

During Sentinel-6 tandem phase with Jason-3, the averaged difference of gridded SLA shows little difference between both missions as they have a very small temporal shift, similar to Jason-2/Jason-3 tandem phase. One noticeable difference between both missions is the dependency of range to SWH for Sentinel-6. This issue is currently under investigation, see [Analysis of the Sentinel-6A SLA bias correction](#). Another significant difference is the equatorial band in the map difference which is also under investigation. So far, the results highlight an anomaly in the Jason series at this latitude.

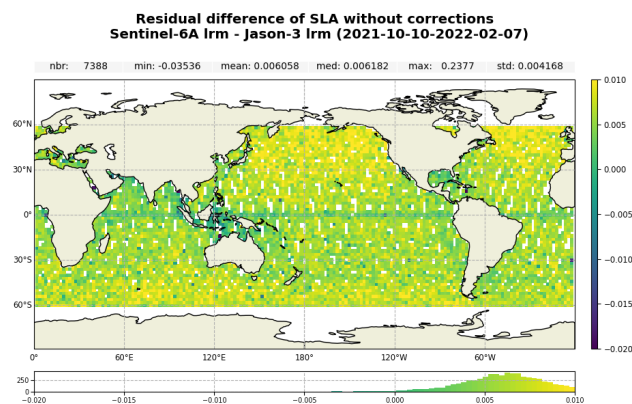


Figure 3 – GDR data. Map of Sentinel-6 and Jason-3 SLA differences for Jason-3 cycles 209 to 221

During the formation flight with Jason-2 (i.e. over cycles 25 to 46 from 12-10-2016 to 17-05-2017) and over Jason-2 LRO phase (until Jason-3 cycle 58, on 14-09-2017), average difference of gridded SLA for Jason-2 and Jason-3 shows high variability regions as Gulf Stream and Antarctic

circumpolar currents are visible (figure 4). This difference is quite noisy as both satellites are shifted in time and sea state changes especially in regions of high ocean variability.

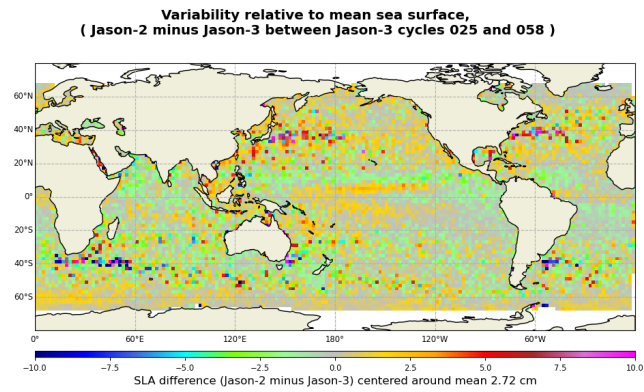


Figure 4 – GDR data. Map of Jason-2 and Jason-3 SLA differences for Jason-3 cycles 025 to 058

Performances at crossover points

Looking at SSH difference at crossovers (red curve on figure 5), a 120 day signal is way less visible than before on the mean for Jason-3 GDR data now that the orbit standard is homogeneous for the whole record (standard-F).

Concerning SSH error at crossover points ($standard\ deviation / \sqrt{2}$), Jason-3 mission show very good and stable performances with an error of 3.39 cm (3.48 cm for Jason-2). This satisfying performance is confirmed from cycle 15 onwards for Sentinel-6.

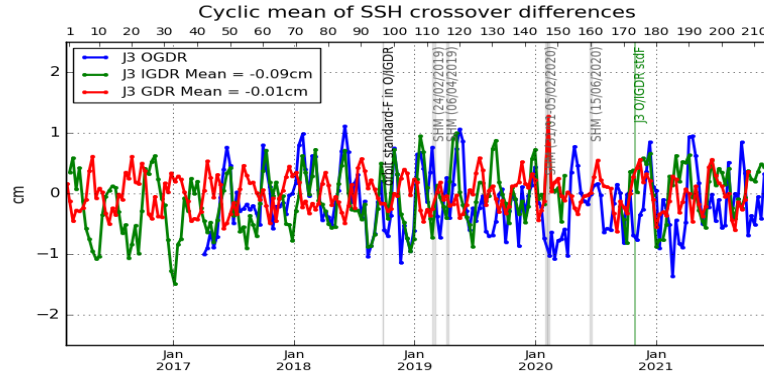


Figure 5 – Monitoring of mean of Jason-3 SSH crossover differences for OGDRs, IGDRs and GDRs. Only data with $|latitude| < 50^\circ$, bathymetry $< -1000m$ and low oceanic variability were selected. (ocean_tide_sol1 = FES is used in SSH computation)

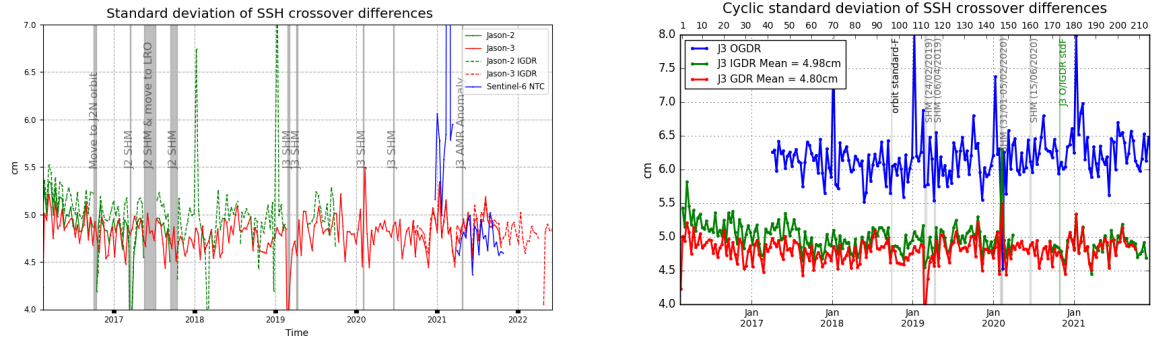


Figure 6 – Cycle by cycle standard deviation of SSH crossover differences for Jason-2, Sentinel-6 and Jason-3 (**left**), and for Jason-3 using OGDRs, IGDRs and GDRs (**right**). Only data with $|latitude| < 50^\circ$, bathymetry $< -1000m$ and low oceanic variability were selected.

The mean SSH differences at Jason 3/Jason 2 crossovers is quite stable and around 3cm in average (figure 7, left). The geographical pattern indicates some hemispheric biases: positive to the west, negative to the east (figure 7, right). It corresponds to orbital signatures observed on sea surface height.

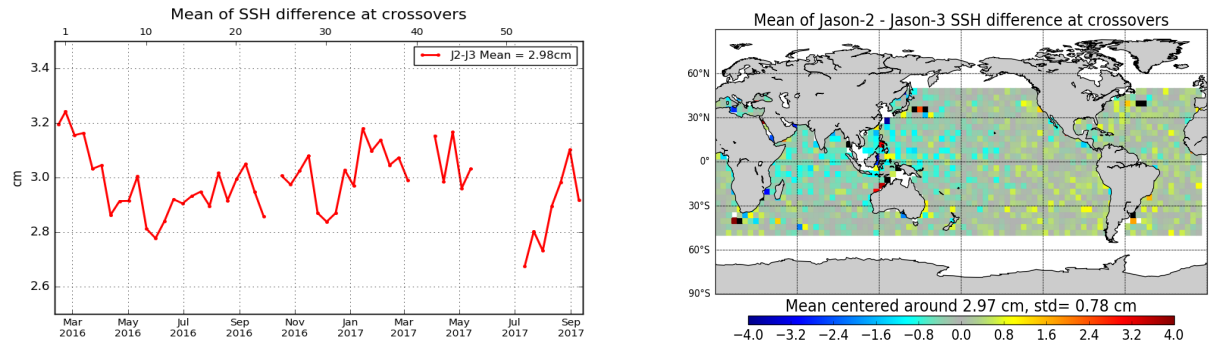


Figure 7 – Cyclic monitoring of Jason-2 - Jason-3 SSH crossover differences mean (left) and map over cycle 1 to 58 (right). Only data with $|\text{latitude}| < 50^\circ$, bathymetry $< -1000\text{m}$ and low oceanic variability were selected. GDR-D datasets are used for both missions on this figure

Contribution to Global Mean Sea Level

Since May 2016 (Jason-3 cycle 11), Jason-3 has been the reference altimetry mission to estimate the Global Mean Sea Level (GMSL), replacing Jason-2. Regional and global biases between missions have to be precisely estimated in order to ensure the quality of the reference GMSL serie. For more precisions, see the dedicated section on AVISO+ website [4].

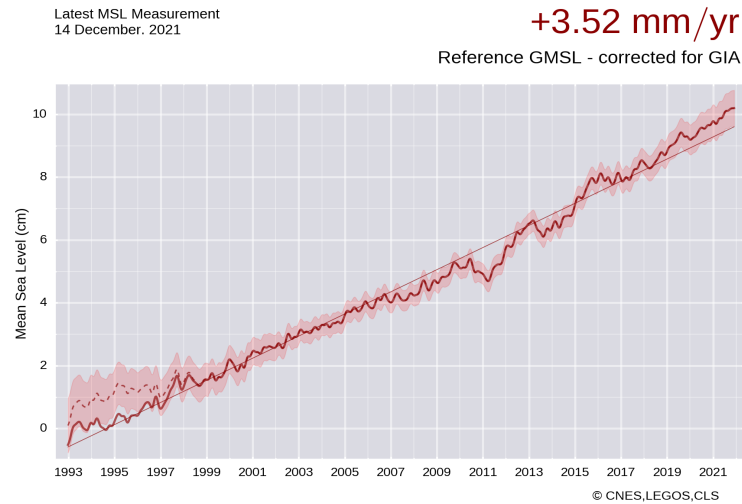


Figure 8 – Global (right) and regional (left) MSL trends from 1993 onwards.

Performances of the adaptive retracking method

The outputs of the adaptive retracking solution are distributed along the historical MLE3/4 ones. With the complete reprocessing of GDR data in standard “F”, various diagnostics have been assessed to compare both adaptive and MLE4 products. See the article presenting the Adaptive retracking advantages for Jason-3 mission [5].

When checking the GMSL data, the adaptive solution conserves the stability of the GMSL record over the 5 years of data. Small differences observed are due to specific events (instrument resets). See the Mean Sea Level chapter of the Jason-3 Annual Report for more information.

The data availability and the along-track performance have been measured for both retrackers to assess the satisfying performances of the adaptive retracking solution. The report dedicated to the reprocessing in standard-F highlights the variance reduction when using the adaptive retracking (see figure 9).

There is a global bias of -2,28cm from MLE4 SLA to adaptive SLA. SLA MLE4 data are globally more rejected than SLA adaptive data (using recommended in handbook procedure). Taking into account valid points for both datasets, performances are better with adaptive solution than with MLE4 (except for coastal distance < 10km).

- variance of SSH difference at crossovers is reduced by -0,52cm²
- variance of along-track SLA is reduced by -0,18cm²

The 20Hz SLA and SWH spectrum also highlight the significant noise reduction when using the adaptive retracking solution.

⁴<https://www.aviso.altimetry.fr/en/data/products/ocean-indicators-products/mean-sea-level.html>

⁵https://www.aviso.altimetry.fr/fileadmin/documents/data/tools/NT-Thibaut_AdaptiveRetrackingForJason3GDRF.pdf

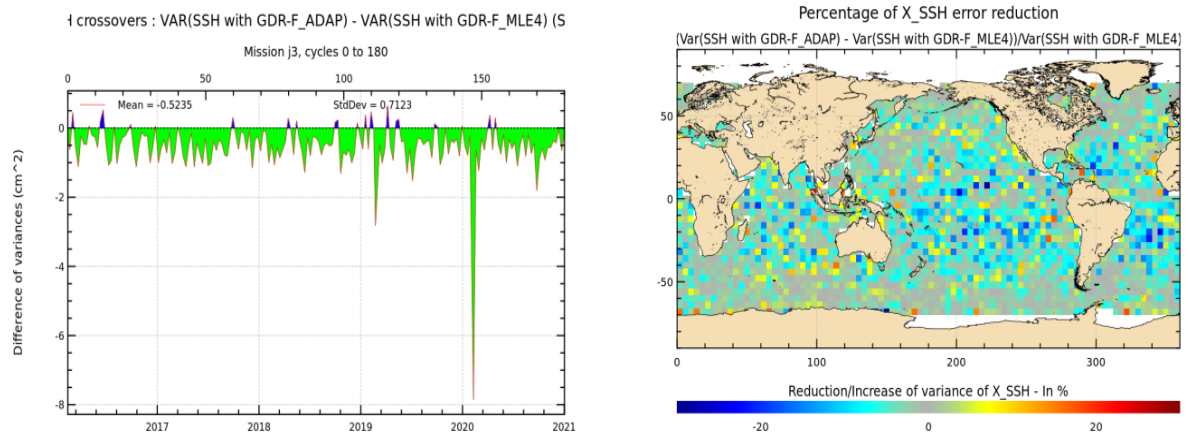


Figure 9 – Difference of SSH at crossover points : Variance difference (left) (selection on common valid points), percentage of error reduction (right).

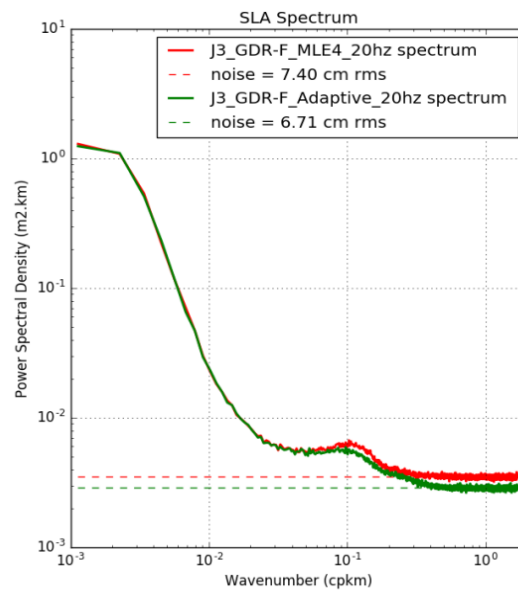


Figure 10 – SLA spectrum 20hz for cycle 174

2. Processing status

2.1. Data Used

Metrics provided in this document are based on Jason-3 dataset from cycle 0 to 208 for GDR products (corresponding to February 10th 2016 to October 10th 2021). This period extends until cycle 214 (December 9th 2021) when IGDR data are considered. Cycle 0 is not included in many statistics because of its available data covering only 5 days. **Note that all GDR data used in this report follow standard “F”, the IGDR data follow standard “F” since cycle 174 included.**

After tandem phase with Jason-2, Jason-3 has become the reference mission in *DUACS* system from mid-september 2016 onwards. Note that in order to improve their product quality (and also to use as possible same corrections for multimission products), *DUACS* system applies some updates to IGDR data. If no precision is done, IGDR results that are presented in this document contain *DUACS* updates (also called here IGDR-L2P).

2.2. List of events

The following table shows the major events during the Jason-3 mission.

Start time → End time	Cycle	Event
15/02/2016 08:00:00 → 18:04:28	0	First calibration in DIODE + DEM mode
16/02/2016 16:07:00 → 16:38:59	0	Poseidon3B instrument CNG calibration
08/03/2016 20:00:00 → 09/03/2016 00:00:01	3	Gyro calibration
11/03/2016 05:09:50 → 05:17:14	3	AMR Cold Sky calibration maneuver
15/03/2016 → 17/03/2016	3	Platform GPS upload
21/03/2016 20:46:00 → 20:46:11	4	DEM patch upload
25/03/2016 09:30:15	4	AMR OFF / ON
06/04/2016 06:05:00 → 06:36:59	5	Poseidon3B instrument CNG calibration
07/04/2016 00:21:27 → 16:32:55	6	DIODE DEM mode

Start time → End time	Cycle	Event
08/04/2016 04:44:30 → 05:00:46 05:11:00 → 05:28:21	6	Poseidon3B instrument CAL2 calibration
27/04/2016 11:38:21 → 12:05:55	8	OPS error
02/05/2016 14:34:23 → 14:37:28	8	DEM patch upload.
06/05/2016 18:16:59 → 16/05/2016 16:15:29	9	DIODE DEM mode
12/05/2016 22:44:59 → 22:52:23	9	AMR Cold Sky calibration maneuver
16/05/2016 10:00:00 → 10:16:15	9	Poseidon3B instrument CAL2 calibration
17/05/2016 02:34:00 → 19/05/2016 03:34:16	10	Poseidon3B instrument CAL2 calibration (5 sequences)
25/06/2016 08:09:39 → 05/07/2016 06:08:10	14	DIODE DEM mode
07/07/2016 15:04:44 → 15:11:15	15	AMR internal error
12/07/2016 04:26:36 → 04:34:00	15	AMR Cold Sky calibration maneuver
05/09/2016 04:24:44 → 04:32:08	21	AMR Cold Sky calibration maneuver
10/2016	24	OSTM/Jason 2 moved to the interleaved orbit, end of the verification phase for Jason 3
07/11/2016 22:21:30 → 22:28:54	27	AMR Cold Sky calibration maneuver
27/11/2016 06:15:00 → 06:46:59	29	Poseidon3B instrument CNG calibration
08/12/2016 04:36:34 → 09/12/2016 12:58:47	30	AMR anomaly
10/01/2017 16:37:35 → 16:44:59	34	AMR Cold Sky calibration maneuver
23/02/2017 11:35:00 → 12:06:59	38	Poseidon3B instrument CNG calibration

Start time → End time	Cycle	Event
26/02/2017 17:13:07 → 17:20:31	38	AMR Cold Sky calibration maneuver
27/04/2017 04:13:16 → 04:20:40	44	AMR Cold Sky calibration maneuver
03/06/2017 15:46:00 → 16:17:59	48	Poseidon3B instrument CNG calibration
28/06/2017 05:10:04 → 05:17:28	51	AMR Cold Sky calibration maneuver
14/08/2017 05:57:05 → 06:04:29	55	AMR Cold Sky calibration maneuver
29/08/2017 13:41:14 → 31/08/2017 16:24:07	57	DEM onboard upload
31/08/2017 21:33:00 → 22:04:59	57	Poseidon3B instrument CNG calibration
04/09/2017 17:32:09 → 17:39:33	58	AMR Cold Sky calibration maneuver
14/09/2017 16:54:56 → 17:52:18	59	Gyro calibration
14/10/2017 15:30:11 → 15:37:35	62	AMR Cold Sky calibration maneuver
02/11/2017 02:05:23 → 02:12:47	63	AMR Cold Sky calibration maneuver
02/12/2017 02:30:00 → 03:01:59	66	Poseidon3B instrument CNG calibration
16/12/2017 02:03:45 → 02:11:09	68	AMR Cold Sky calibration maneuver
05/01/2018 20:45:36 → 20:53:00	70	AMR Cold Sky calibration maneuver
04/02/2018 16:46:42 → 16:54:06	73	AMR Cold Sky calibration maneuver
26/02/2018 02:36:17 → 02:43:41	75	AMR Cold Sky calibration maneuver
01/03/2018 08:17:00 → 08:48:59	75	Poseidon3B instrument CNG calibration

Start time → End time	Cycle	Event
07/04/2018 23:25:16 → 23:32:40	79	AMR Cold Sky calibration maneuver
25/04/2018 20:34:10 → 20:41:34	81	AMR Cold Sky calibration maneuver
29/05/2018 14:05:00 → 14:36:59	84	Poseidon3B instrument CNG calibration
30/05/2018 13:08:34 → 13:17:02 14:41:24 → 14:42:47	85	Poseidon BDR update (2 sequences)
10/06/2018 00:41:29 → 00:48:53	86	AMR Cold Sky calibration maneuver
07/07/2018 19:27:47 → 19:35:10	88	AMR Cold Sky calibration maneuver
31/07/2018 01:05:47 → 01:13:11	91	AMR Cold Sky calibration maneuver
22/08/2018 01:25:28 → 01:32:52	93	AMR Cold Sky calibration maneuver
29/08/2018 19:00:00 → 19:31:59	94	Poseidon3B instrument CNG calibration
02/10/2018 18:53:50 → 19:01:14	97	AMR Cold Sky calibration maneuver
21/10/2018 14:32:55 → 14:40:19	99	AMR Cold Sky calibration maneuver
01/12/2018 00:25:00 → 00:59:59	103	Poseidon3B instrument CNG calibration
04/12/2018 01:36:39 → 01:44:03	103	AMR Cold Sky calibration maneuver
25/12/2018 18:48:13 → 18:55:37	106	AMR Cold Sky calibration maneuver
22/01/2019 15:56:15 → 16:03:39	108	AMR Cold Sky calibration maneuver
28/01/2019 21:50:00	109	AMR Reset
12/02/2019 22:04:38 → 22:12:02	111	AMR Cold Sky calibration maneuver

Start time → End time	Cycle	Event
24/02/2019 09:57:16 → 06/03/2019 08:44:21	112-113	Safe Hold Mode (SHM)
27/02/2019	112	Doris Software patch update (during recovery)
28/02/2019	112	Upload of the GPS software (version N) on PMB (during recovery)
07/03/2019 14:30:00 → 15:25:00	113	Gyro calibration
27/03/2019 02:53:30 → 03:00:54	115	AMR Cold Sky calibration maneuver
06/04/2019 23:17:22 → 12/04/2019 02:20:01	116	Safe Hold Mode (SHM)
29/05/2019 05:50:23 → 05:57:47	121	AMR Cold Sky calibration maneuver
31/05/2019 11:10:00 → 11:41:59	121	Poseidon3B instrument CNG calibration
18/06/2019 18:36:47 → 18:44:11	123	AMR Cold Sky calibration maneuver
18/07/2019 00:15:34 → 00:22:58	126	AMR Cold Sky calibration maneuver
08/08/2019 21:00:06 → 21:07:30	128	AMR Cold Sky calibration maneuver
18/08/2019 11:10:00 → 11:41:59	129	Poseidon3B instrument CNG calibration
20/09/2019 20:18:57 → 20:26:21	133	AMR Cold Sky calibration maneuver
09/10/2019 15:58:18 → 16:05:42	135	AMR Cold Sky calibration maneuver
21/11/2019 19:38:16 → 19:45:40	139	AMR Cold Sky calibration maneuver
25/11/2019 22:42:00 → 23:13:59	139	Poseidon3B instrument CNG calibration
13/12/2019 20:13:34 → 20:20:58	141	AMR Cold Sky calibration maneuver

Start time → End time	Cycle	Event
09/01/2020 20:51:16 → 20:58:40	144	AMR Cold Sky calibration maneuver
31/01/2020 15:43:05 → 15:50:29	146	AMR Cold Sky calibration maneuver
31/01/2020 04:51:17 → 05/02/2020 09:37:14	146- 147	Safe Hold Mode (SHM)
05/02/2020 21:00:53 → 13/02/2020 08:42:44	147	Safe Hold Mode (SHM)
04/03/2020 02:28:00 → 02:29:59	149	Poseidon3B instrument CNG calibration
14/03/2020 02:27:18 → 02:34:42	150	AMR Cold Sky calibration maneuver
01/04/2020 16:30:06 → 16:37:30	152	AMR Cold Sky calibration maneuver
15/05/2020 23:47:54 → 23:47:54	157	AMR Cold Sky calibration maneuver
29/05/2020 09:05:00 → 09:36:59	158	Poseidon3B instrument CNG calibration
06/06/2020 01:44:40 → 01:52:04	159	AMR Cold Sky calibration maneuver
15/06/2020 21:50:42 → 19/06/2020 07:32:46	160	Safe Hold Mode (SHM)
04/07/2020 01:20:01 → 01:27:25	162	AMR Cold Sky calibration maneuver
12/08/2020 17:15:00 → 17:46:59	166	Poseidon3B instrument CNG calibration
01/09/2020 17:15:00 → 03/09/2020 14:13:40	168	DEM onboard upload
07/09/2020 23:45:32 → 23:52:56	168	AMR Cold Sky calibration maneuver
09/09/2020 22:13:36 → 23:04:55	169	Gyro calibration
26/09/2020 02:38:06 → 02:45:30	170	AMR Cold Sky calibration maneuver

Start time → End time	Cycle	Event
27/10/2020 13:23:01 → 29/10/2020 11:36:00	173- 174	DORIS anomaly
08/11/2020 03:52:22 → 03:59:46	175	AMR Cold Sky calibration maneuver
26/11/2020 19:50:00 → 20:21:59	176	Poseidon3B instrument CNG calibration
29/11/2020 17:23:40 → 17:31:05	177	AMR Cold Sky calibration maneuver
27/12/2020 16:32:49 → 16:40:13	180	AMR Cold Sky calibration maneuver
17/01/2021 16:46:07 → 16:53:31	182	AMR Cold Sky calibration maneuver
24/02/2021 01:35:00 → 02:06:59	185	Poseidon3B instrument CNG calibration
03/03/2021 00:24:03 → 00:31:27	186	AMR Cold Sky calibration maneuver
08/03/2021 08:19:28 → 09:27:29	187	DORIS on-board software upgrade
19/03/2021 23:06:47 → 23:14:11	188	AMR Cold Sky calibration maneuver
02/04/2021 20:46:22 → 21:12:41	189	Ground control segment anomaly
07/04/2021 13:27:46 → 13:27:59	190	DEM onboard upload
24/04/2021 15:33:15 → 25/04/2021 01:19:22	191	AMR anomaly
02/05/2021 06:05:37 → 06:13:01	192	AMR Cold Sky calibration maneuver
05/05/2021 13:54:41 → 13:54:55	193	DEM onboard upload
22/05/2021 02:02:41 → 02:10:05	194	AMR Cold Sky calibration maneuver
24/05/2021 07:22:00 → 07:53:59	194	Poseidon3B instrument CNG calibration

Start time → End time	Cycle	Event
22/06/2021 06:27:41 → 06:35:05	197	AMR Cold Sky calibration maneuver
29/06/2021 16:54:30	198	AMR reset performed on rev 25487 due to error 32 (RAM!=ROM) and error count rising
12/07/2021 23:14:40 → 23:22:04	199	AMR Cold Sky calibration maneuver
27/08/2021 23:43:32 → 23:50:56	204	AMR Cold Sky calibration maneuver
28/08/2021 11:57:00 → 12:28:59	204	Poseidon3B instrument CNG calibration
12/09/2021 03:21:30 → 03:28:54	206	AMR Cold Sky calibration maneuver
26/10/2021 20:13:41 → 20:21:05	210	AMR Cold Sky calibration maneuver
16/11/2021 14:44:21 → 14:51:45	212	AMR Cold Sky calibration maneuver
28/11/2021 16:55:00 → 17:26:59	213	Poseidon3B instrument CNG calibration

Table 1 – Events on Jason-3 mission

2.3. Tracking and acquisition mode

Jason-3 can use two on-board tracking modes: Diode/DEM (open loop) and median tracker. In addition, a tracking automatic transition is possible, which means that when authorized: acquisition mode switches automatically from autonomous DIODE acquisition mode over land to Diode/DEM over ocean and referenced inland water. The status of tracking and acquisition modes are detailed in table 2.

Cycle	Acquisition Mode over land	Acquisition Mode over ocean and all referenced inland waters	Comment
Cycle 000	Median tracker + autonomous acquisition / tracking + DEM	Median tracker + autonomous acquisition / tracking + DEM	tracking automatic transition inhibited except for 7 passes

Cycle	Acquisition Mode over land	Acquisition Mode over ocean and all referenced inland waters	Comment
Cycles 001 to 005	Median tracker	Median tracker	tracking automatic transition inhibited.
Cycles 006	see dedicated point below	see dedicated point below	
Cycles 007	Median tracker	Median tracker	tracking automatic transition inhibited everywhere.
Cycles 008	mainly Median tracker	mainly Median tracker	autonomous acquisition / tracking for passes 144 to 148 (DEM patch upload on 2016-05-02). tracking automatic transition inhibited everywhere.
Cycle 009 Pass 001 to mid-248	Median tracker	DEM	mid-pass 248 = CAL2 event on 2016-05-16 10:00)
Cycle 009 Pass mid-248 to 254	Median tracker	Median tracker	mid-pass 248 = CAL2 event on 2016-05-16 10:00)
Cycle 010	Median tracker	Median tracker	tracking automatic transition inhibited
Cycles 011 to 019	Median tracker	DEM	tracking automatic transition authorized
Cycle 020	Median tracker	Median tracker	tracking automatic transition inhibited
Cycles 021 to 056	Median tracker	DEM	tracking automatic transition authorized
Cycle 057			DEM upload
Cycles 058 to 167	Median tracker	DEM	tracking automatic transition authorized
Cycle 168			DEM upload
Cycles 168 onwards	Mainly DEM (see dedicated point below)	DEM	tracking automatic transition authorized

Table 2 – Acquisition mode

- About cycle 006: Altimeter state flag for tracking mode is set to 1 by three times (=0 everywhere else):

- for passes 018 to 029 from 2016-04-07 16:32:57 to 2016-04-08 03:13:59 :
>DIODE Acquisition/Autonomous mode (Altimeter state flag for acquisition mode is set to 9) due to operation error after transponder calibration : back to DIODE DEM mode after the next routine calibration.
 - for passes 065 to 070, from 2016-04-09 12:46:05 to 2016-04-09 17:25:10 :
>Auto Acquisition/Autonomous tracking mode (Altimeter state flag for acquisition mode is set to 8) due to automatic reinitialisation in POS3B default mode, triggered on-board by GPS reinit : back to DIODE DEM mode after the next routine calibration
 - for passes 113 to 116, from 2016-04-11 10:03:37 to 2016-04-11 12:20:28 :
>Auto Acquisition/Autonomous tracking mode (Altimeter state flag for acquisition mode is set to 8) due to automatic reinitialisation in POS3B default mode, triggered on-board by GPS OFF-ON : back to DIODE DEM mode after the next routine calibration
- From cycle 21 onwards, except during DEM upload on cycles 057 and 168, tracking automatic transition is activated.

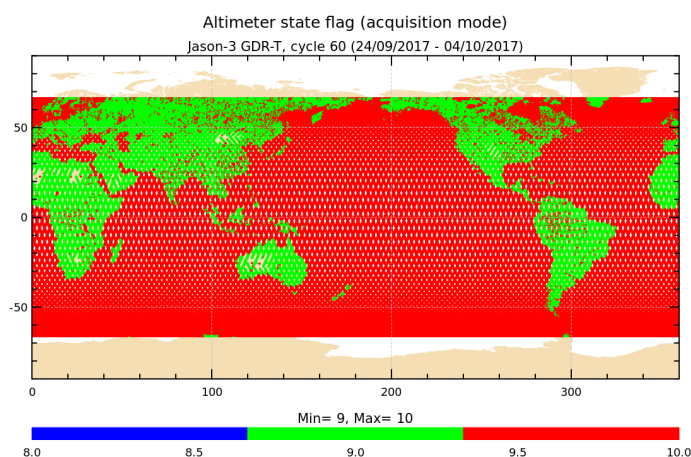


Figure 1 – Acquisition mode for cycle 060 (identical to acquisition mode automatic switch for cycles 6, 9, 11-19, 21-56, 58-167). 8 = autonomous acquisition / tracking, 9 = autonomous DIODE acquisition / tracking, 10 = DIODE + Digital Elevation Model tracking

- About cycle 057, some passes are entirely autonomous acquisition / tracking, and some passes entirely median tracker. DEM upload during this cycle is detailed in [12].
- During cycle 168, some passes are entirely autonomous acquisition / tracking, and some passes entirely median tracker. DEM upload during this cycle is detailed in [7] in the SHM investigation.
- From cycle 169 onwards, tracking automatic transition is activated. Due to the new database of targets used to define onboard elevation commands over continental surfaces, a very low part of measurements are in median mode (see green points on left of Figure 2).

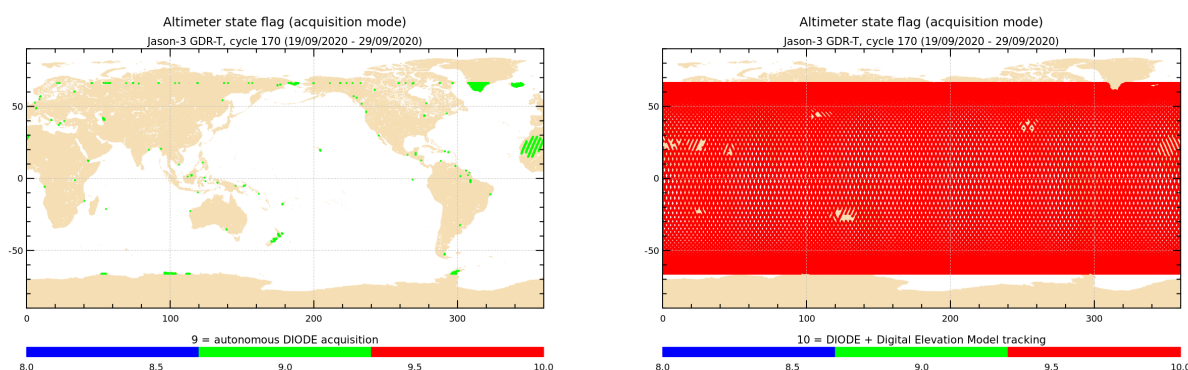


Figure 2 – Acquisition mode for cycle 170 (identical to acquisition mode automatic switch for cycles 169-214). **Left:** 9 = autonomous DIODE acquisition / tracking. **Right:** 10 = DIODE + Digital Elevation Model tracking

2.4. Models and standards

The standards previously used in version “D” are listed in Table 3. Now that the reprocessing of all cycles has been performed, GDR products are in standard “F”. OGDR and IGDR products are in standard “F” since the cycle 174 (2020/10).

The main differences between the O/IGDRs versions “T” and “D” are summarized hereafter:

- CAL-2 calibration processing are based on typical ocean AGC values, correcting the negative squared-attitude values that were observed from the start of the mission.
- Backscatter (sigma-0) values are adjusted internally during ground processing. A calibration bias of +0.14 dB and +0.109 dB is added to the measured (and reported) MLE-4 and MLE-3 Ku-band sigma-0, respectively, prior to wind speed computation; a calibration bias of -0.231 dB and -0.012 dB is added to the measured (and reported) MLE-3 Ku- and C-band sigma-0, respectively, prior to rain flag computation and rain flag values. This ensure that they are properly aligned with the adopted algorithms, so that rain flagging and wind speed values are in-line with those from Jason-2.

The main differences between the O/IGDRs versions “D” and “F” are summarized hereafter:

- Move from TOPEX/Poseidon reference ellipsoid to WGS84.
- Precision of the CAL1 total power of the PTR from 10^{-2} to 10^{-4} .
- Change in the CAL2 (LPF) normalization.
- Backscatter (sigma-0) values are adjusted internally during ground processing. A calibration bias of +0.06 dB and +0.109 dB is added to the measured (and reported) MLE-4 and MLE-3 Ku-band sigma-0, respectively, prior to wind speed computation; no more bias to apply to sigma0 before rain flag computation as a new table based on preliminary GDR-F data is used.

Model	Product version “D”	(version “F” for O/IGDR from cycle 174 onwards and for all GDR)
Orbit	Based on Doris onboard navigator solution for OGDRs.	

Model	Product version "D"	(version "F" for O/IGDR from cycle 174 onwards and for all GDR)
	<p>DORIS tracking data for IGDRs (orbit standard MOE-E until cycle 094 and MOE-F from cycle 095 onwards).</p> <p>From Feb.2019 onwards, a DORIS+GPS solution is used for MOE computation</p> <p>DORIS and/or GPS tracking data for GDRs (orbit standard POE-E until cycle 094 and POE-F from cycle 095 onwards).</p>	
Altimeter Retracking	<p>OceanMLE4 retracking: MLE4 fit from 2nd order Brown model: MLE4 simultaneously retrieves the following 4 parameters from the altimeter waveforms:</p> <ul style="list-style-type: none"> • Epoch (tracker range offset) → altimeter range • Composite Sigma → SWH • Amplitude → Sigma0 • Trailing Edge slope → Square of mispointing angle (Ku band only, a null value is used in input of the C band retracking algorithm) <p>OceanMLE3 retracking: MLE3 fit from first order Brown analytical model: MLE3 simultaneously retrieves the 3 parameters that can be inverted from the altimeter waveforms:</p> <ul style="list-style-type: none"> • Epoch (tracker range offset) → altimeter range • Composite Sigma → SWH • Amplitude → Sigma0 <p>"Ice" retracking: Geometrical analysis of the altimeter waveforms, which retrieves the following parameters:</p> <ul style="list-style-type: none"> • Epoch (tracker range offset) → altimeter range • Amplitude → Sigma0 	

Model	Product version "D"	(version "F" for O/IGDR from cycle 174 onwards and for all GDR)
Altimeter Instrument Corrections	Two sets: one set consistent with MLE4 retracking and one set consistent with MLE3 retracking	
Jason3 Advanced Microwave Radiometer (AMR) Parameters	Using parameters derived from long term calibration tool developed and operated by NASA/JPL	
Dry Troposphere Range Correction	From ECMWF atmospheric pressures and model for S1 and S2 atmospheric tides	Two solutions: <ul style="list-style-type: none"> • From ECMWF atmospheric pressures at sea level and model for S1 and S2 atmospheric tides • From ECMWF atmospheric pressures at measurement level and model for S1 and S2 atmospheric tides
Wet Troposphere Range Correction from Model	From ECMWF model	identical
Ionosphere correction from model	Based on Global Ionosphere TEC Maps from JPL	identical
Sea State Bias Model	Two empirical models: <ul style="list-style-type: none"> • MLE4 version derived from 1 year of MLE4 Jason-2 altimeter data with version "D" geophysical models • MLE3 version derived from 1 year of MLE3 Jason-2 altimeter data with version "D" geophysical models 	Two empirical models (in IGDR): <ul style="list-style-type: none"> • MLE4 version derived from 1 year of MLE4 Jason-3 altimeter data with version "F" geophysical models • MLE3 version derived from 1 year of MLE3 Jason-3 altimeter data with version "F" geophysical models
Mean Sea Surface Model	MSS_CNES-CLS11 (reference 7 years)	Two models: <ul style="list-style-type: none"> • MSS_CNES-CLS15 (reference 20 years) • MSS_DTU-18
Mean Dynamic Topography Model	MDT_CNES-CLS09	MDT_CNES-CLS18
Geoid	EGM96	EGM2008
Bathymetry Model	DTM2000.1	ACE-2
Inverse Barometer Correction	Computed from ECMWF atmospheric pressures after removing S1 and S2 atmospheric tides	identical

Model	Product version “D”	(version “F” for O/IGDR from cycle 174 onwards and for all GDR)
Non-tidal High-frequency De-aliasing Correction	Mog2D high resolution ocean model on I/GDRs. None on OGDRs. Ocean model forced by ECMWF atmospheric pressures after removing S1 and S2 atmospheric tides.	identical
Tide Solution 1	GOT4.8 + S1 ocean tide. S1 load tide ignored. <i>Note that this solution is used in ssha computation variable.</i>	GOT4.10
Tide Solution 2	FES2004 + S1 and M4 ocean tides. S1 and M4 load tides ignored	FES2014B. <i>Note that this solution is used in ssha computation variable.</i>
Equilibrium long-period ocean tide model.	From Cartwright and Taylor tidal potential.	identical
Non-equilibrium long-period ocean tide model.	Mm, Mf, Mtm, and Msqm from FES2004	Mm, Mf, Mtm, Msqm, Sa and Ssa from FES2014B
Solid Earth Tide Model	From Cartwright and Taylor tidal potential.	identical
Pole Tide Model	Equilibrium model WAHR85	DESAI2015 with 2017 coefficients for mean pole location
Wind Speed from Model	ECMWF model	identical
Rain Flag	Derived from comparisons to thresholds of the radiometer-derived integrated liquid water content and of the difference between the measured and the expected Ku-band backscatter coefficient	Use of preliminary GDR-F data to compute rain flag table
Ice Flag	Derived from comparison of the model wet tropospheric correction to a dual-frequency wet tropospheric correction retrieved from radiometer brightness temperatures, with a default value issued from a climatology table	

Table 3 – List of GDR version “D” standard (version “F” for O/IGDR from cycle 174 onwards and for all GDR)

2.5. Processing versions

OGDR and IGDR products are publicly available since June 30th 2016. OGDRs were generated in version “T” until cycle 18/pass 137, in version “D” until cycle 173/pass 222, and then turned in “F” version.

→ The first OGDR “D” file is: *JA3.OPN_2PdS018.137_20160809_080914_20160809_100739.nc*

→ The first OGDR “F” file is: *JA3.OPN_2PfS174.018_20201029_121148_20201029_140842.nc*

Concerning IGDRs, they turned from “T” to “D” version a few days before OGDRs on June 27th(cycle 14/pass

143). They were generated in version “D” until cycle 173/pass 222, and then turned in “F” version.

→ The first IGDR “D” file is: *JA3_IPN_2PdP014.043_20160626_233040_20160627_002653.nc*

→ The first IGDR “F” file is: *JA3_IPN_2PfP174.017_20201029_111312_20201029_120925.nc*

GDRs products have been computed in version “D” until cycle 177. Data were available in version “F” since cycle 171 and along the way. From cycle 178 onwards, the operational version of the GDR products have only been computed in version “F” (see [5]).

2.6. Cautions

Caution (see part 8.4. “Caution about qual inst corr 1hz sig0 ku”)

Natural evolution of PTR results in a gradual increase of the Ku-band sigma0 instrumental correction, this correction exceeded the corresponding threshold: there was a first threshold exceeding from cycle 72 onwards. Since IGDR data have not been reprocessed, the flag ‘qual_inst_corr_1hz_sig0_ku’ is thus considered invalid for IGDR data from cycle 72 until cycle 99 and the adjustment of the threshold in the processing chain. Thanks to the GDR reprocessing, the flag for cycles 72 to 99 is considered valid into GDR-F, contrary to the IGDR. Again, a gradual increase of the Ku-band sigma0 instrumental correction leads to the exceed of this correction over the corresponding threshold from cycle 206 onwards. The threshold was once more increased in the processing chain and this change will be taken into account in the beginning of April 2022.

Caution (see part “Caution about qual inst corr 1hz sig0 C” in 2020 annual report [7]):

The nominal evolution (aging) of the altimeter forced a gradual increase of the C-band sigma0 instrument correction, which has exceeded thresholds for flagging from cycle 160 onwards.

The flag ‘qual_inst_corr_1hz_sig0_c’ parameter has an abnormal number of points with value set to 1 over ocean and should not be used then. This has no impact on data quality or system performance.

Note that the threshold used to set the flag qual_inst_corr_1hz_sig0_c has been adjusted in the standard F processing chain. As a consequence the flag qual_inst_corr_1hz_sig0_c is back ok for a standard use from IGDR and GDR cycles.

3. Data coverage and edited measurements

3.1. Missing measurements

3.1.1. Over land and ocean

Determination of missing measurements relative to the theoretically expected orbit ground pattern is an essential tool to detect missing telemetry or satellite events for instance. Applying the same procedure for Jason-2 and Jason-3, the comparison of the percentage of missing measurements has been performed.

Figure 3 shows the percentage of available measurements for Jason-3 and Jason-2 for all kinds of surfaces observed, computed with respect to a theoretical possible number of measurements. In average Jason-3 provides 99.0% of measurements over 208 cycles (without taking into accounts cycles with explained anomalies or safe hold mode), which shows an improvement compared to Jason-2 tracking capabilities.

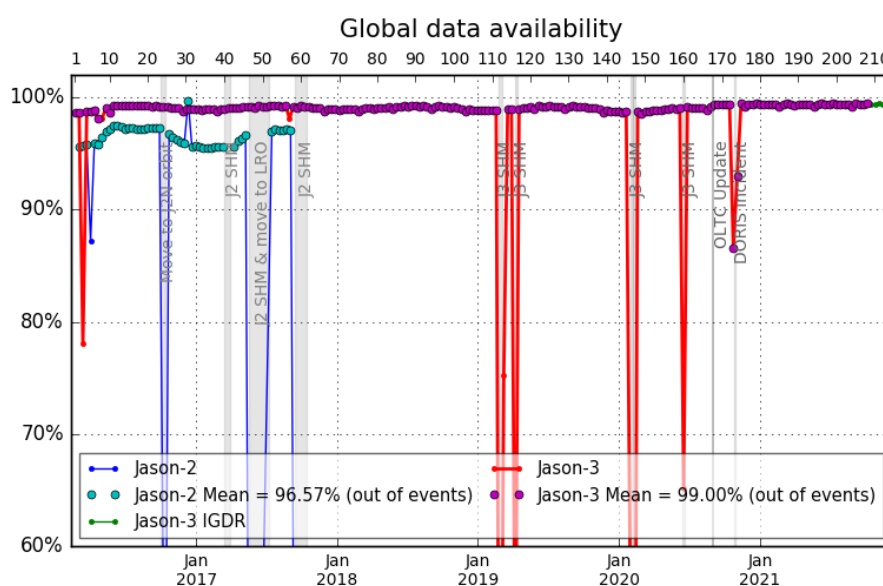


Figure 3 – Global GDRs data availability per cycle

Out of Jason-2 SHM or move of orbit, missing measurements on Jason-2 and Jason-3 since the beginning of Jason-3 mission are:

- **Jason-3 Cycle 3:** GPS platform upload interrupted the data production for two days.
- **Jason-2 Cycle 285:** Data are missing in 2016 between April, 5 at 13:35:10 and April, 6 at 12:02:40. No scientific products have been processed during this period to allow the upload of new GPS On Board software.
- **Jason-3 Cycle 57:** DEM onboard upload interrupted the data production for a few passes.

-
- **Jason-3 Cycles 112-113**: Jason-3 SHM (Safe Hold Mode) occurred from 24/02/2019 09:57:16 until 06/03/2019 08:44:21. Over this SHM event, missing data rate is 79.89% for cycle 112 and 24.21% for cycle 113.
 - **Jason-3 Cycle 116**: SHM occurred from 06/04/2019 23:17:22 until 12/04/2019 02:20:01. Over this SHM event, missing data rate is 53.19% for cycle 116.
 - **Jason-3 Cycles 146-147**: SHM occurred from 31/01/2020 04:51:17 until 05/02/2020 09:37:14. And from 05/02/2020 21:00:53 until 13/02/2020 08:42:44. Over those SHM events, missing data rate is 38.94% for cycle 146 and 88.81% for cycle 147.
 - **Jason-3 Cycle 160**: SHM occurred from 15/06/2020 21:50:42 until 19/06/2020 07:32:46. Over this SHM event, missing data rate is 33.58% for cycle 160.
 - **Jason-3 Cycles 173-174**: DORIS anomaly from 27/10/2020 13:23:01 until 29/10/2020 11:36:00. Over this event, missing data rate is 13.49% for cycle 173 and 7.06% for cycle 174.

Jason-2 in median tracker mode and Jason-3 in DEM mode: For **almost all cycles**, available data percentage is greater for Jason-3 than for Jason-2. This is due to differences in tracking and acquisition modes (Jason-3 uses DEM mode over ocean and inland waters and Jason-2 uses median tracker everywhere): Jason-3 data coverage over land surface can be slightly different regarding to Jason-2 (as shown on top of figure 4).

Jason-2 and Jason-3 both in median tracker: Available data percentage is greater for Jason-3 than for Jason-2 even over cycles where median tracker is used on Jason-2 (all except Jason-2 cycle 311) and only median tracker is used on **Jason-3 (cycles 1 to 5, 7-8, 10 and 20: see 2.3.)**. This difference is probably due to a limitation imposed on Jason-2 tracking to avoid ghost echoes.

Jason-2 and Jason-3 both in DEM mode: Note that **Jason-2 cycle 311 (partly over Jason-3 cycles 30 and 31)** is in DEM mode, so that availability of measurements over this cycle is quite 100% (but more data are rejected). Bottom part of figure 4 shows that these additional measurements for Jason-2 (right) compared to Jason-3 (left) are mainly located over Asia.

Table 4 gives an overview of missing passes and reasons for Jason-3.

Date	Jason-3 Cycle/Pass	Reason
Before 12/02/2016 01:11:09	C000 / P001-116	Final ground-track reached on 12-02-2016 01:11:09
	C000 / P201, 203, 236	Due to calibration events, passes 201 (~10%), 203 (~12%) and 236 (~8%) partly missing
08/03/2016 20:00:00 → 09/03/2016 00:00:01	C003	Due to Gyro calibration , data gap on pass 018.
11/03/2016 05:14:00 → 05:34:00	C003	AMR Cold Sky calibration maneuver

Date	Jason-3 Cycle/Pass	Reason
15/03/2016 07:15:04 to 17/03/2016 08:06:13	C003 / P181-233	Due to platform GPS software upload, passes 182 to 232 are entirely missing, as well as part of passes 181 and 233
06/04/2016 06:05:00 → 06:36:59	C005 / P235	Due to Poseidon3B instrument CNG calibration, data gap on pass 235, that mainly concerns land data acquisition and a portion of Red Sea.
26/04/2016 20:18:29 → 2016-05-06 18:16:59	C008	Due to Poseidon3B instrument CAL2 calibrations , data gaps over land on passes 55, 53, 27, 5, 38, 12 and 29
27/04/2016 11:38:11 to 12:05:55	C008 / P017	Due to OPS error, pass 017 has 49.39% of missing measurements (42.44% over ocean)
08/04/2016 04:44:30 → 05:00:46 05:11:00 → 05:28:21	C006	Due to Poseidon3B instrument CAL2 calibration, data gaps over land
02/05/2016 10:17:04 to 10:28:14 and 14:34:22 to 14:37:28	C008 / P144,148	Due to DEM upload: <ul style="list-style-type: none"> • Pass 144 has 20.33% of missing measurements (13.27% over ocean, Norwegian Sea) • Pass 148 has 6.60% of missing measurements over ocean (western african coast)
12/05/2016 22:44:59 → 22:52:23	C009	AMR Cold Sky calibration maneuver
16/05/2016 10:00:00 → 10:16:15	C009	Due to Poseidon3B instrument CAL2 calibration, data gap over land on pass 248
17/05/2016 02:34:00 → 19/05/2016 03:34:16	C010	Due to Poseidon3B instrument CAL2 calibration (5 sequences), data gaps over land on passes 31, 64, 38, 12, and 44
12/07/2016 04:26:36 → 04:34:00	C015	AMR Cold Sky calibration maneuver
05/09/2016 04:24:44 → 04:32:08	C021	AMR Cold Sky calibration maneuver
07/11/2016 22:21:30 → 22:28:54	C027	AMR Cold Sky calibration maneuver

Date	Jason-3 Cycle/Pass	Reason
27/11/2016 06:15:00 to 06:46:58	C029 / P159, 160	Due to CNG calibration, parts of passes 159 and 160 are missing (mostly over land). Pass 159 has 54.73% of missing measurements (10.54% over ocean).
10/01/2017 16:37:35 → 16:44:59	C034	AMR Cold Sky calibration maneuver
23/02/2017 11:35:00 → 12:06:59	C038	Poseidon3B instrument CNG calibration
26/02/2017 17:13:07 → 17:20:31	C038	AMR Cold Sky calibration maneuver
27/04/2017 04:13:16 → 04:20:40	C044	AMR Cold Sky calibration maneuver
03/06/2017 from 15:46:00 to 16:17:59	C048 / P159	Due to CNG calibration, pass 159 has 56.55% of missing data mostly over land (10.54% over ocean)
28/06/2017 05:10:04 → 05:17:28	C051	AMR Cold Sky calibration maneuver
14/08/2017 05:57:05 → 06:04:29	C055	AMR Cold Sky calibration maneuver
30/08/2017 12:07:15 to 14:10:33	C057 / P123-125	Due to DEM upload: <ul style="list-style-type: none"> • Pass 123 has 23.91% of missing measurement (15.44% over ocean). • Pass 124 is missing • Pass 125 has 96.16% of missing measurement (100% over ocean).
31/08/2017 14:22:58 to 16:26:10	C057 / P151-153	Due to DEM upload: <ul style="list-style-type: none"> • Pass 151 has 12.40% of missing measurement (8.57% over ocean). • Pass 152 has 100% of missing measurement over ocean • Pass 153 has 98.40% of missing measurement (100% over ocean).

Date	Jason-3 Cycle/Pass	Reason
31/08/2017 21:33:00 to 22:04:59	C057 / P159	Due to CNG calibration, pass 159 has 56.17% of missing measurement (10.54% over ocean).
04/09/2017 17:32:09 → 17:39:33	C058	AMR Cold Sky calibration maneuver
14/09/2017 from 16:54:56 to 17:52:18	C059 / P005	Due to Gyro calibration, pass 5 has 47.22% of missing measurements (0.07% over ocean)
14/10/2017 15:30:11 → 15:37:35	C062	AMR Cold Sky calibration maneuver
02/11/2017 02:05:23 → 02:12:47	C063	AMR Cold Sky calibration maneuver
02/12/2017 02:30:00 → 03:01:59	C066 / P235	Due to CNG calibration, pass 235 has 57.16% of missing measurement (8.33% over ocean).
16/12/2017 02:03:45 → 02:11:09	C068	AMR Cold Sky calibration maneuver
26/12/2017 23:03:32 → 23:06:25	C069	Pass 110 has 5.88% of missing measurement (5.66% over ocean) probably due to connection to Usingen anomaly.
05/01/2018 20:45:36 → 20:53:00	C070	AMR Cold Sky calibration maneuver
04/02/2018 16:46:42 → 16:54:06	C073	AMR Cold Sky calibration maneuver
26/02/2018 02:36:17 → 02:43:41	C075	AMR Cold Sky calibration maneuver
01/03/2018 08:17:00 → 08:48:59	C075 / P235	Due to CNG calibration, pass 235 has 57.03% of missing measurement (8.33% over ocean).
07/04/2018 23:25:16 → 23:32:40	C079	AMR Cold Sky calibration maneuver
25/04/2018 20:34:10 → 20:41:34	C081	AMR Cold Sky calibration maneuver
29/05/2018 14:05:00 → 14:36:59	C084 / P235	Due to CNG calibration, pass 235 has 57.00% of missing measurement (8.33% over ocean).

Date	Jason-3 Cycle/Pass	Reason
30/05/2018 13:08:34 → 13:17:02 14:41:24 → 14:42:47	C085 / P006-007	Due to BDR update: <ul style="list-style-type: none"> • Pass 6 has 15.31% of missing measurement (10.80% over ocean). • Pass 7 has 2.84% of missing measurement (4.86% over ocean).
10/06/2018 00:41:29 → 00:48:53	C086	AMR Cold Sky calibration maneuver
07/07/2018 19:27:47 → 19:35:10	C088	AMR Cold Sky calibration maneuver
31/07/2018 01:05:47 → 01:13:11	C091	AMR Cold Sky calibration maneuver
22/08/2018 01:25:28 → 01:32:52	C093	AMR Cold Sky calibration maneuver
29/08/2018 19:00:00 → 19:31:59	C094 / P057	Due to CNG calibration, pass 057 has 57.00% of missing measurement (12.67% over ocean).
02/10/2018 18:53:50 → 19:01:14	C097	AMR Cold Sky calibration maneuver
21/10/2018 14:35:37 → 14:40:19	C099	AMR Cold Sky calibration maneuver
01/12/2018 00:25:00 → 00:56:59	C103 / P159	Due to CNG calibration, pass 159 has 56.43% of missing measurement (10.54% over ocean).
04/12/2018 01:36:39 → 01:44:03	C103	AMR Cold Sky calibration maneuver
25/12/2018 18:48:13 → 18:55:37	C106	AMR Cold Sky calibration maneuver
22/01/2019 15:56:15 → 16:03:39	C108	AMR Cold Sky calibration maneuver
12/02/2019 22:04:38 → 22:12:02	C111	AMR Cold Sky calibration maneuver
24/02/2019 09:57:16 → 06/03/2019 08:44:21	C112 P050 / C113 P061	Safe Hold Mode. Passes 050 to 254 of cycle 112 and passes 001 to 060 of cycle 113 are missing.

Date	Jason-3 Cycle/Pass	Reason
07/03/2019 14:30:00 → 15:25:00	C113 / P093 and 094	Due to Gyro calibration, passes 093 and 094 have respectively 19.2% and 23.9% of missing measurements (all over ocean)
27/03/2019 02:53:30 → 03:00:54	C115	AMR Cold Sky calibration maneuver
06/04/2019 23:17:22 → 12/04/2019 02:20:01	C116	Safe Hold Mode. Passes 108 to 245 are completely missing and pass 246 has 16.37% of missing measurement (15,46% over ocean).
30/04/2019 07:43:45 → 07:47:01	C118	Due to PLTM gaps, pass 199 has 26 non-continuous missing points over ocean.
29/05/2019 05:50:23 → 05:57:47	C121	AMR Cold Sky calibration maneuver
31/05/2019 11:10:00 → 11:41:59	C121 / P235	Due to CNG calibration, pass 235 has 59.96% of missing measurement (8.00% over ocean).
11/06/2019 → 13/06/2019	C123	Due to PLTM gaps, passes 021 and 071 have 47 and 33 non-continuous missing points over ocean.
18/06/2019 18:36:47 → 18:44:11	C123	AMR Cold Sky calibration maneuver
18/07/2019 00:15:34 → 00:22:58	C126	AMR Cold Sky calibration maneuver
08/08/2019 21:00:06 → 21:07:30	C128	AMR Cold Sky calibration maneuver
18/08/2018 18:58:00 → 19:29:59	C129 / P235	Due to CNG calibration, pass 235 has 55.42% of missing measurement (7.98% over ocean).
20/09/2019 20:18:57 → 20:26:21	C133	AMR Cold Sky calibration maneuver
09/10/2019 15:58:18 → 16:05:42	C135	AMR Cold Sky calibration maneuver
04/11/2019 22:08:50 and 22:14:46	C137	Due to PLTM gaps, pass 204 has 2.63% of missing points over ocean.
21/11/2019 19:38:16 → 19:45:40	C139	AMR Cold Sky calibration maneuver

Date	Jason-3 Cycle/Pass	Reason
25/11/2019 22:42:00 → 23:13:59	C139 / P235	Due to CNG calibration, pass 235 has 57.19% of missing measurement (8.40% over ocean).
13/12/2019 20:13:34 → 20:20:58	C141	AMR Cold Sky calibration maneuver
09/01/2020 20:51:16 → 20:58:40	C144	AMR Cold Sky calibration maneuver
31/01/2020 04:51:17→ 05/02/2020 09:37:14	C146 P153 / C147 P033	Safe Hold Mode. Passes 154 to 254 of cycle 146 and passes 001 to 032 of cycle 147 are missing.
05/02/2020 21:00:53→ 13/02/2020 08:42:44	C147 P044-237	Safe Hold Mode. Passes 045 to 236 of cycle 147 are missing.
04/03/2020 02:28:00 → 02:29:59	C149 / P235	Due to CNG calibration, pass 235 has 55.42% of missing measurement (8.08% over ocean).
14/03/2020 02:27:18 → 02:34:42	C150	AMR Cold Sky calibration maneuver
01/04/2020 16:30:06 → 16:37:30	C152	AMR Cold Sky calibration maneuver
15/05/2020 23:40:30 → 23:47:54	C157	AMR Cold Sky calibration maneuver
29/05/2020 09:05:00 → 09:36:59	C158 / P159	Due to CNG calibration, pass 159 has 51.21% of missing measurement (10.11% over ocean).
06/06/2020 01:44:40 → 01:52:04	C159	AMR Cold Sky calibration maneuver
15/06/2020 21:50:42→ 19/06/2020 07:32:46	C160 P100-187	Safe Hold Mode. Passes 101 to 186 of cycle 160 are missing.
04/07/2020 01:20:01 → 01:27:25	C162	AMR Cold Sky calibration maneuver
26/07/2020 01:40:45 → 01:48:09	C164	AMR Cold Sky calibration maneuver
12/08/2020 17:15:00 → 17:46:59	C166 / P057	Due to CNG calibration, pass 057 has 55.44% of missing measurement (11.62% over ocean).

Date	Jason-3 Cycle/Pass	Reason
01/09/2020 13:03:18 → 03/09/2020 14:13:40	C168 / P053-109	Due to DEM upload: <ul style="list-style-type: none"> • Pass 083 has 14.06% of missing measurement (9.27% over ocean). • Pass 109 has 3.35% of missing measurement (1.72% over ocean).
27/10/2020 13:23:01 → 29/10/2020 11:36:00	C173 P222 / C174 P017	Due to DORIS anomaly: <ul style="list-style-type: none"> • Pass 222 of cycle 173 has 90.30% of missing measurement (88.77% over ocean). • Passes 223 of cycle 173 to 016 of cycle 174 are entirely missing. • Pass 017 of cycle 174 has 42.78% of missing measurement (52.00% over ocean).
26/11/2020 19:50:00 → 20:21:59	C176 / P235	Due to CNG calibration, pass 235 has 55.67% of missing measurement (2.78% over ocean).
29/11/2020 17:23:41 → 17:31:05	C177	AMR Cold Sky calibration maneuver
27/12/2020 16:32:49 → 16:40:13	C180	AMR Cold Sky calibration maneuver
17/01/2021 16:46:07 → 16:53:31	C182	AMR Cold Sky calibration maneuver
24/02/2021 01:35:00 → 02:06:59	C186 / P235	Due to CNG calibration, pass 235 has 56.9% of missing measurement (2.54% over ocean).
19/03/2021 23:06:47 → 23:14:11	C188	AMR Cold Sky calibration maneuver
02/04/2021 20:46:22 → 21:12:41	C189	Ground control segment anomaly
02/05/2021 06:05:37 → 06:13:01	C192	AMR Cold Sky calibration maneuver

Date	Jason-3 Cycle/Pass	Reason
22/05/2021 02:02:41 → 02:10:05	C194	AMR Cold Sky calibration maneuver
24/05/2021 07:22:00 → 07:53:59	C194 / P235	Due to CNG calibration, pass 235 has 56.9% of missing measurement (2.46% over ocean).
22/06/2021 06:27:41 → 06:35:05	C197	AMR Cold Sky calibration maneuver
12/07/2021 23:14:40 → 23:22:04	C199	AMR Cold Sky calibration maneuver
02/08/2021 11:32:28 → 11/09/2021 03:26:35	C202 to C205	Caution : Altimeter calibrations wrongly planned over ocean
27/08/2021 23:43:32 → 23:50:56	C204	AMR Cold Sky calibration maneuver
28/08/2021 11:57:00 → 12:28:59	C204 / P235	Due to CNG calibration, pass 235 has around 55% of missing measurement (around 2% over ocean).
12/09/2021 03:21:30 → 03:28:54	C206	AMR Cold Sky calibration maneuver
26/10/2021 20:13:41 → 20:21:05	C210	AMR Cold Sky calibration maneuver
16/11/2021 14:44:21 → 14:51:45	C212	AMR Cold Sky calibration maneuver
28/11/2021 16:55:00 → 17:26:59	C213 / P235	Due to CNG calibration, pass 235 has 56.43% of missing measurement (2.62% over ocean).

Table 4 – List of missing Jason-3 passes

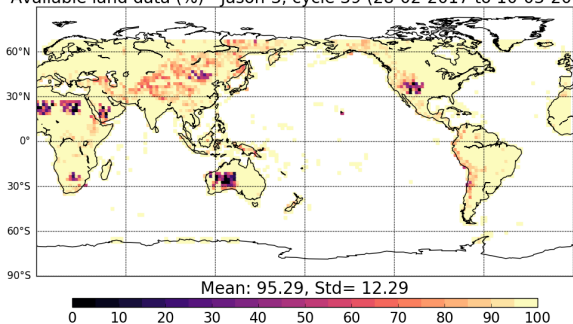
3.1.2. Over ocean

The behaviour of Jason-3 over ocean is excellent and conform to what is observed with Jason-2 during tandem phase (on the same ground track, with 80 seconds of difference), and even after on interleaved groundtrack.

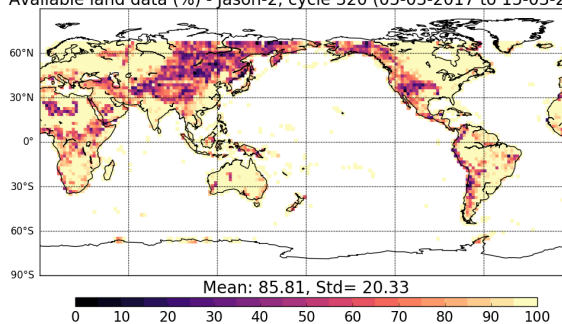
Looking at data over ocean, Jason-3 is always available (ocean is fully covered) out of specific events (see figure 5)

- 21.03% of missing measurements due to GPS platform upload during cycle 3.

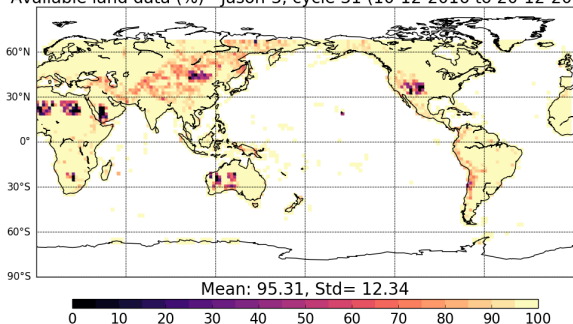
Available land data (%) - Jason-3, cycle 39 (28-02-2017 to 10-03-2017)



Available land data (%) - Jason-2, cycle 320 (05-03-2017 to 15-03-2017)



Available land data (%) - Jason-3, cycle 31 (10-12-2016 to 20-12-2016)



Available land data (%) - Jason-2, cycle 311 (05-12-2016 to 15-12-2016)

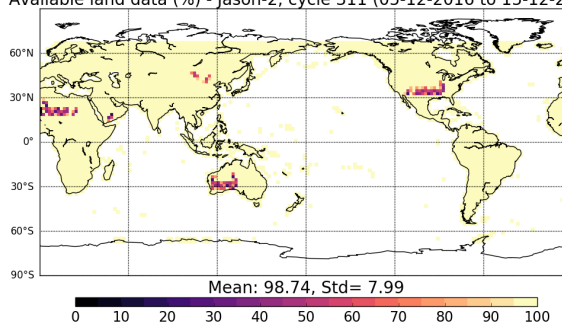


Figure 4 – Map of percentage of available measurements over land for Jason-3 (left) and for Jason-2 (right). **Top:** Jason-3 cycle 039 in DEM mode and Jason-2 cycle 320 in median mode. **Bottom:** Jason-3 cycle 031 in DEM mode and Jason-2 cycle 311 in DEM mode

- 0.3% of missing measurements over cycle 8 due to operator error.
- 1.74% of missing measurements due to the DEM-onboard upload during cycle 57.
- 79.82% of missing measurements due to safe hold mode during cycle 112.
- 22.92% of missing measurements due to safe hold mode during cycle 113.
- 53.16% of missing measurements due to safe hold mode during cycle 116.
- 38.94% of missing measurements due to safe hold mode during cycle 146.
- 88.81% of missing measurements due to safe hold mode during cycle 147.
- 33.58% of missing measurements due to safe hold mode during cycle 160.
- 0.03% of missing measurements due to the DEM-onboard upload during cycle 168.
- 13.21% of missing measurements due to DORIS anomaly during cycle 173.
- 6.27% of missing measurements due to DORIS anomaly during cycle 174.
- 0.18% of missing measurements due to the altimeter calibrations over ocean during cycle 202.
- 0.62% of missing measurements due to the altimeter calibrations over ocean during cycle 203.
- 0.63% of missing measurements due to the altimeter calibrations over ocean during cycle 204.
- 0.32% of missing measurements due to the altimeter calibrations over ocean during cycle 205.

See specific cyclic reports at [2] for the four last altimeter calibrations mentionned (cycle 202 to 205).

In addition, please note the following events that slightly impact the data coverage (only a few number of ocean missing points):

- A few missing points per cycle were observed on the beginning of 2021 (respectively cycles 182, 184, 185, 186, 187, 189, 190, 191, 192). This was due to an anomaly with the ground stations partially receiving the data produced onboard.
- An anomaly of calibration over Australia was also recurrently observed over pass 177, inducing a few missing points (< 5) for cycles 171, 172, 173, 174, 175, 176, 177, 181, 183, 184, 185, 186, 187, 188, 189, 190, 195.

Note that Jason-2 missing measurements reason until end of 2017 is detailed in Jason-2 2017 annual report [16].

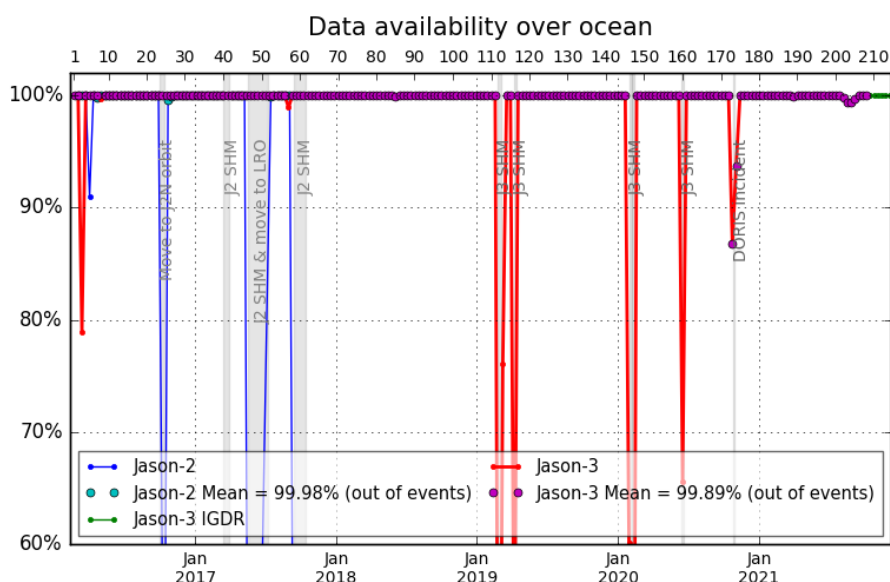


Figure 5 – Jason-2 and Jason-3 GDR data availability over ocean (per cycle)

3.2. Edited measurements

Editing criteria allow to select only measurements considered as valid over ocean. This editing process is structured in 4 main steps:

1. Measurements over land are removed, only measurements over ocean and lakes are kept
2. Measurements over ice are removed
3. Threshold criteria are applied on altimeter, radiometer and geophysical parameters as described in the following table 5. Except for the dual frequency ionosphere correction, only Ku-band measurements are used in this editing procedure, as they mainly represent the end user dataset.
4. A spline criterion is applied to remove the remaining spurious data.

3.2.1. Global editing

The percentage of total edited measurements is monitored on a cyclic basis. The average of total edited measurements is 37.6% (see Figure 6). A small annual cycle is visible due to ice coverage signal (see dedicated part 3.2.2.): the total percentage is slightly lower during March/April/May (30-35%), then increasing during May to July and remains around 38-42%, and start to slowly decrease in mid-September. This expected behaviour is related to sea ice coverage, and was already observed on previous altimetry missions such as OSTM/Jason 2. The peak detected on cycle 30 is due to an AMR anomaly that occurred from 08/12/2016 04:36:34 to 09/12/2016 12:58:47. The second peak visible on cycle 112 is due to edited data before SHM (see details about SHM in 2019 Annual report [17]). The peak visible on cycle 147 is due to SHM (not significant figure as there are less than 2 days for this cycle). The peak visible on cycle 191 is due to a radiometer yellow alarm which brought a data gap.

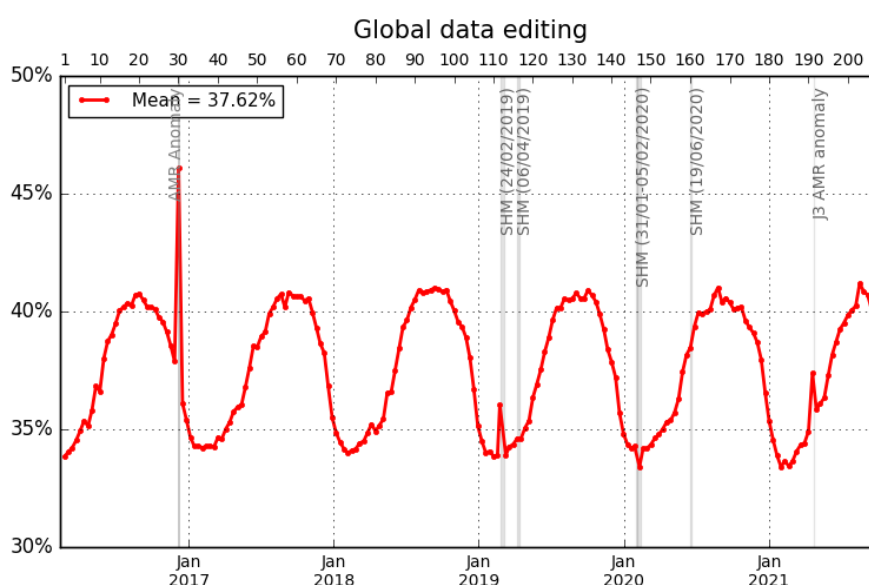


Figure 6 – Jason-3 data editing average by cycle.

3.2.2. Flagging quality criterion: Ice flag

The ice flag (from GDR) is used to remove the ice and sea ice data. Figure 7 shows cycle per cycle percentage of measurements edited by this criterion in comparison with Jason-2 (only ocean and big lakes measurements are kept). Jason-2 and Jason-3 ice flag show similar features while on repetitive orbit. The number of measures flagged according to this criterion is higher with standard “F” than with standard “D”, this is due to a change in the surface classification between both standards (see [5]).

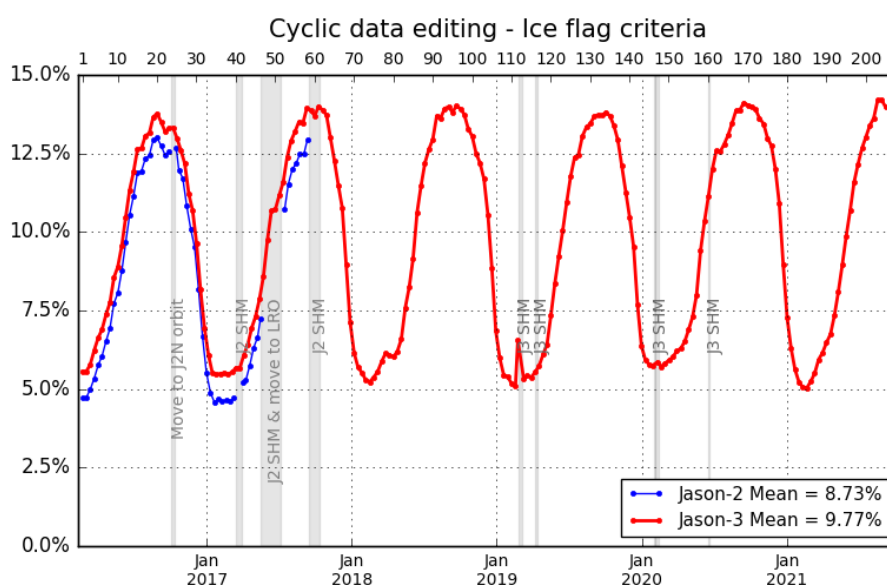


Figure 7 – Cycle per cycle monitoring of the percentage of edited measurements by ice flag criterion.

Over the shown period, no anomalous trend is detected but the nominal annual cycle is visible. Indeed, the maximum number of points over ice is reached during the southern winter (i.e. July - September). As Jason-3 takes measurements between 66° north and south, it does not detect thawing of sea ice (due to global warming), which takes place especially in northern hemisphere over 66°N.

3.2.3. Flagging quality criterion: Rain flag

Though the altimeter rain flag is available in GDR, it is not used hereafter during the editing procedure. The percentage of measurements where rain flag is set to 1 is plotted in figure 8 top panel. Using the altimeter rain flag would lead to edit 1.36% of additional measurements compared to recommended editing procedure (see figure 8 bottom panels for comparison). This is way less than the 5.85% of flagged with the standard “D” (see [5]).

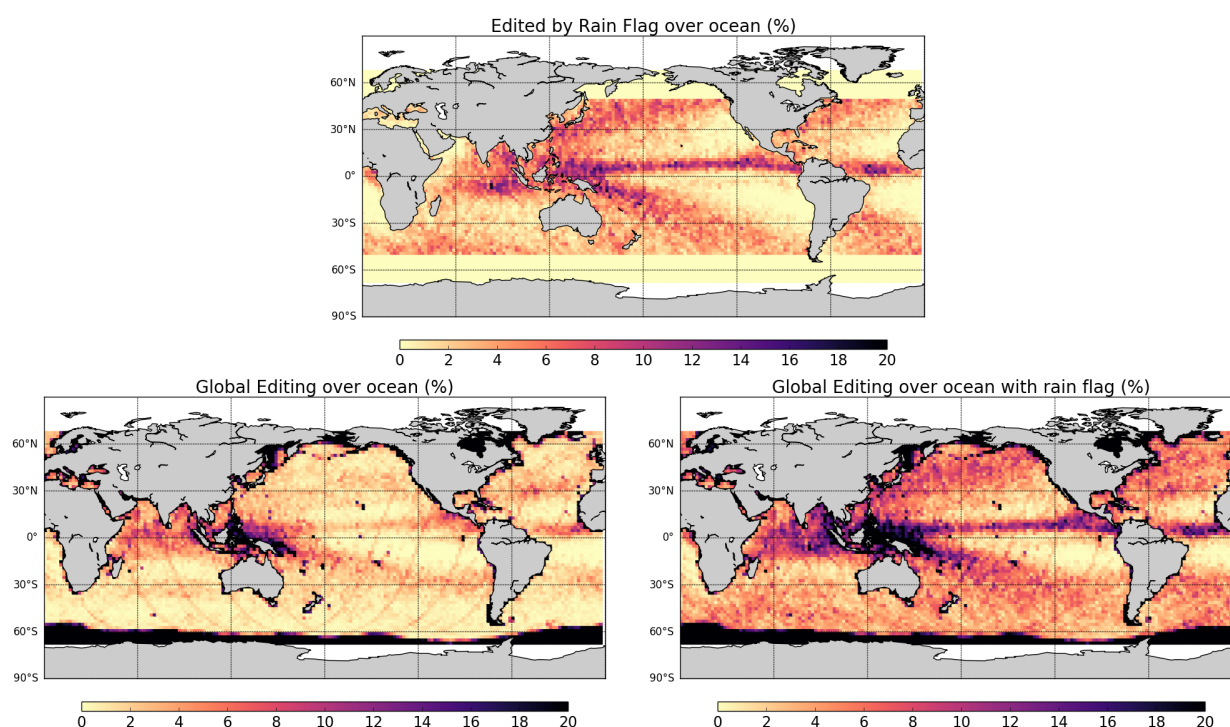


Figure 8 – Top: Percentage of edited measurements by altimeter rain flag criterion. Bottom left: Map of global edited measurements without considering the rain flag. Bottom right: Map of global edited measurements using all criteria and considering the rain flag. All figures are computed over ocean and from cycle 171 to 208.

3.2.4. Editing on thresholds criteria

After quality flag analysis, instrumental parameters have also been analyzed from comparison with thresholds. The average of total edited measurements following threshold criterion is around 3.38% (Figure 9). For each criterion, cycle percentage of edited measurements is monitored (detailed from part 3.2.4.1. to 3.2.4.11.). This allows detection of anomalies in the number of removed data, which could have instrumental, geophysical or algorithmic origins. In particular, note that no measurement is edited by the following corrections (these parameters are only verified in order to detect data at default values, which might happen during a processing anomaly):

- dry troposphere correction,
- inverted barometer correction (including DAC),
- equilibrium tide,
- earth tide,
- pole tide.

Threshold criteria applied on altimeter, radiometer and geophysical parameters are described in the following table 5. The last column represents the mean of rejected data on each criterion over GDR cycles 1 to 208.

Parameter	Min thresholds	Max thresholds	Mean edited
Sea surface height	−130 <i>m</i>	100 <i>m</i>	0.82%
Sea level anomaly	−2.0 <i>m</i>	2.0 <i>m</i>	1.45%
Number measurements of range	10	<i>Not applicable</i>	1.1%
Standard deviation of range	0	0.2 <i>m</i>	1.4%
Squared off-nadir angle	−0.2 <i>deg</i> ²	0.64 <i>deg</i> ²	0.65%
Dry troposphere correction	−2.5 <i>m</i>	−1.9 <i>m</i>	0.00%
Inverted barometer correction	−2.0 <i>m</i>	2.0 <i>m</i>	0.00%
AMR wet troposphere correction	−0.5 <i>m</i>	−0.001 <i>m</i>	0.16%
Ionosphere correction	−0.4 <i>m</i>	0.04 <i>m</i>	0.89%
Significant wave height	0.0 <i>m</i>	11.0 <i>m</i>	0.64%
Sea State Bias	−0.5 <i>m</i>	0.0 <i>m</i>	0.58%
Number measurements of Ku-band Sigma0	10	<i>Not applicable</i>	1.09%
Standard deviation of Ku-band Sigma0	0	1.0 <i>dB</i>	2.14%

Parameter	Min thresholds	Max thresholds	Mean edited
Ku-band Sigma0	7.0 dB	30.0 dB	0.62%
Ocean tide	-5.0 m	5.0 m	0.01%
Equilibrium tide	-0.5 m	0.5 m	0.00%
Earth tide	-1.0 m	1.0 m	0.00%
Pole tide	-15.0 m	15.0 m	0.00%
Altimeter wind speed	0 m.s ⁻¹	30.0 m.s ⁻¹	1.08%
All together	-	-	3.38%

Table 5 – Editing criteria over cycles 1 to 208

The peak detected on cycle 30 (Figure 9) is due to an AMR anomaly that occurred from 08/12/2016 04:36:34 to 09/12/2016 12:58:47. The second peak is located on cycle 112, where occurred SHM. Before going into SHM, data is rejected by several parameters out of threshold (square off nadir angle, rms of range, backscattering coefficient, significant wave height, altimeter ionosphere, sea state bias, wind speed, sea surface height, sea level anomaly). The third pic is due to an AMR anomaly that occurred from 24/04/2021 17:18:33 to 25/04/2021 01:21:54. Except those anomalies the rate of rejected by thresholds data is quite stable.

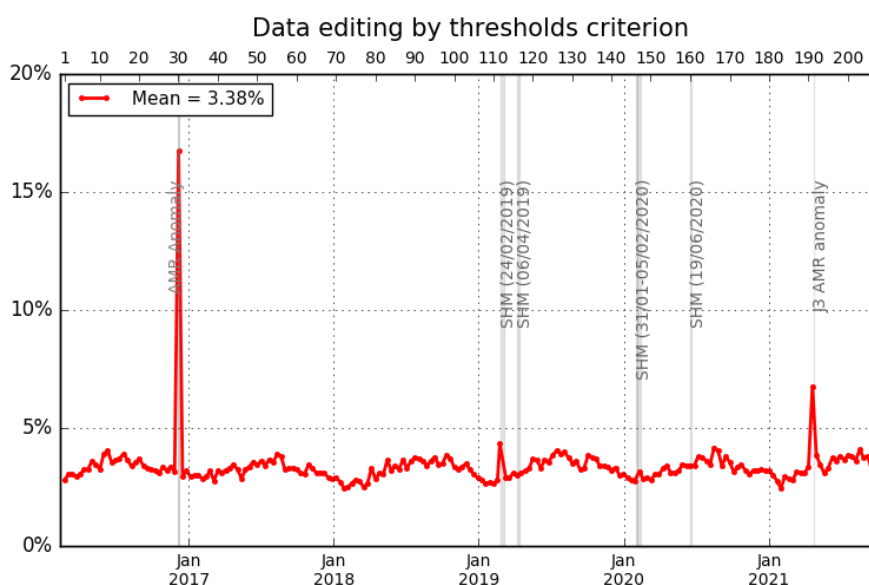


Figure 9 – Jason-3 data editing by thresholds average by cycle.

3.2.4.1. Threshold criteria: 20-Hz range measurements number and standard deviation

1Hz range measurements computed with less than 10 full resolutions (20Hz, 20 measurements/seconds) are removed. Indeed they are considered as not consistent to compute 1Hz resolution range. Such situation usually occurs in regions with disturbed sea state or heavy rain, as shown on Figure 10 top right. Indeed waveforms are distorted by rain cells, which makes them often meaningless for SSH calculation. As a consequence, edited measurements due to several altimetric criteria are often correlated with wet areas.

For Jason-3, the average percentage of removed measurements using this criterion is 1.1% whereas it is 1.04% for Jason-2. The two missions provide very close values (Figure 10 top right).

Using the threshold editing on 20Hz measurements standard deviation (Figure 10 bottom), 1.4% of data are removed in average for Jason-3, which is very close to Jason-2 (1.41%). An annual signal appears here for both missions. As for 20Hz range measurements number, edited measurements are correlated with wet areas.

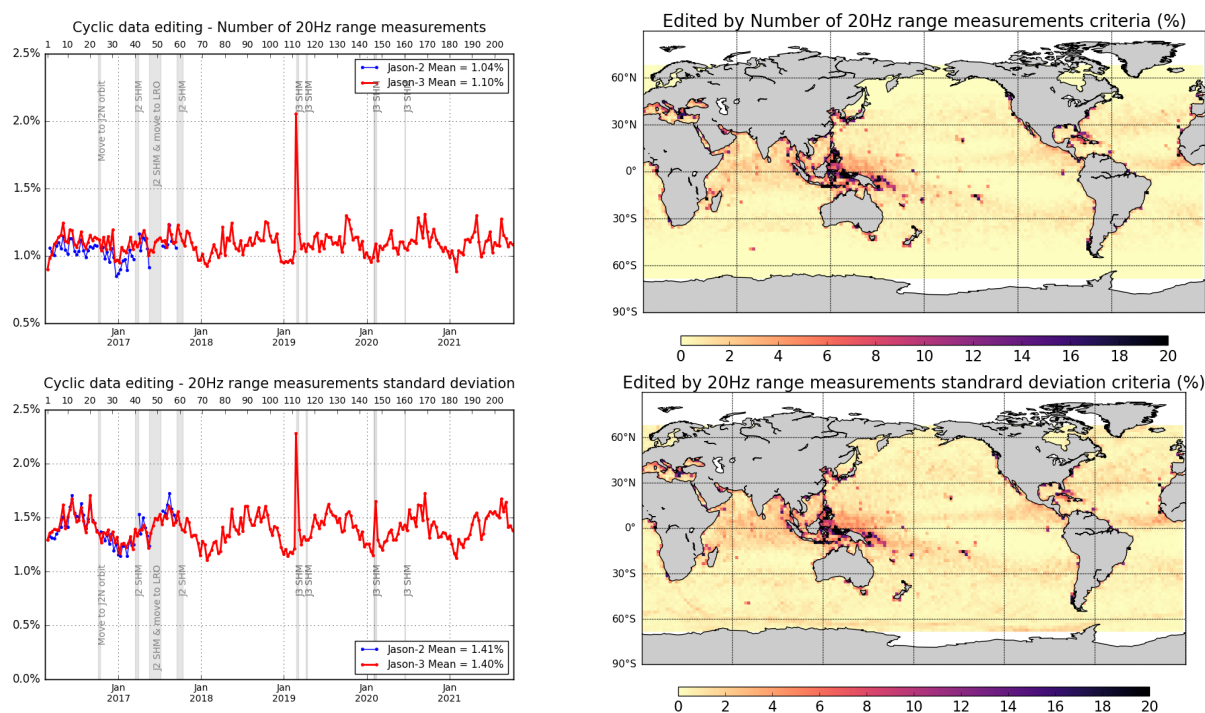


Figure 10 – Percentage of edited measurements by 20Hz range measurements threshold criterion (top) and by 20Hz range measurements standard deviation threshold criteria (bottom). Cycle per cycle monitoring compared with Jason-2 (left) and Jason-3 averaged map from cycle 171 to 208 (right).

3.2.4.2. Threshold criteria: Significant wave height (swh)

The percentage of edited measurements due to significant wave heights criterion is represented on Figure 11, and is about 0.64%. They are mostly due to set to default values data, and are located near coasts, in the equatorial regions and in circumpolar areas.

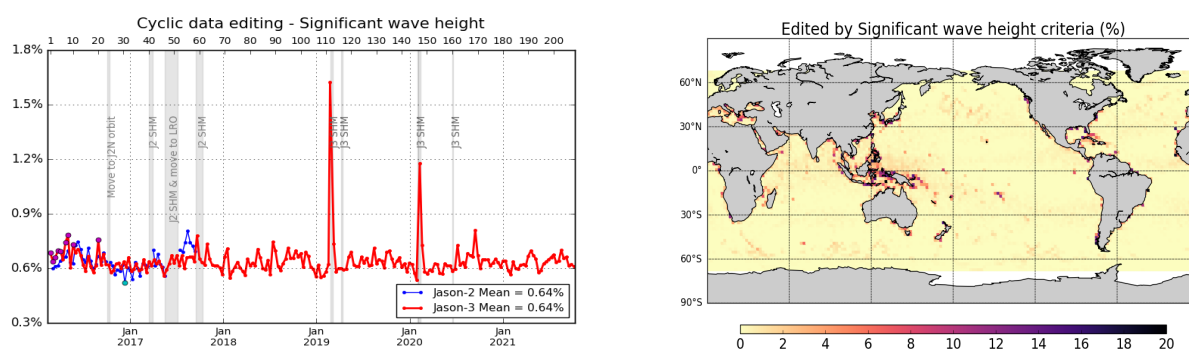


Figure 11 – Percentage of edited measurements by SWH threshold criterion. Left: Cycle per cycle monitoring compared with Jason-2 (Jason-2 DEM cycle in cyan. Jason-3 median tracker cycles in purple.) Right: Jason-3 averaged map from cycle 171 to 208 .

3.2.4.3. Threshold criteria: Backscatter coefficient (sigma0)

The percentage of edited measurements due to backscatter coefficient criterion is represented on top of Figure 12. It is about 0.62%, compared to 0.61% for Jason-2. The bottom part of Figure 12 shows again close values between the two missions for the 20Hz sigma0 standard deviation criterion. However, there are more rejected measurements with this criterion on Jason-3 (2.14%) than Jason-2 (1.95%). The number of measures flagged according to this criterion is higher with standard “F” than with standard “D”, this is due to a change in the surface classification between both standards (see [5]). In addition differences seem to be linked to acquisition modes:

- For Jason-3 cycles 1 to 5, 7-8, 10, and 20, both missions are using median tracker: rejected data rate on this criterion are equivalent for both missions.
- For almost all cycles, Jason-2 uses median tracker and Jason-3 uses Diode/DEM automatic switch: there are less data removed for Jason-2 than for Jason-3.
- For Jason-2 cycle 311 (over Jason-3 cycles 30 and 31), both missions are in Diode/DEM mode: the results are quite equivalent.

Edited measurements are especially found in regions with disturbed waveforms, as shown on the maps.

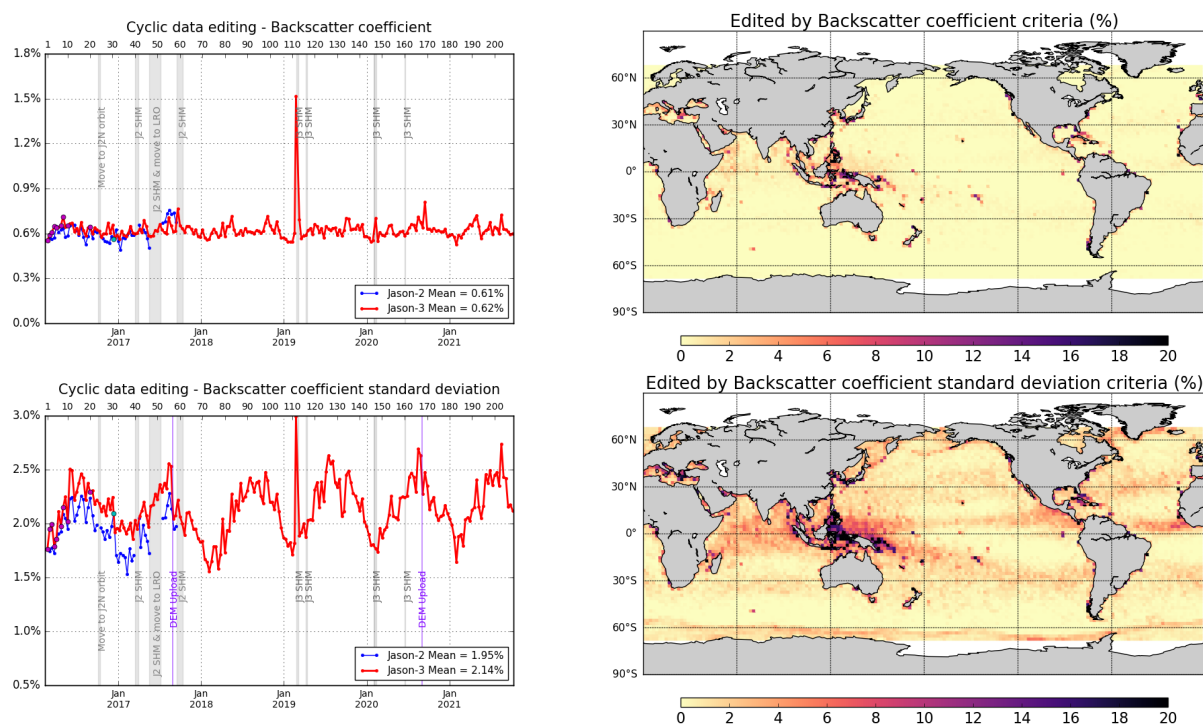


Figure 12 – Percentage of edited measurements by backscatter coefficient threshold criterion (top) and by 20Hz backscatter coefficient standard deviation threshold criteria (bottom). Cycle per cycle monitoring compared with Jason-2 (left, Jason-2 DEM cycle in cyan. Jason-3 median tracker cycles in purple) and Jason-3 averaged map from cycle 171 to 208 (right).

3.2.4.4. Threshold criteria: Radiometer wet troposphere correction

The percentage of edited measurements due to radiometer wet troposphere correction criterion is represented in figure 13. It is about 0.16%. When removing cycles which experienced problems, percentage of edited measurements drops to 0.08%. For some cycles, the percentage of edited measurements is higher than usual. For cycle 30, this unusual value (13.85%) is due to an AMR anomaly that occurred from 08/12/2016 04:36:34 to 09/12/2016 12:58:47. For cycle 191, the edited measurements (3.4%) correspond to another AMR anomaly occurring from 24/04/2021 17:18:33 to 25/04/2021 01:21:54. Compared to Jason-2 values, they are within the same order of magnitude, except specific events or anomalies (Jason-2 AMR anomalies during cycle 285 and cycle 326, that correspond respectively to Jason-3 cycle 5 and cycle 45 datation).

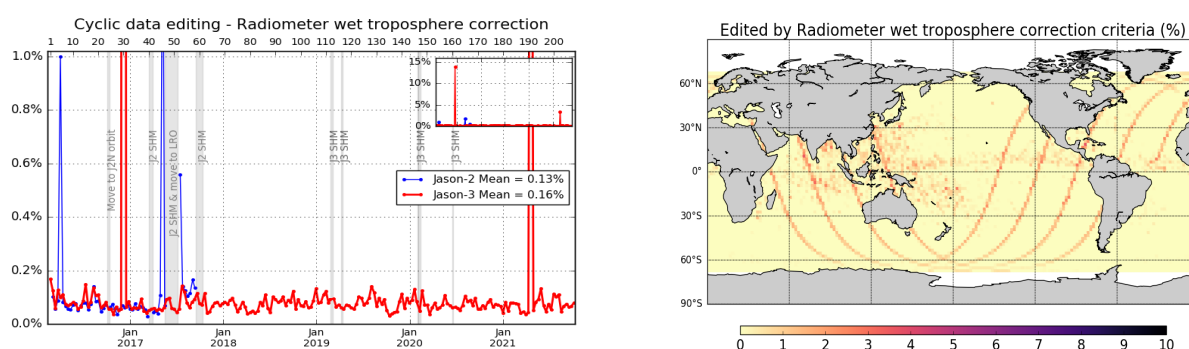


Figure 13 – Percentage of edited measurements by radiometer wet troposphere correction threshold criterion. Left: Cycle per cycle monitoring compared with Jason-2. Right: Jason-3 averaged map from cycle 171 to 208.

3.2.4.5. Threshold criteria: Ionospheric correction

The mean percentage of edited data by threshold criterion on ionospheric correction is 0.89%. It is much lower than Jason-2 mean (1.18%) and this gain is explained by the filtered version of the ionospheric correction used in the standard “F” (see [5] and [11]). The map on figure 14 shows that measurements edited by filtered dual frequency ionosphere correction are mostly found near coasts and at ice frontiers.

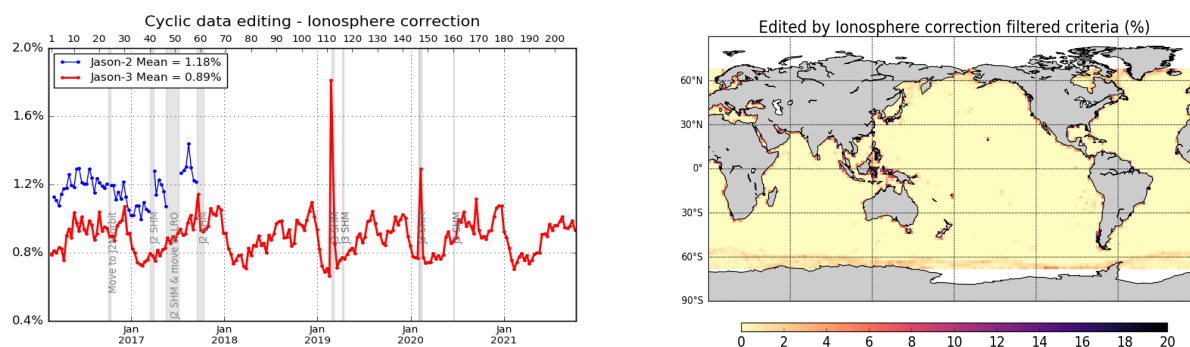


Figure 14 – Percentage of edited measurements by ionospheric correction threshold criterion. Left: Cycle per cycle monitoring compared with Jason-2. Right: Jason-3 averaged map from cycle 171 to 208.

3.2.4.6. Threshold criteria: Altimeter wind speed

The percentage of edited measurements due to altimeter wind speed criterion is represented on figure 15. It is about 1.08%, and in accordance with Jason-2 (1.03%). Measurements are usually edited because of default values. This is the case when sigma0 itself is at default value, or when it shows very high values (higher than 25 dB), which occurs during sigma bloom situations and also over sea ice. Indeed, the wind speed algorithm (which uses backscatter coefficient and significant wave height) can not retrieve values for sigma0 higher than 25 dB.

Wind speed is also edited when it includes negative values, which can occur in GDR products. Nevertheless, sea state bias is available even for negative wind speed values. Therefore, the percentage of edited altimeter wind speed data is higher than the percentage of edited sea state bias data (see 3.2.4.7.).

The map 15 showing percentage of measurements edited by altimeter wind speed criterion is correlated with maps 11 (swh) and 16 (ssb).

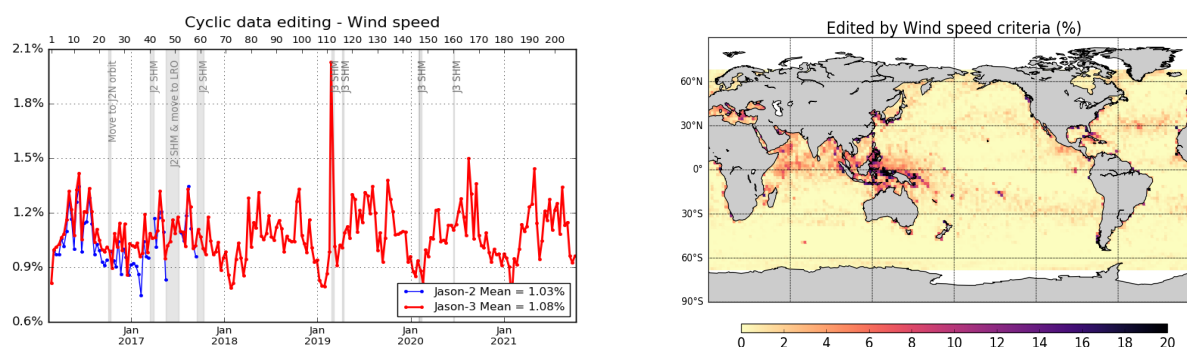


Figure 15 – Percentage of edited measurements by wind speed threshold criterion. Left: Cycle per cycle monitoring compared with Jason-2. Right: Jason-3 averaged map from cycle 171 to 208.

3.2.4.7. Threshold criteria: Sea State Bias

Regarding the sea state bias criterion, the percentage of Jason-3 edited measurements is about 0.58% and 0.63% for Jason-2. The difference can also be observed on the sigma0 and the significant wave height threshold criteria (which are both used for SSB computation).

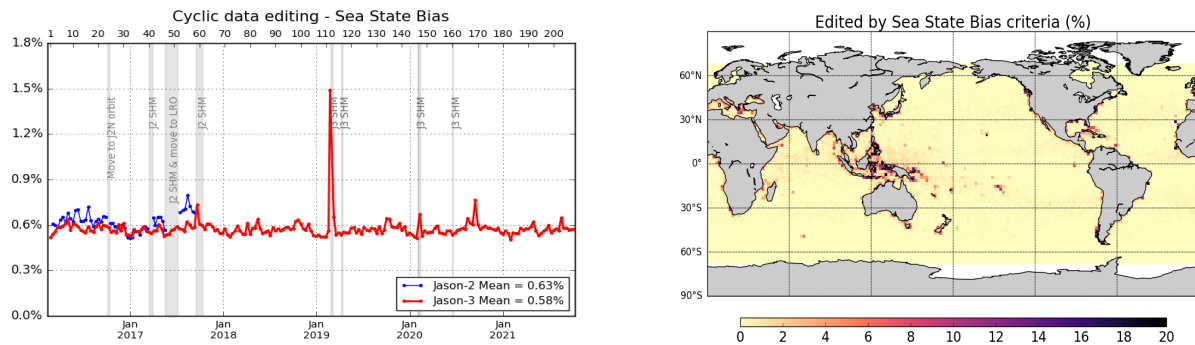


Figure 16 – Percentage of edited measurements by sea state bias threshold criterion. Left: Cycle per cycle monitoring compared with Jason-2. Right: Jason-3 averaged map from cycle 171 to 208.

3.2.4.8. Threshold criteria: Ocean tide

The percentage of edited measurements due to ocean tide is lower than 0.01% for both missions. The ocean tide correction is a model output, there should therefore be no edited measurement. Indeed there are no measurements edited in open ocean areas, but only very few near coasts (Alaska, Kamchatka, Labrador). These measurements are mostly at default values. The level of edited measurements decreases or increases with move of orbit for Jason-2 : this is related to the new ground track, which no longer overflows the same areas. Two different models are used for both missions : Jason-3 uses the FES14B model while Jason-2 uses the GOT4.8.

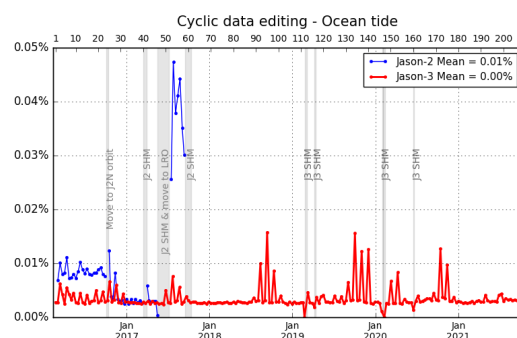


Figure 17 – Percentage of edited measurements by ocean tide threshold criterion. Cycle per cycle monitoring compared with Jason-2.

3.2.4.9. Threshold criteria: Square off nadir angle

The percentage of edited data is a little higher for Jason-3 (0.65%) than it is for Jason-2, this is due to the difference in the surface type mask as explained in [5] (part 3.2.3). An increase in Jason-2 edited measurements is observed from July 2017 after Jason-2 move to drifting orbit. The map 18 shows that edited measurements are mostly found in coastal regions and regions with disturbed waveforms.

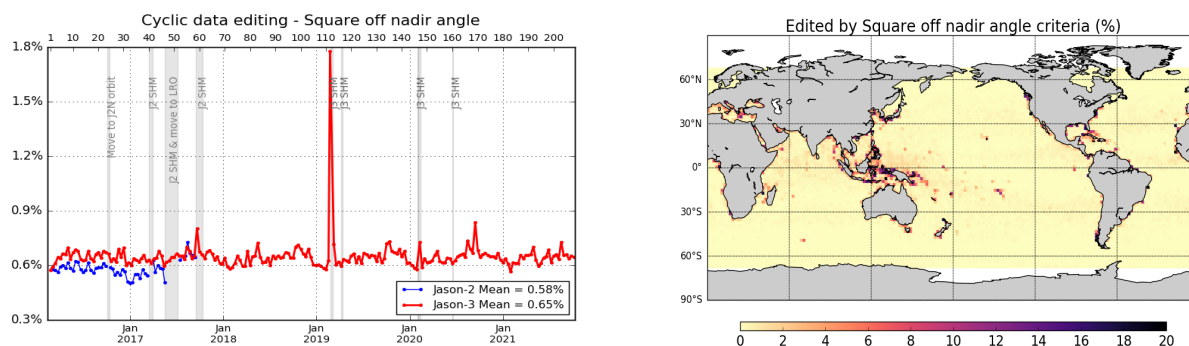


Figure 18 – Percentage of edited measurements by square off nadir angle threshold criterion. Left: Cycle per cycle monitoring compared with Jason-2. Right: Jason-3 averaged map from cycle 171 to 208.

3.2.4.10. Threshold criteria: Sea surface height

Sea surface height represents the difference between the orbit and the altimeter range in Ku band. Figure 19 summarizes the editing resulting from the sea surface height threshold criterion. It removes in average 0.82% of data for Jason 3 whereas it removes 0.77% of data for Jason 2. The editing is usually due to range measurements at default values near coast in equatorial and mid-latitude regions, as well as regions with low significant wave heights.

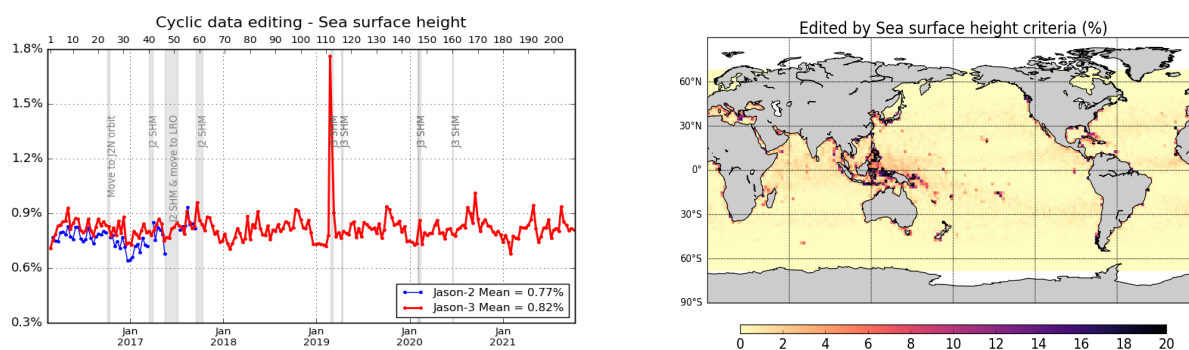


Figure 19 – Percentage of edited measurements by sea surface height threshold criterion. Left: Cycle per cycle monitoring compared with Jason-2. Right: Jason-3 averaged map from cycle 171 to 208.

3.2.4.11. Threshold criteria: Sea Level Anomaly

The percentage of edited data by threshold criterion is 1.45% for Jason-3. As the wet tropospheric correction is used in the SLA computation, percentage of edited SLA measurement presents the same peak on cycle 30. In the same way edited data due to derive from altimeter corrections before SHM at cycle 112 are rejected for this criterion (second peak in february 2019). The radiometer yellow alarm from cycle 191 also produces another lack of wet tropospheric correction which results in a SLA editing as well, this event is seen in the figure 20 over of a few tracks. When removing these cycles, the percentage of edited measurements drops to lower than 1%. The rate of rejected data for Jason-3 is a little higher than for Jason-2 (0.93%), this is due to the special editing of the filtered ionospheric correction in coastal areas (see [5] part 3.2.1 and 3.2.4). As in Jason-3, higher points on Jason-2 monitoring are mainly due to Jason-2 wet troposphere contribution, where AMR was unavailable during cycle 285 (Jason-3 cycle 5), cycle 326 (Jason-3 cycle 45), and for restart after SHM, leading to an increase of the quantity of edited data (point out of plot scale).

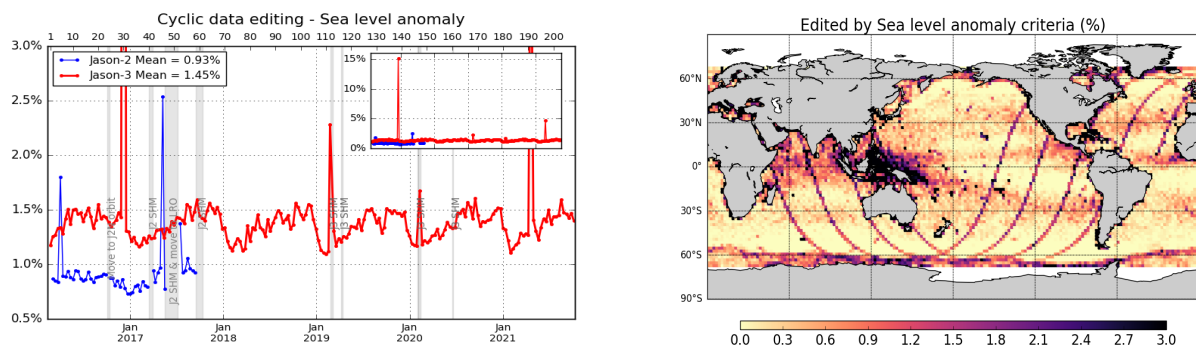


Figure 20 – Percentage of edited measurements by sea level anomaly threshold criterion. Left: Cycle per cycle monitoring compared with Jason-2. Right: Jason-3 averaged map from cycle 171 to 208.

4. Monitoring of altimeter and radiometer parameters

4.1. Methodology

Mean and standard deviation of Jason-3 main parameters have both been monitored since the beginning of the mission. Moreover, a comparison with Jason-2 parameters has been performed: it allows to monitor the bias between the parameters of the 2 missions.

- Till Jason-3 cycle 23, Jason-3 and Jason-2 are on the same ground track and are spaced out about 80 seconds apart (tandem phase), the mean of the Jason-2 - Jason-3 differences can be computed using a point by point repeat track analysis (referred as 'residuals' in plots).
- From Jason-3 cycle 24, a maneuver sequence was conducted (from end of Jason-2 cycle 303) to move Jason-2 to the new formation flight mission orbit. Jason-2 has a repeat ground-track which is interleaved with Jason-3. It is the same ground-track as already used by Topex/Poseidon during its formation flight phase with Jason-1, and Jason-1 with Jason-2. Because of a time shift of 5 days, geographical variations are then too strong to directly compare Jason-3 and Jason-2 parameters on a point by point basis. Therefore day per day global differences have been carried out to monitor differences between the two missions. A filter over 11 days was applied. Nevertheless the differences are still quite noisy, especially for corrections which vary rapidly in time and space. Therefore occasional small jumps might be covered by the noise of the differences. Nevertheless it should be possible to detect drifts and permanent jumps. Jason-3 and Jason-2 were in this formation flight phase from Jason-3 cycles 25 to 46 (Jason-2 cycles 305 to 327).

In March and May 2017, Jason-2 experienced several safe holds caused by gyro anomalies. It was decided to move Jason-2 to an End-of-Life (EOL) Long Repeat Orbit (LRO). Jason-2 mission phase is detailed in [16]. Science data on the first LRO are available from 11th of July 2017 to 16th of July 2018. Note that the first cycle on the new orbit starts with cycle 500 (this corresponds to mid-Jason-3 cycle 52) and this first interleaved ground track ends on cycle 537 (end of Jason-3 cycle 89). Note that after this first LRO, Jason-2 was moved to a second interleaved ground track (iLRO) on 18th of July 2018. Science data restart on 25th of July 2018 with cycle 600. Jason-2 mission ended on October 1st 2019 during cycle 644.

As during the formation flight phase, day per day global differences of the parameters have been carried out to monitor differences between the two missions (only until Jason-2 cycle 506 (14th of September 2017)): differences are done over Jason-3 cycles 1 to 58, corresponding to Jason-2 cycles 281 to 506.

4.2. 20 Hz range measurements

The monitoring of the number and standard deviation of 20 Hz elementary range measurements used to derive 1 Hz data is presented here. These two parameters are computed during the altimeter ground processing. For both Jason-2 and Jason-3, before performing a regression to derive the 1 Hz range from 20 Hz data, a MQE (mean quadratic error) criterion is used to select valid 20 Hz measurements. This first step of selection consists in verifying that the 20 Hz waveforms can be approximated by a Brown echo model (Brown, 1977 [13]) (Thibaut et al. 2002 [14]).

Then, through an iterative regression process, elementary ranges too far from the regression line are discarded until convergence is reached. Thus, monitoring the number of 20 Hz range measurements and the standard deviation computed among them is likely to reveal changes at instrumental level.

4.2.1. 20 Hz range measurements number in Ku-Band and C-Band

Jason-3 number of elementary 20 Hz range measurements starts with values slightly higher than Jason-2 until cycle 3. During cycle 3, new calibration (CAL2) filter turned the square off-nadir angle to zero, which implies the absence of waveform mispointing, a higher MQE and a smaller number of elementary measurements. Then from cycle 4 onwards, Jason-3 number of elementary 20 Hz range measurements is very similar to Jason-2 with an average of 19.61 versus 19.60 in Ku-band (left of figure 21) and 19.24 versus 19.25 in C-band (right of figure 21).

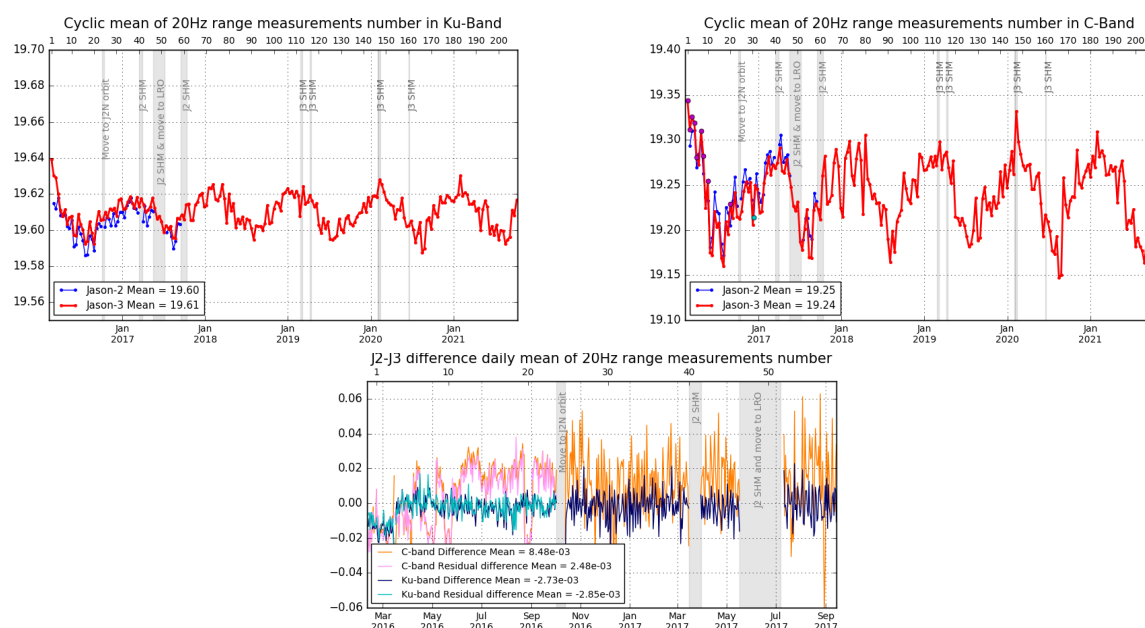


Figure 21 – **Top:** Cyclic monitoring of number of elementary 20 Hz range measurements for Jason-2 and Jason-3 for Ku-band and C-band. **Bottom:** Jason-2 - Jason-3 difference daily monitoring of elementary 20 Hz range measurements number (until september 2017). Note that the bottom figure was computed using GDR-D data for both Jason-3 and Jason-2.

Elementary number of measurements used to compute a 1Hz measurement is correlated to significant wave height (4.5): figure 22 shows less elementary range measurements around Indonesia, the Mediterranean Sea and close to coasts, which are all regions of low significant wave heights.

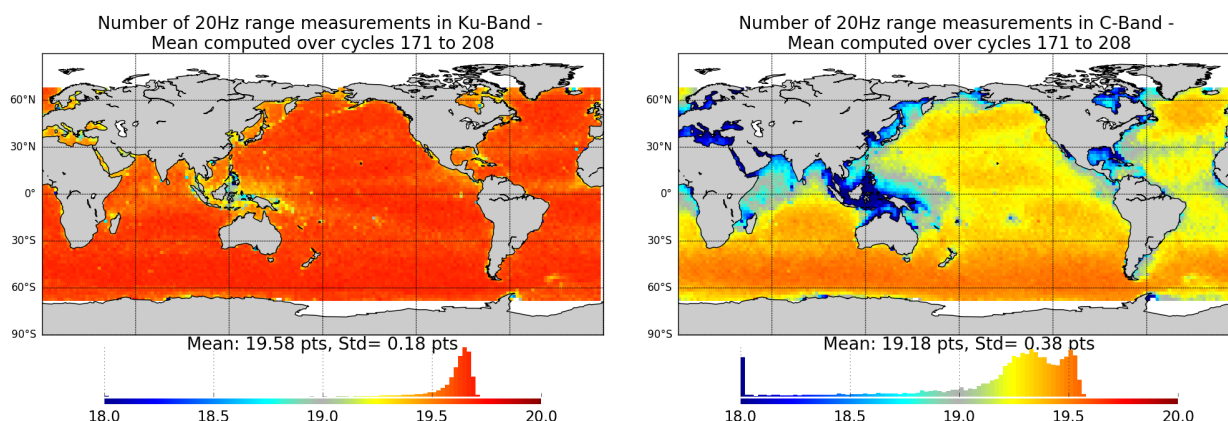


Figure 22 – Map of number of 20 Hz range measurements for Jason-3 averaged over cycles 171 to 208, in Ku-band (left) and in C-band (right).

4.2.2. 20 Hz range measurements standard deviation in Ku-Band and C-Band

Figure 23 shows the monitoring of Jason-3 and Jason-2 20 Hz range measurements standard deviation, in Ku-band (left) and C-band (right). Jason-3 standard deviation of the 20 Hz measurements is 8.00 cm for Ku-Band and 17.57 cm for C-Band. It is similar to Jason-2 data (8.00 cm in Ku-Band and 17.43 cm in C-Band). 20 Hz range measurements standard deviation is higher on C-band than on Ku-band due to the onboard averaging that is performed over less waveforms (onboard averaging of 90 measurements for each 20 Hz Ku-band value, against 15 in case of C-band), which leads to an increased noise.

Standard deviation of measurements is correlated to significant wave height (swh dedicated part: 4.5.).

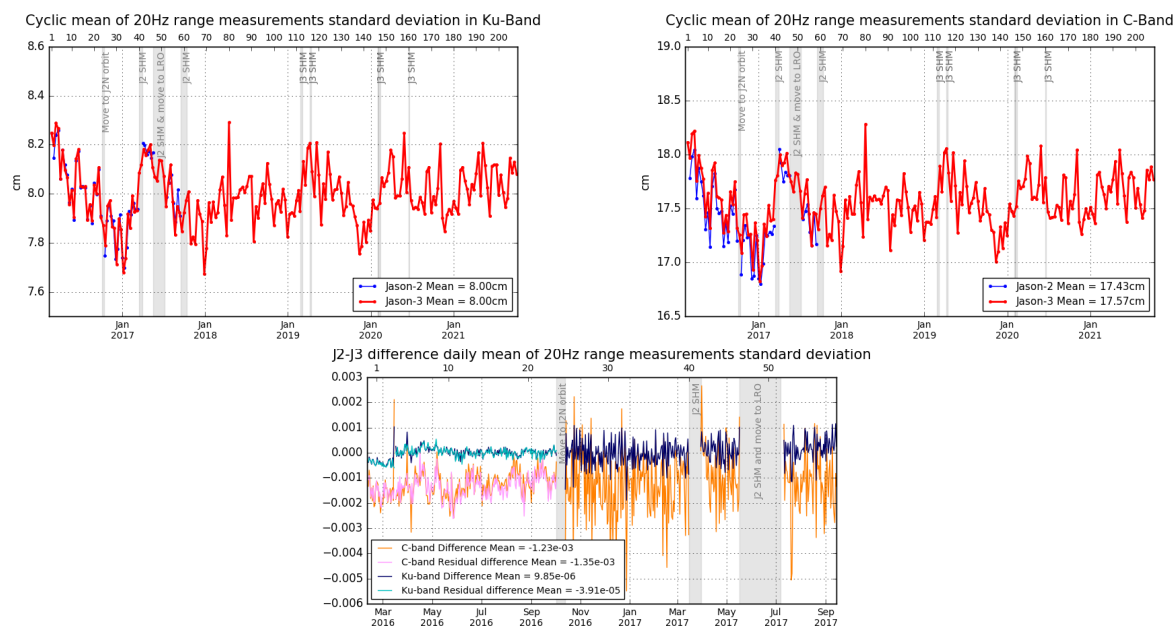


Figure 23 – **Top:** Cyclic monitoring of elementary 20 Hz range measurements standard deviation for Jason-2 and Jason-3 for Ku-band and C-band. **Bottom:** Jason-2 - Jason-3 difference daily monitoring of elementary 20 Hz range measurements standard deviation. Note that the bottom figure was computed using GDR-D data for both Jason-3 and Jason-2.

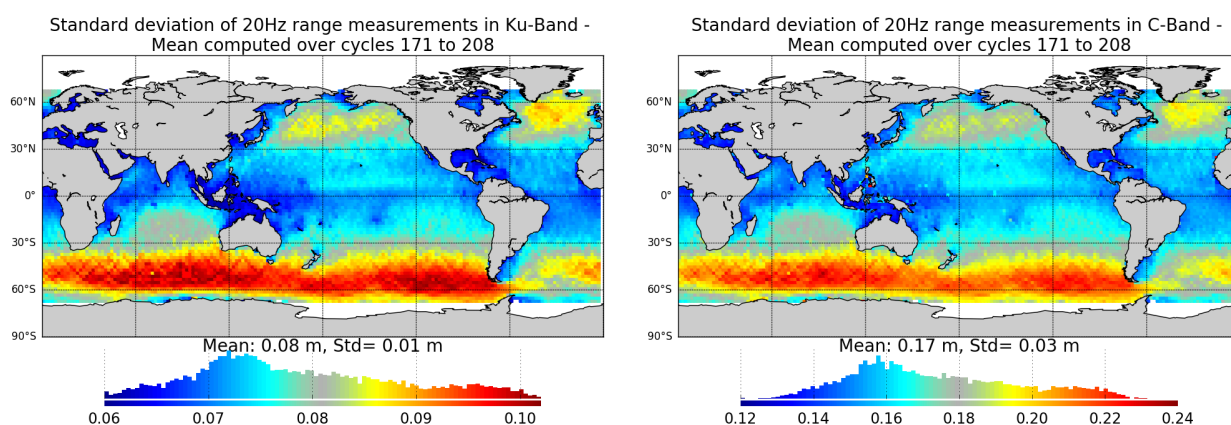


Figure 24 – Map of 20 Hz range measurements standard deviation for Jason-3 averaged over cycles 171 to 208, in Ku-band (left) and in C-band (right).

4.3. Off-Nadir Angle from waveforms

The off-nadir angle is derived from the slope of the trailing edge of the waveform during the altimeter processing: it can either be caused by real platform mispointing or by backscattering properties of the surface. The square of the off-nadir angle, averaged on a cyclic basis (taking into account valid measurements only), has been plotted for Jason-3 and Jason-2 on figure 25.

At the beginning of the mission, Jason-3 altimeter mispointing was deeply analysed to understand the negative values observed from cycle 3 after GPS upload. Mispointing is actually related to CAL2 filter shapes, which depends on automatic gain control settings for Jason-3. During the first cycles, the in-flight calibration (CAL2) filters were measured using a different Automatic Gain Control code than the one used during waveform acquisition over ocean, in order to optimize the CAL2 measurement numerical accuracy (quantification optimization). It has however an impact on the filter slope and fully explains the observed mispointing negative values. The filter slope was modified during cycle 14 (June 26th, 2016) and explains the jump to zero on the IGDR curve. This correction was applied during GDR production, which explains the difference between red and green curves between cycles 4 and 14, so that GDR mispointing has been close to zero from cycle 4.

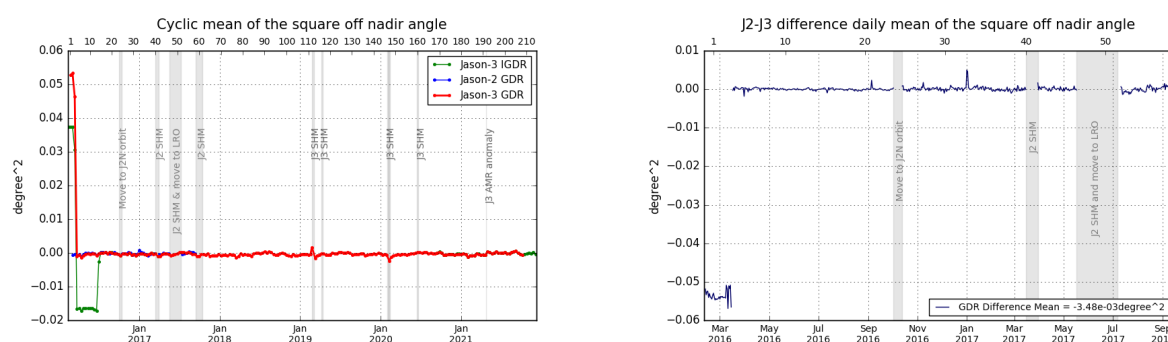


Figure 25 – **Left:** Cyclic monitoring of the square off-nadir angle for Jason-2 and Jason-3 for GDRs (blue and red curves) and Jason-3 IGDRs (product IGDR for cycles 1 to 41, and IGDR L2P from cycle 25 to 132 in green). **Right:** Jason-2 - Jason-3 difference daily monitoring of the square off-nadir angle (Note that the figure on right panel was computed using GDR-D data for both Jason-3 and Jason-2.).

Except round SHM in 2019 and 2020, no mispointing event occurred on Jason-3 over the considered period. The map figure 26 is generally slightly negative, except for regions around Indonesia, and close to coasts.

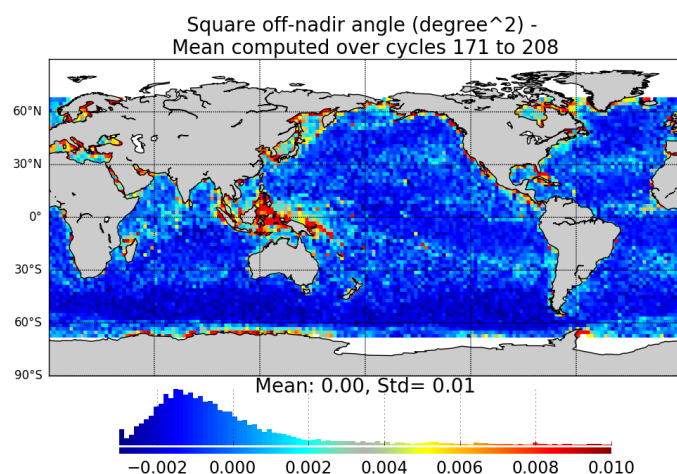


Figure 26 – Map of the square off-nadir angle for Jason-3 averaged over cycles 171 to 208.

Without taking into account the first three cycles, square off-nadir angle is monitored year by year on the left part of figure 27, highlighting a small annual signal (global mean is higher during summer). Also, a small higher value of square off-nadir angle is visible before SHM at cycle 112 and just after SHM at cycle 147. Square off-nadir angle slightly depends on significant wave height as shown on right part of figure 27: considering this monitoring for swh between 2m and 6m, slope is $-0.0004 \text{ deg}^2/\text{m}$.

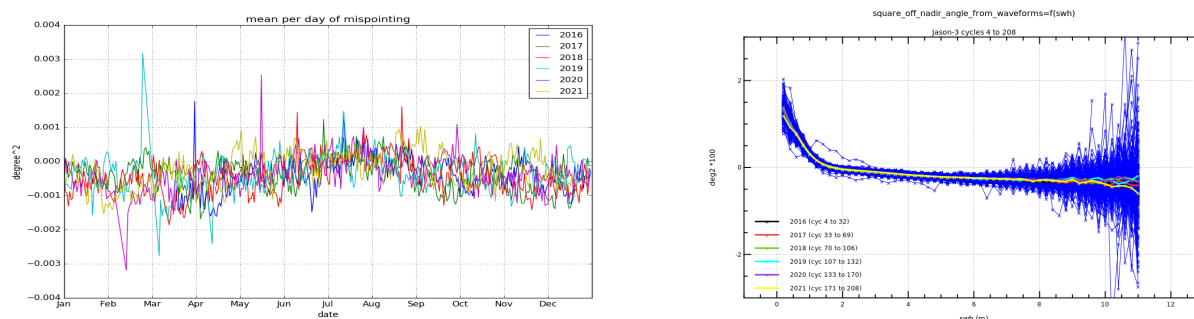


Figure 27 – **Left:** Mean per day of mispointing for Jason-3 from cycle 4. **Right:** Square off nadir angle against swh.

4.4. Backscatter coefficient

The Jason-3 Ku-band and C-band backscatter coefficients show good agreement with Jason-2 as visible on cyclic monitoring (figure 29). Jason-3 backscatter coefficient is about 13.70 dB for Ku-band (15.50 dB for C-band) while for Jason-2 it is about 13.51 dB (15.40 dB). The difference between the two missions is about -0.25 dB (-0.11 dB) and presents a good stability. However, this was different from cycle 0 to cycle 4, where slight mispointing on Jason-3 caused a higher difference of sigma0 between missions.

During the tandem flight, Jason-3 sigma0 was modified with a new altimeter characterization file, an update of the Look Up Tables (LUT, Patch 6) and a new CAL2 filter (cycle 14, June 26th, 2016). All of them were applied on all GDR cycles. As a consequence, there is a bias between backscatter coefficient in GDR and IGDR products until cycle 14. In addition, a new AMR calibration file is applied for IGDR cycle 17 (see part 4.7.), so that IGDR and GDR sigma0 are slightly different until cycle 17 due to atmospheric attenuation applied to sigma0 (as the atmospheric attenuation is derived from radiometer parameters).

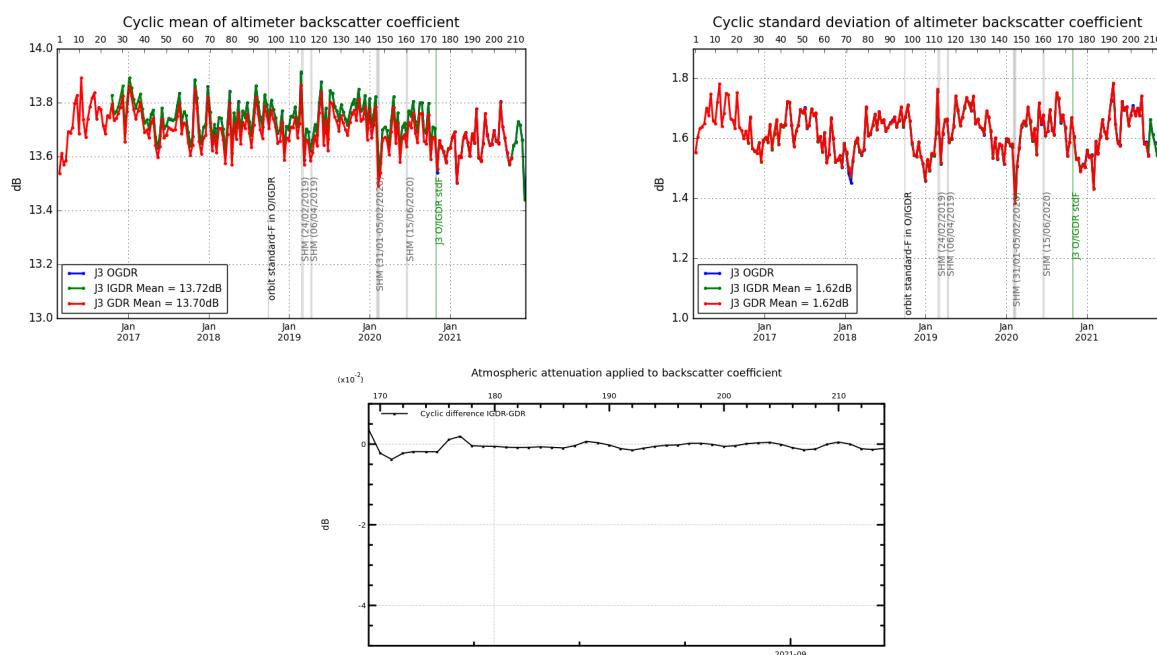


Figure 28 – **Top:** Cyclic monitoring of backscatter coefficient for Jason-3 (Ku-band) OGDR/IGDR/GDR. **Bottom:** difference of atmospheric attenuation applied to sigma0 between IGDR and GDR products.

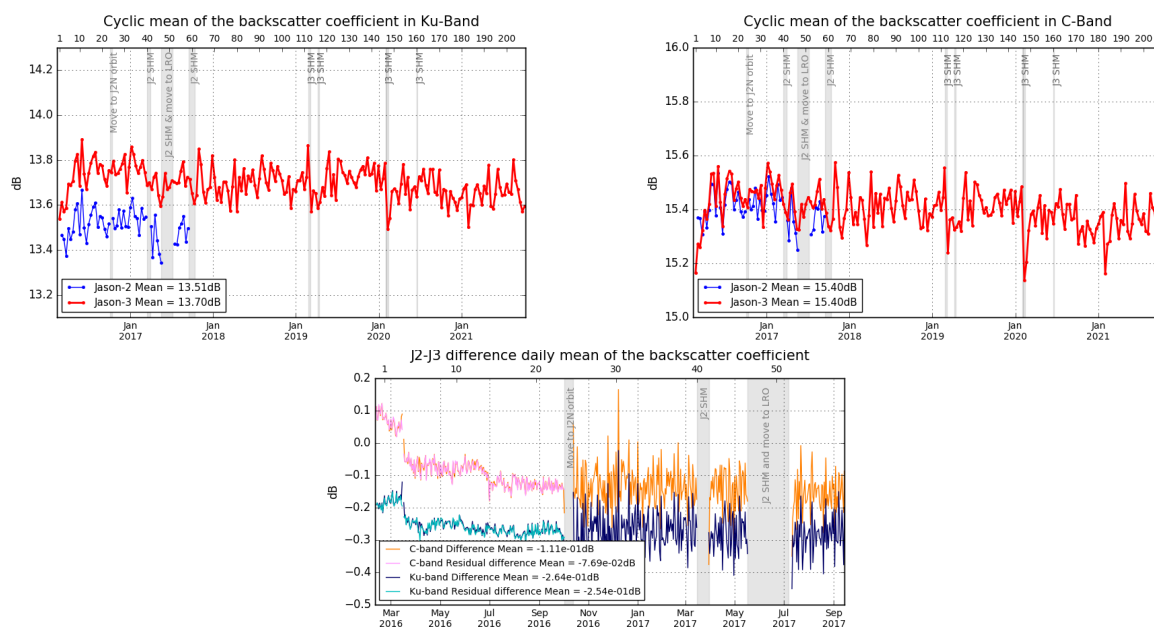


Figure 29 – **Top:** Cyclic monitoring of backscatter coefficient for Jason-2 and Jason-3 for Ku-band (left) C-band (right). **Bottom:** daily monitoring of Jason-2 - Jason-3 GDR difference of the backscatter coefficient. Note that the bottom figure was computed using GDR-D data for both Jason-3 and Jason-2.

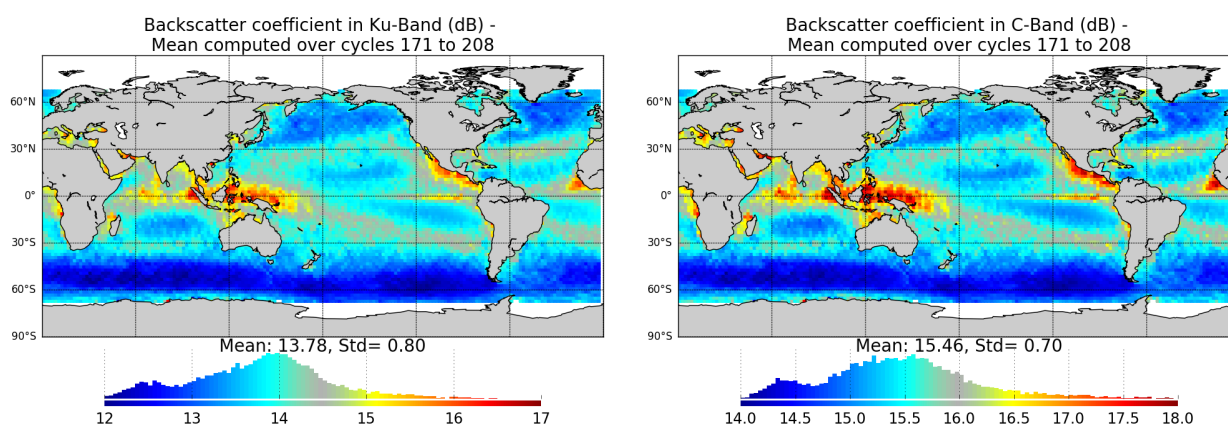


Figure 30 – Map of backscatter coefficient for Jason-3 averaged over cycles 171 to 208, in Ku-band (left) and in C-band (right).

4.5. Significant wave height

As for sigma0 parameter, a very good consistency between both Jason-2 and Jason-3 significant wave height is shown (see figure 32). In addition, until Jason-3 cycle 23 (tandem phase, observing the same ocean with only 1'20" apart), Jason-2 and Jason-3 measurements are identical. After Jason-2 move to interleaved orbit, the two missions are not as close as during tandem phase and measured swh are slightly different, but there is still no bias between Jason-2 and Jason-3 measured wave height in average (see bottom of figure 32).

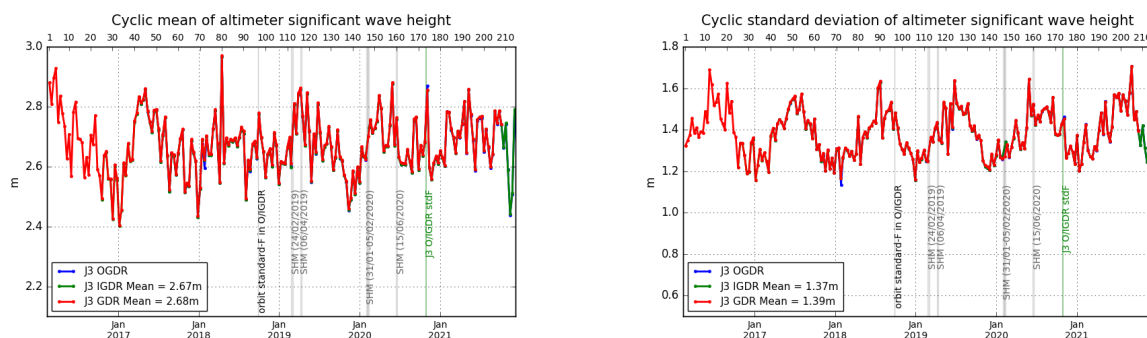


Figure 31 – Cyclic monitoring of significant wave height for Jason-3 (Ku-band) *OGDR/IGDR/GDR*.

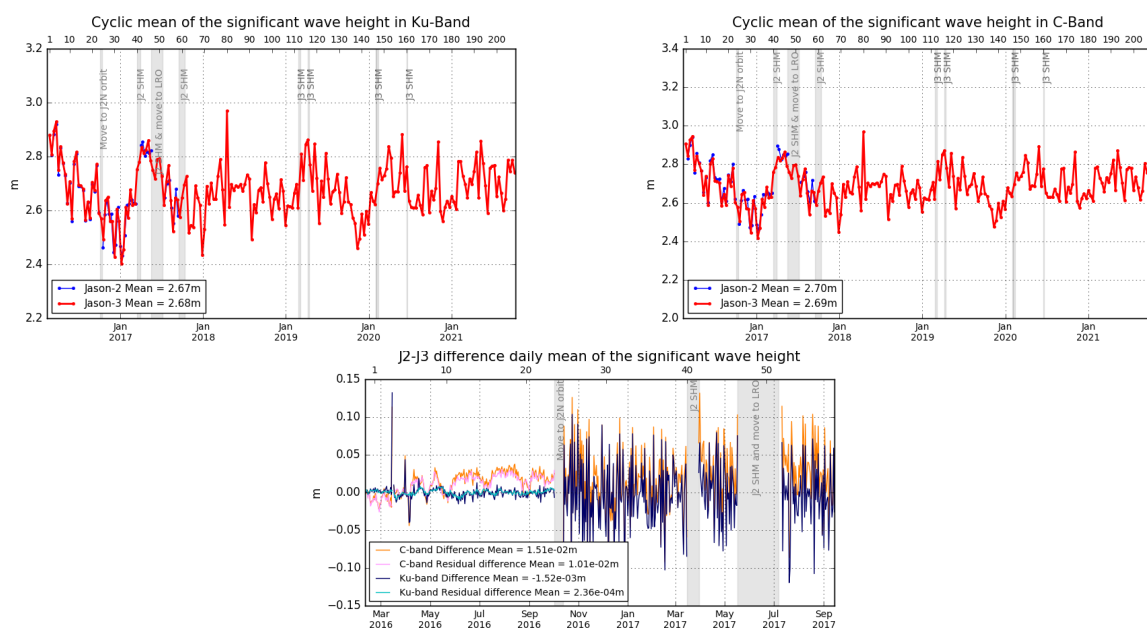


Figure 32 – Cyclic monitoring of significant wave height for Jason-2 and Jason-3 for Ku-band (left) and for C-band (right). Jason-2 - Jason-3 difference daily monitoring of significant wave height (bottom). Note that the bottom figure was computed using GDR-D data for both Jason-3 and Jason-2.

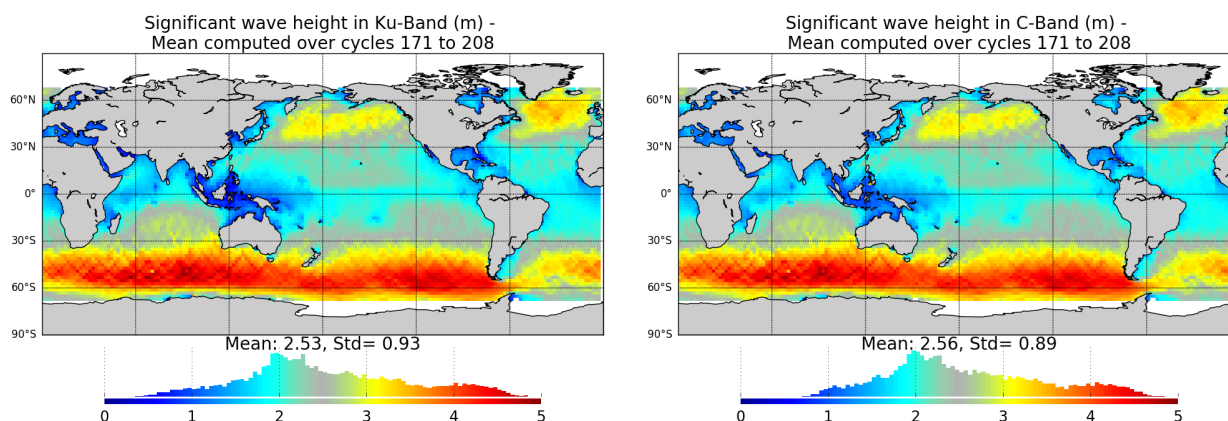


Figure 33 – Map of significant wave height for Jason-3 averaged over cycles 171 to 208, in Ku-band (left) and in C-band (right).

4.6. Dual-frequency ionosphere correction

The dual frequency ionosphere corrections derived from the Jason-3 and Jason-2 altimeters show a mean difference of about 0.87 cm (figure 34), with cycle to cycle variations lower than 1 mm.

Until the LUT changes that occurred during cycle 14 (for O/IGDRs), the mean bias between the two missions was 1 cm (for O/IGDRs). It turns then to 0.55 cm following “jumps” of Ku range (5 mm), C Range (1.5 cm) and sea state bias (0.1 mm). This event has an impact on Sea Level Anomalies retrieved from OGDRs and IGDRs products. For GDR products, the same LUT was used for the whole mission period, hence the absence of jump (see bottom and right of figure 34).

Note that as IGDR are produced following standard F, a filtered solution of altimeter ionospheric correction has been available in the products from IGDR cycle 174 onwards (see [11]). The maps were produced with the bifrequency ionospheric correction and not the filtered one.

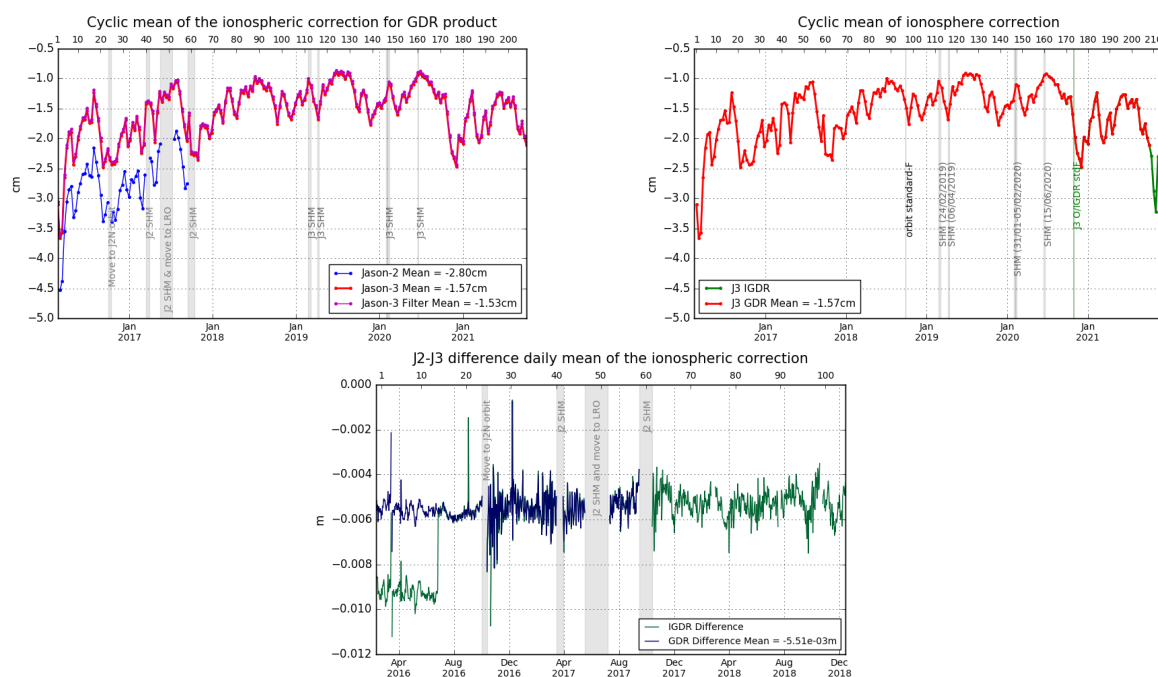


Figure 34 – Cyclic monitoring of ionospheric correction for Jason-2 and Jason-3. **(left)**. Cyclic monitoring of Jason-3 ionospheric correction for IGDR and GDR data **(right)**. Jason-2 - Jason-3 difference daily monitoring of ionospheric correction **(bottom)**. Note that the bottom figure was computed using GDR-D data for both Jason-3 and Jason-2.

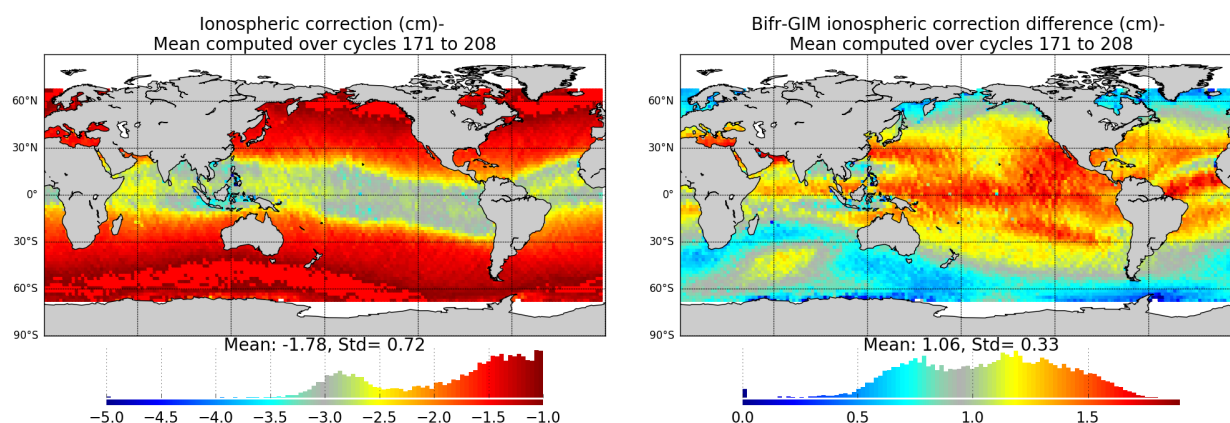


Figure 35 – **Left**: Map of ionospheric correction for Jason-3 averaged over cycles 171 to 208. **Right**: Map of dual-frequency minus GIM ionospheric correction solutions.

When comparing altimeter ionosphere correction to GIM correction (figure 36), mean as well as standard deviation of this difference present same variation for both missions.

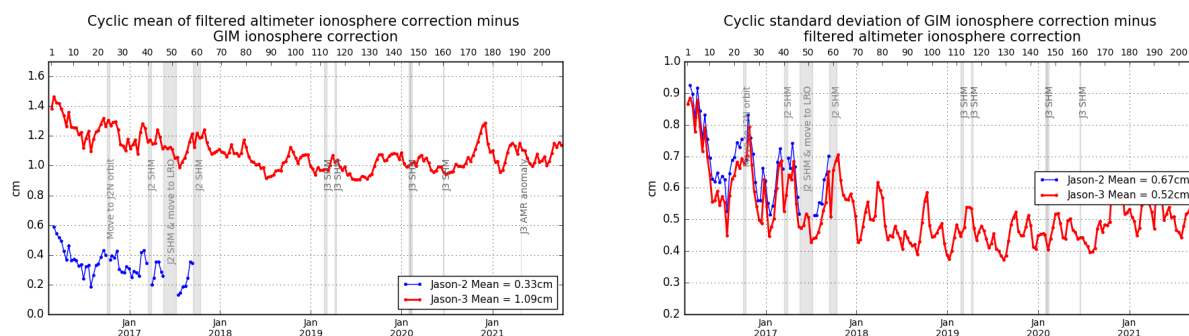


Figure 36 – Cyclic monitoring of GIM ionosphere correction minus filtered altimeter ionosphere correction for Jason-2 and Jason-3. Left: mean, right: standard deviation.

Several ionospheric correction solutions are available in Jason-3 GDR-F:

- `model : iono_cor_gim`
- `dual-frequencies:`
 - `iono_cor_alt,`
 - `iono_cor_alt_mle3,`
 - and `iono_cor_alt_adaptive`
- `filtered from dual-frequencies:`
 - `iono_cor_alt_filtered,`
 - `iono_cor_alt_filtered_mle3,`
 - and `iono_cor_alt_filtered_adaptive`

Filtering process of dual-frequencies ionospheric correction is described in [11].

As already shown in Jason-3 GDR-F reprocessing report [5], the system performances for SLA estimations over open ocean is significantly improved thanks to filtering of the dual-frequencies ionospheric correction. Nevertheless, the filtering process tends to set the correction to default value near coast and ice frontiers, and as a consequence a loss of SLA valid points over these areas.

We propose here to evaluate a composite solution, taking advantage of the filtering method over open ocean, avoiding the loss of points when filtering is not possible (ionospheric correction = filtered, but raw values are used if filtered solution is set to default value).

Figure 37 shows the difference in number of SLA valid points (i.e. same process as described in dedicated part, but using a different ionospheric correction solution). With MLE4 retracking, the use of the filtered solution allows to retrieve 367 points over open ocean in average, but the global loss of points is near 538 points due to the 905 points over coastal and near ice default values. The loss of valid points is mainly located near coasts and can reach 4000 points (more than 5000 points in case of adaptive retracking) per cycle for coastal distances round 5km to 10km (Figure 38).

The analysis of the number of valid points with regard to distance to coast from both mle4 or adaptive retracking outputs (Figure 38) clearly highlights it is significantly lower using filtered solution instead of raw data (red/orange curves), but using a composite solution allows to improve the ionospheric correction availability for distance to coast below 10km (green curves). This is visible both considering sea ice areas (continuous lines) or not (dotted lines, selection on $|latitude| < 50$).

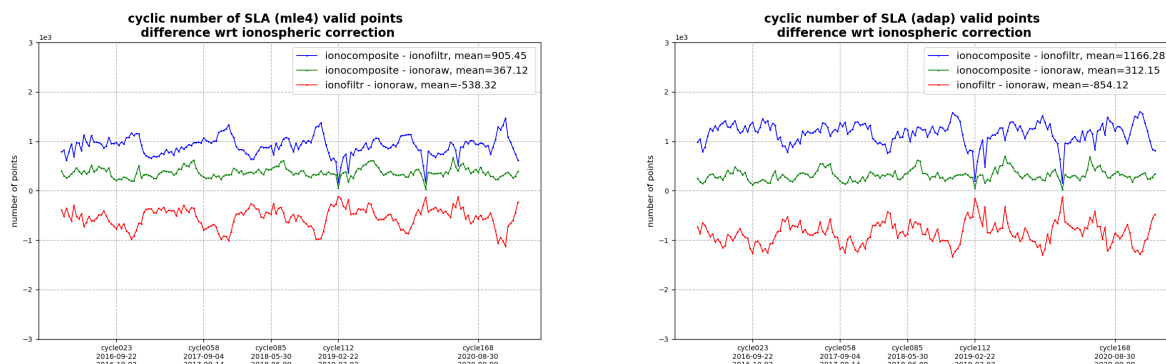


Figure 37 – Global difference in number of valid points (i.e. within thresholds) between ionospheric correction solutions. MLE4 retracking (left) or adaptive retracking (right). Statistics are computed over cycles 001 (17/02/2016) to 184 (14/02/2021)

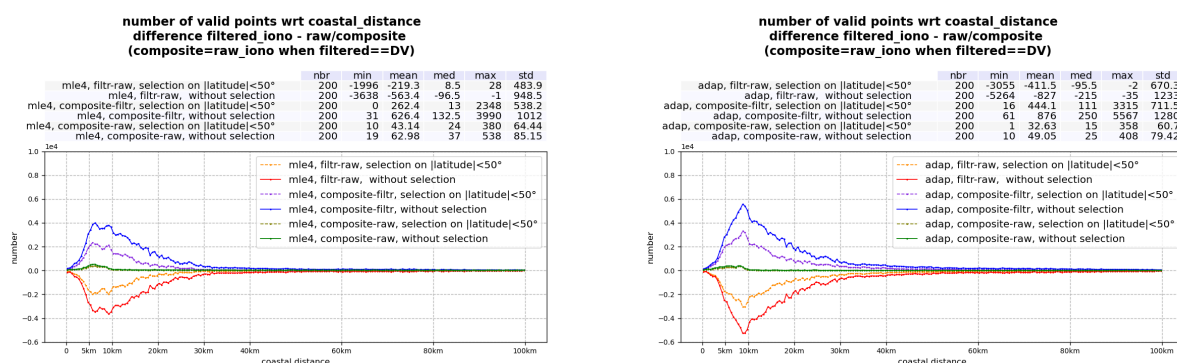


Figure 38 – Difference in number of valid points (i.e. within thresholds) between ionospheric correction solutions wrt distance to coast. MLE4 retracking (left) or adaptive retracking (right). Statistics are computed over cycles 001 (17/02/2016) to 184 (14/02/2021)

The use of the filtered solution instead of raw dual-frequencies ionospheric correction allows a reduction of 0.17cm on along-track SLA standard deviation with MLE4 retracking (from 10.83cm to 10.66cm on Figure 39), which represents a significant reduction of 3.67cm² on global SLA variance (Figure 40). The impact on adaptive SLA performances is slightly lower with -0.13cm on along-track standard deviation (-2.82cm² on variance).

The along-track SLA performances using the composite (filtered/raw) solution analysis show a global improvement slightly lower than with the filtered solution, but significant with regard to the non filtered one (-2.99cm² for MLE4 and -1.73cm² for adaptive using composite solution wrt raw dual-frequencies ionospheric correction).

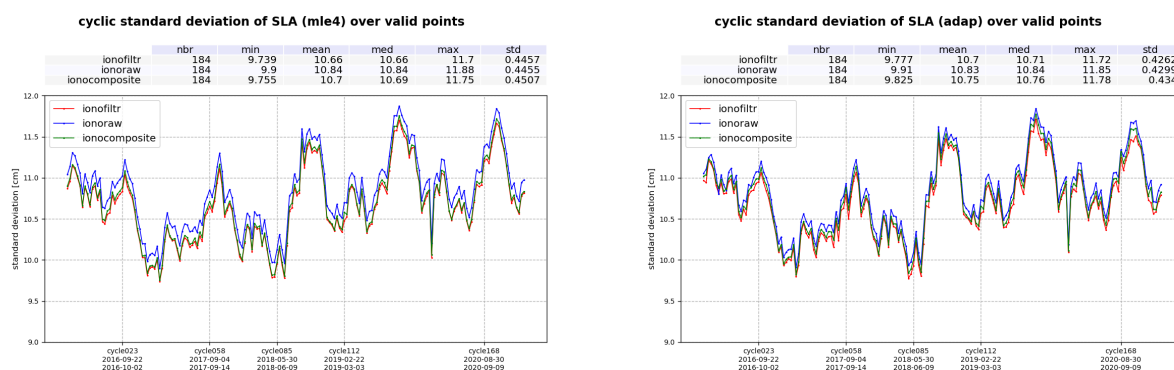


Figure 39 – Difference in number of valid points (i.e. within thresholds) between ionospheric correction solutions. Statistics are computed over cycles 001 (17/02/2016) to 184 (14/02/2021)

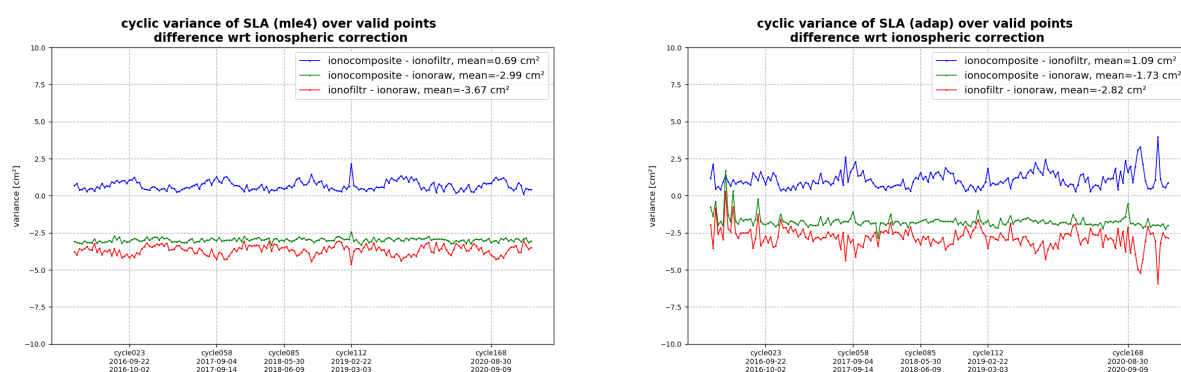


Figure 40 – Difference in number of valid points (i.e. within thresholds) between ionospheric correction solutions. Statistics are computed over cycles 001 (17/02/2016) to 184 (14/02/2021)

In conclusions, the use of a composite solution from filtered/non filtered ionospheric corrections both available in GDR-F L2 products allows to significantly improve the global system performance on along-track SLA estimations with regard to the use of non filtered solution only, avoiding the loss of valid points for distance to coast lower than 10km and near ice areas when using the filtered solution only.

4.7. AMR Wet Troposphere Correction

4.7.1. Overview

In order to evaluate radiometer wet troposphere correction, liquid water content, water vapor content and atmospheric attenuation, Jason-3 uses a three-frequency AMR radiometer (18.7, 23.8 and 34.0 GHz), similar to the one used on Jason-2.

Note that the 23.8 GHz channel is the primary water vapor sensing channel, meaning a higher water vapor concentration leads to larger 23.8 GHz brightness temperature values. As a consequence, top right and bottom right parts of figure 41 are correlated. Moreover, the 34 GHz channel and the 18.7 GHz channel, which have less sensitivity to water vapor, facilitate the removal of the contributions from cloud liquid water and excess surface emissivity of the ocean surface due to wind, which also act to increase the 23.8 GHz brightness temperature.

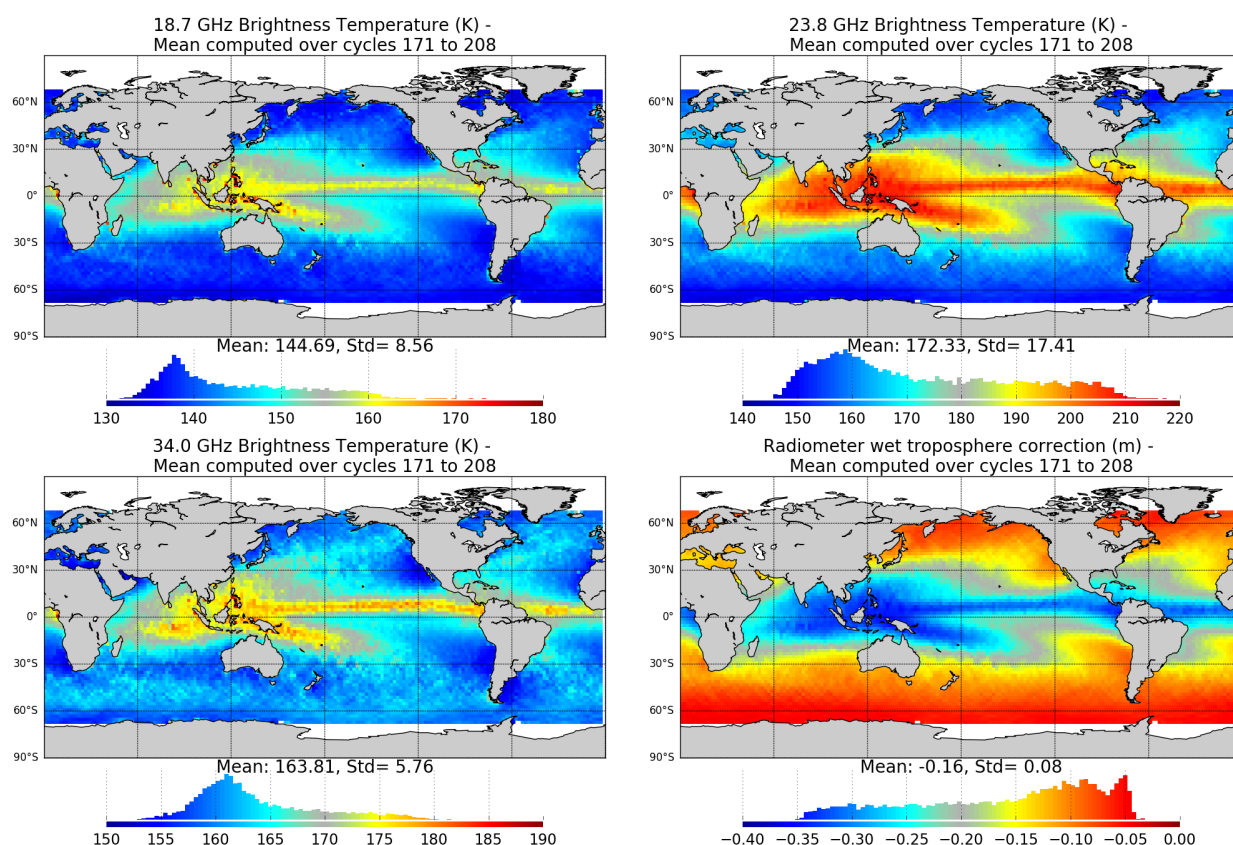


Figure 41 – Map of Jason-3 brightness temperatures averaged over cycles 171 to 208: 18.7 GHz channel (top left), 23.8 GHz channel (top right) and 34.0 GHz channel (bottom left). Map of AMR wet troposphere correction for Jason-3 averaged over cycles 171 to 208 (bottom right)

4.7.2. Comparison with the ECMWF model

The wet troposphere correction computed from ECMWF model data has been used to check the Jason-2 and Jason-3 radiometer corrections. The cross-comparison between all radiometers and models available is necessary to analyze the stability of each wet troposphere correction. An overview of the wet troposphere correction importance for mean sea level is given in Obligis et al. [15]. The difference between AMR and model data is computed on a daily basis and is plotted on figure 43 for Jason-3 IGDR and GDR, and Jason-2 GDR for comparisons. As observed, Jason-3 AMR correction has a drift of more than half a millimetre per cycle for IGDRs (and OGDRs, not shown). Such behaviour is routinely monitored by JPL instrument expert team. Impact of drift is corrected through ground calibration (ARCS, Autonomous Radiometer Calibration System), also accounting for cold sky calibrations. The first ARCS calibration occurred at the end of cycle 17 and is visible on IGDR monitoring. As regards GDR data, AMR radiometer correction is calibrated at each cycle and the calibration coefficients are modified if necessary. It allows to correct the drift for GDR data (red curve on figure 43), nevertheless small drifts and jumps persist of up to 2 mm amplitude.

Due to an ECMWF model change of version on June 6th 2019, a jump is visible in the monitoring of radiometer minus model wet troposphere correction mid-2019.

Due to an ECMWF model change of version on September 2021, a jump is visible in the monitoring of radiometer minus model wet troposphere correction in October 2021.

Due to the change of version for O/IGDR products for standard “F” on 29th October 2020, an expected jump of about -6.4mm is visible on IGDR data. Note that the jump between 24/11/2020 and 30/11/2020 on IGDR data (seen on figure 42) is due to the use of a wrong AMR calibration file for the product generation.

In GDR, Jason-3 AMR-ECMWF model daily difference is about 0.2 mm and about 5.3 mm for Jason-2. Though Jason-3 radiometer wet troposphere correction is more stable for GDRs, Jason-3 and Jason-2 do not have exactly the same behaviour, with an inflexion point around cycle 13 and another one after Jason-2 moved to its new interleaved groundtrack on October 2016. With 2017 Safe Hold Modes, Jason-2 shows some jumps that are known to occur after restart. The jump visible on January 2020 on Jason-3 is due to the SHM that occurs over cycle 143.

Standard deviation of radiometer minus model wet troposphere correction is equivalent around 1.2 cm for Jason-2 and around 1,1 cm for Jason-3 (right of figure 43).

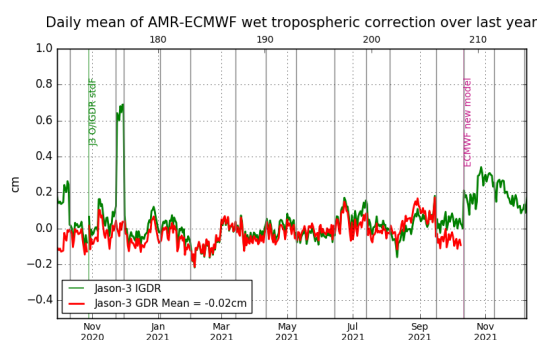


Figure 42 – Daily monitoring of AMR minus ECMWF model wet tropospheric correction over one year.

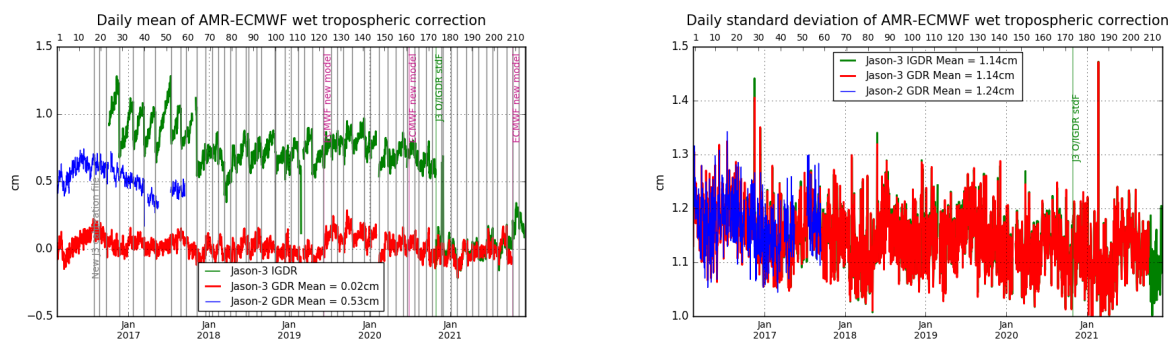


Figure 43 – Daily monitoring of AMR minus ECMWF model wet tropospheric correction. mean (left) and standard deviation (right)

4.7.3. Wet Tropospheric Correction model comparison

Since the reprocessing of all Jason-3 GDR data into standard “F”, two wet tropospheric correction models can be used :

- WTC_{MODEL} which is the correction currently used
- $WTC_{MODEL.3D}$ which is a reanalysis from ECMWF of the WTC model allowing for a complete continuity in the correction.

The first thing to highlight is the closeness of both solutions in terms of long-term stability, as seen in figure 44. The difference is minor, about $\sim 0.1mm$, in average. The daily monitoring of the difference shows a sub-millimetric 59 days signal (right of figure 44), that might be correlated to an anomaly in S1S2 waves correction for $WTC_{MODEL.3D}$ solution (as seen for model dry tropospheric correction in 8.5.), to be confirmed.

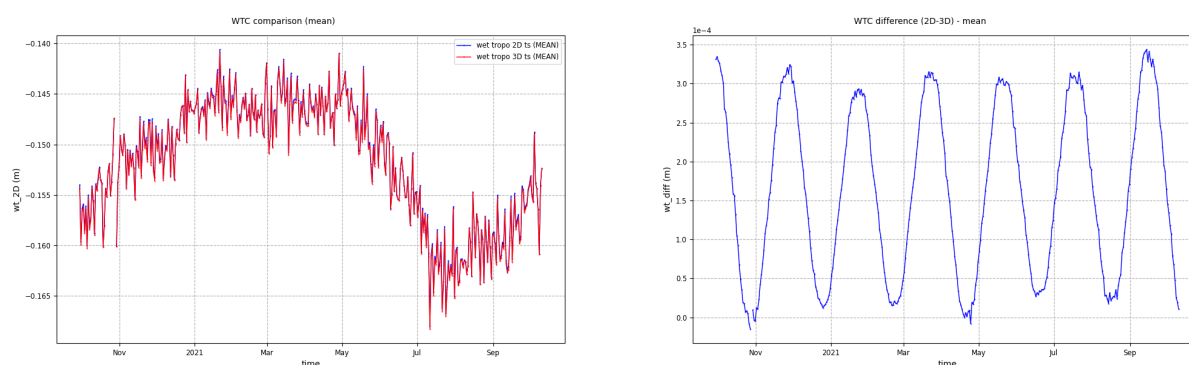


Figure 44 – Jason-3 evolution of both WTC models over 2021. Left: mean per day. Right: mean per day of difference.

Since these models are used to monitor the wet tropospheric correction deduced from the radiometer, figure 45 shows the comparison of the difference (model - rad) using both models. The difference is once again sub-millimetric, with a slight exceed for the (model3D - rad). Both models benefit from the same updates and show thus the same evolutions (e.g. Change in the ECMWF radiometer model during october 2021).

This investigation confirmed the high level of similarity between both models. One specificity highlighted is the cyclic difference between both models with a 59 days frequency.

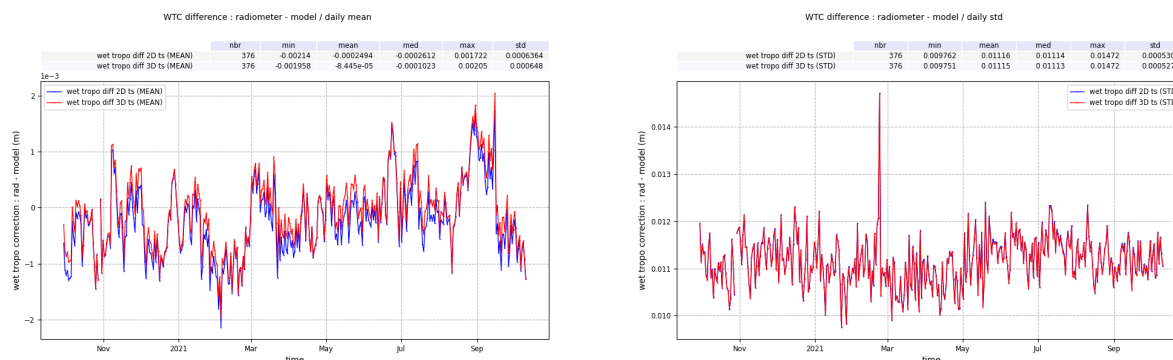


Figure 45 – Jason-3 difference WTC model - rad over 2021. **Left:** mean per day. **Right:** std per day.

4.7.4. Drift of the Jason-3 Radiometer

An investigation performed in the scope of the MSL activities (see [19]) rises the question of a potential drift trend over Jason-3 radiometer instrument. This was deduced from comparing the Wet Tropospheric Correction difference (radiometer - model) for Jason-3, SARAL-Altika and Sentinel-3A.

Figure 46 shows the evolution of the radiometer minus model wet tropospheric correction since the beginning of the Jason-3 mission. In this figure (especially the right one), we can clearly observe a drift in the difference $WTC_{othermission} - WTC_{J3}$. Since it is observed with two distinct satellites (and also with a WTC computed from a water vapour Climate Data Record (CDR) based on the SSMIs radiometer data), the drift is attributed to Jason-3.

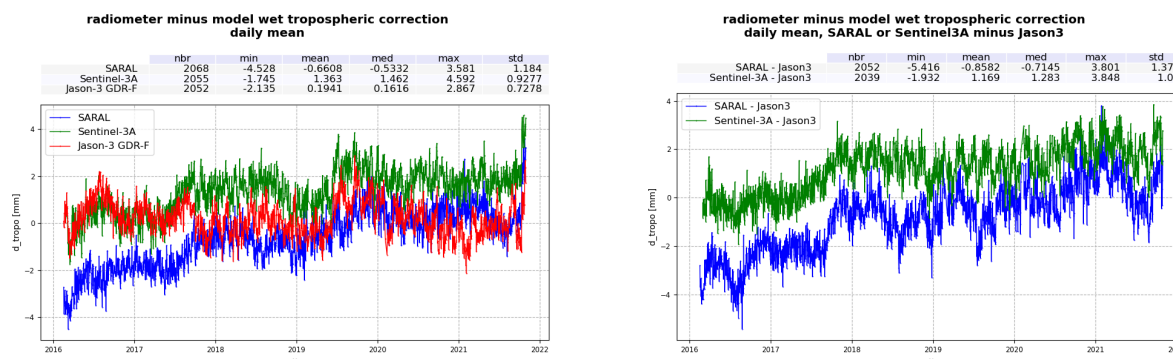


Figure 46 – Wet tropospheric correction : **left** compared to other missions and **right** using the two available correction models.

This investigation quantified the drift to $\sim 0.6 \pm 0.3 \text{ mm.yr}^{-1}$ over the period 2016-2021.

4.8. Altimeter wind speed

Jason-3 and Jason-2 present very close results in terms of wind speed. Jason-2 provides lower wind values than Jason-3 (7.80 vs 7.98 m.s⁻¹, figure 47). The evolution from GDR-D to GDR-F wind speed computation is detailed in [5] part 5.4.4. The difference between the two missions is 0.23 m.s⁻¹ and can be separated in two phases: before and after 16-03-2016. The uploading of updated parameters for STR1 and gyros to correct misalignments occurred on March, 16th 2016 (Cycle 3) and corrected the square off nadir angle, i.e. the mispointing of the platform. Then from the restart of data production (March 18th) mispointing was set to value close to zero, which increases the sigma0 and decreases the wind speed.

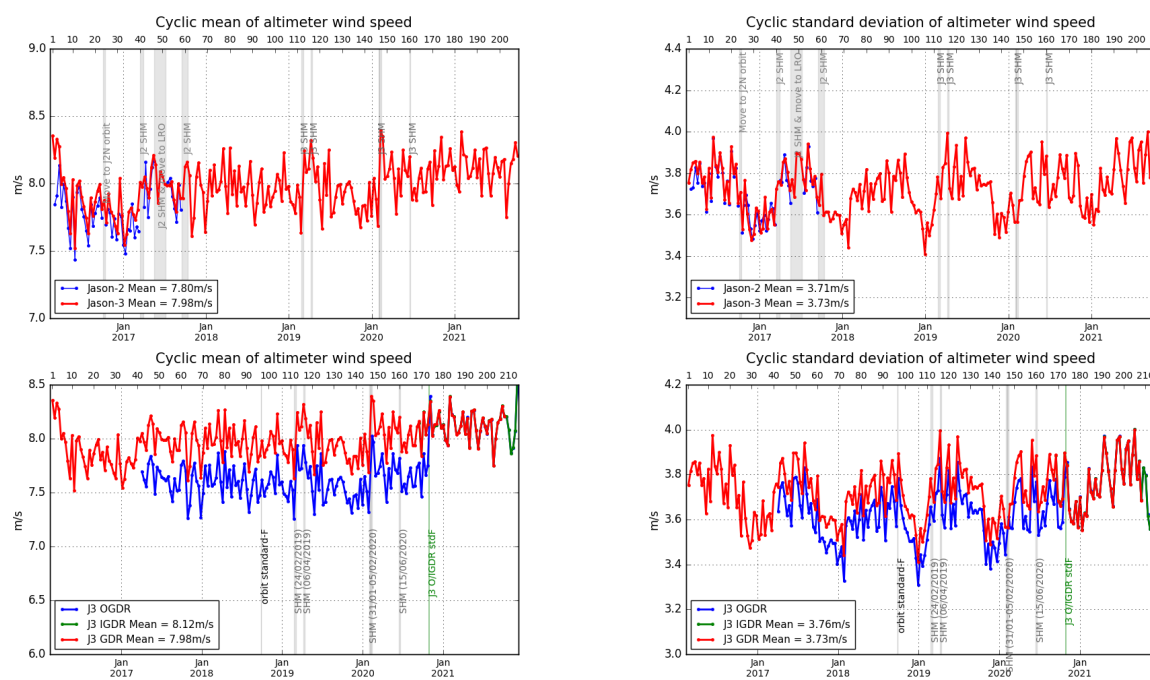


Figure 47 – Cyclic monitoring of altimeter wind speed mean (left) and standard deviation (right). **Top:** for Jason-2 and Jason-3. **Bottom:** for Jason-3 GDR, IGDR and OGDR data.

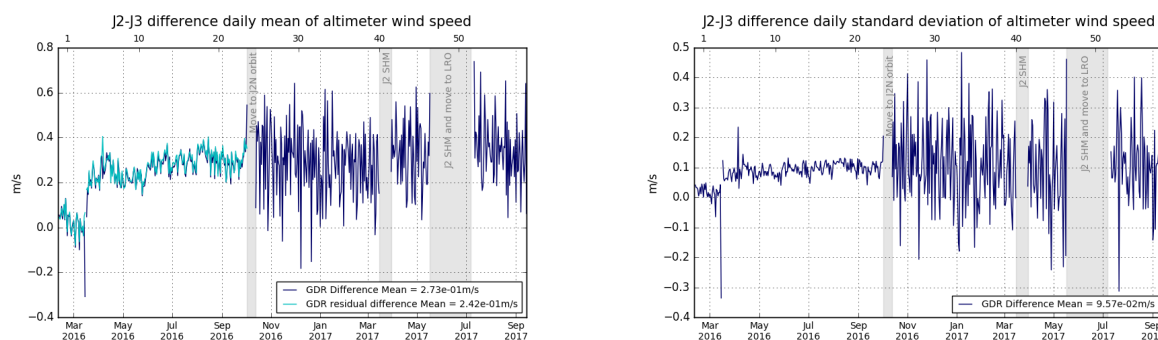


Figure 48 – Jason-2 - Jason-3 difference daily monitoring of altimeter wind speed mean (left) and standard deviation (right). Both were computed using GDRD data. Note that the bottom figure was computed using GDR-D data for both Jason-3 and Jason-2.

Due to the change of version for IGDR products for standard “F” on 29th October 2020, an expected jump is visible on IGDR data (bottom left of figure 47). An adjustment is done before computing wind speed values (bias on sigma0) so that wind speed values in standard “F” are more coherent with ERA5 model distribution as seen on figure 49 and detailed in [5].

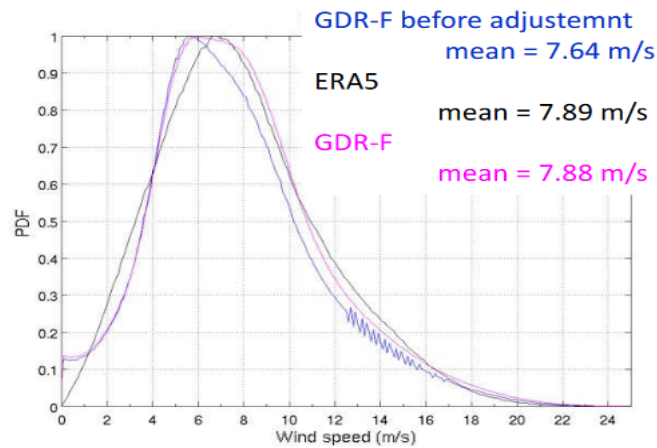


Figure 49 – Wind speed comparison product and ERA5 model

4.9. Sea state bias

GDR Sea state bias (SSB) in Ku band from Jason-3 (-8.40 cm) and Jason-2 (-8.44 cm) present an excellent agreement both in average and in standard deviation (4.61 cm for both missions).

Due to the change of version for IGDR products for standard “F” on 29th October 2020, an expected jump of about -1.9cm is visible on IGDR data (figure 50).

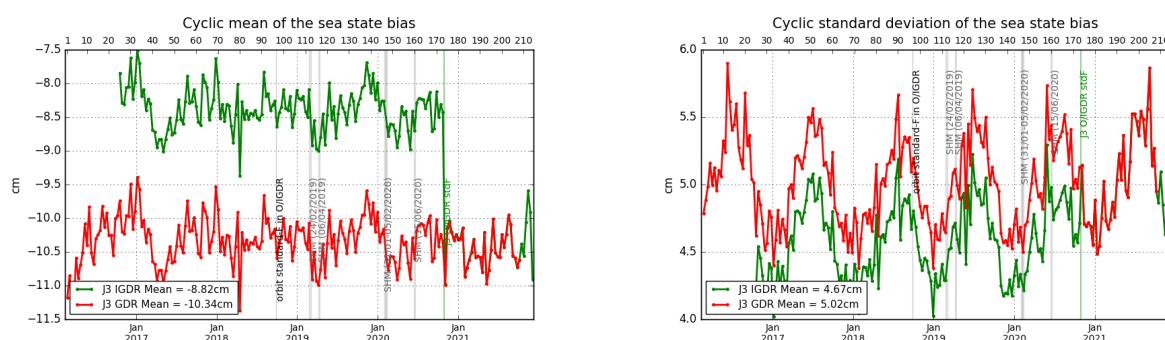


Figure 50 – Cyclic monitoring of the sea state bias mean and standard deviation for Jason-3 IGDR/GDR.

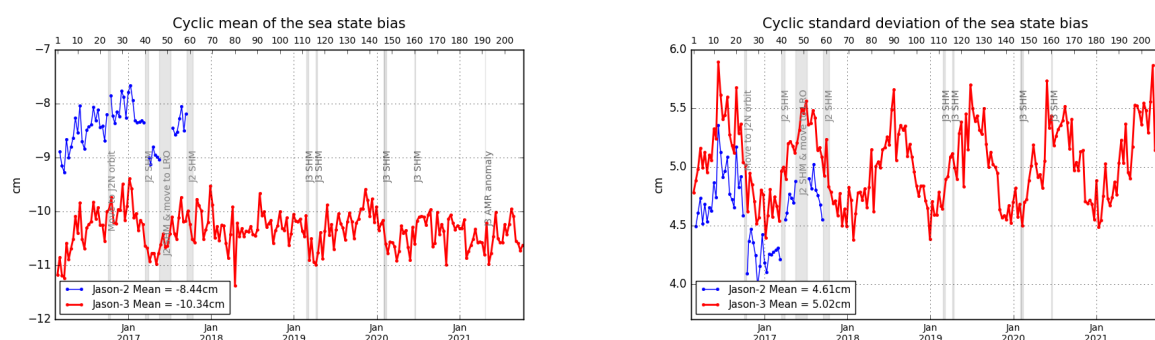


Figure 51 – Cyclic monitoring of the sea state bias mean and standard deviation for Jason-2 and Jason-3

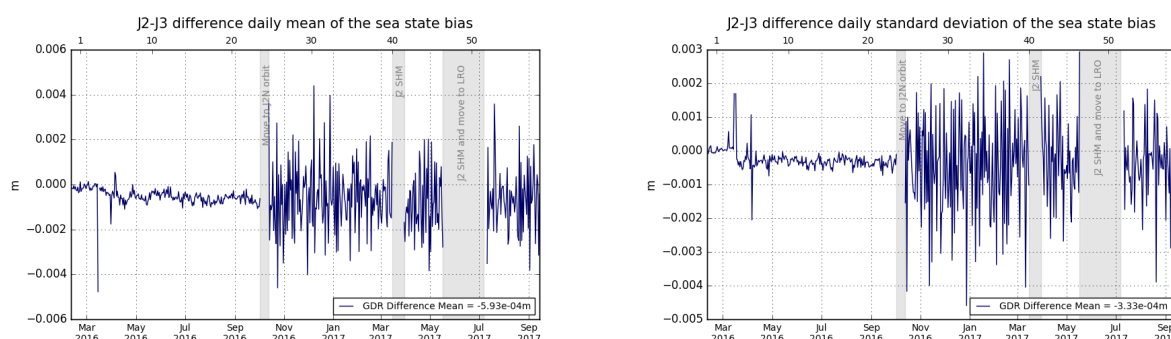


Figure 52 – Jason-2 - Jason-3 difference daily monitoring of the sea state bias mean (left) and standard deviation (right). Note that the figures were computed using GDR-D data for both Jason-3 and Jason-2..

5. SSH crossover analysis

5.1. Overview

SSH crossover differences are the main tool to estimate the whole altimetry system performances. They allow to analyze the SSH consistency between ascending and descending passes: it should not be significantly different from zero. More importantly, special care is given to the geographical homogeneity of the mean difference at crossovers. However in order to reduce the impact of oceanic variability, we select crossovers with a maximum time lag of 10 days. Mean and standard deviation of SSH crossover differences are computed from the valid dataset to perform maps or a cycle by cycle monitoring over all the altimeter period. In order to monitor the performances over stable surfaces, additional editing is applied to remove shallow waters (bathymetry above -1000m), areas of high ocean variability (variability above 20 cm rms) and high latitudes ($> |50|deg$). SSH performances are then always estimated with equivalent conditions. The main SSH calculation for Jason-3 (and Jason-2) are defined below.

$$SSH = Orbit - Altimeter Range - \sum_{i=1}^n Correction_i$$

with $Jason - 3 Orbit = CNES orbit$ for GDR products, and

$$\begin{aligned} \sum_{i=1}^n Correction_i = & \text{Non parametric sea state bias correction} \\ & + \text{Dual frequency ionospheric correction (filtered)} \\ & + \text{Radiometer wet troposphere correction} \\ & + \text{Dry troposphere correction} \\ & + \text{Dynamical atmospheric correction} \\ & + \text{Ocean tide correction (including loading tide)} \\ & + \text{Internal tide correction} \\ & + \text{Earth tide height} \\ & + \text{Pole tide height} \end{aligned}$$

In this part, performance indicators from IGDR input products or IGDR L2P (used in DUACS system) are presented. L2P updates that are then applied (ocean tide correction, mean sea surface model, mog2d dynamical atmospheric correction) are detailed in [20]. Note that comparisons between Jason-3 and Jason-2 have been done from Jason-3 cycle 1 to 58 only (Jason-2 cycles 281 to 506).

5.2. Mean of SSH crossover differences

The cycle by cycle mean of SSH differences is plotted in figure 53 for Jason-3 for OGDRs, IGDRs and GDRs. Mean of SSH differences at crossovers for Jason-3 IGDR products has noticeable negative values in average (-0.09cm for IGDR versus -0.01cm for GDR): mainly link to negative values over IGDR in standard D period.

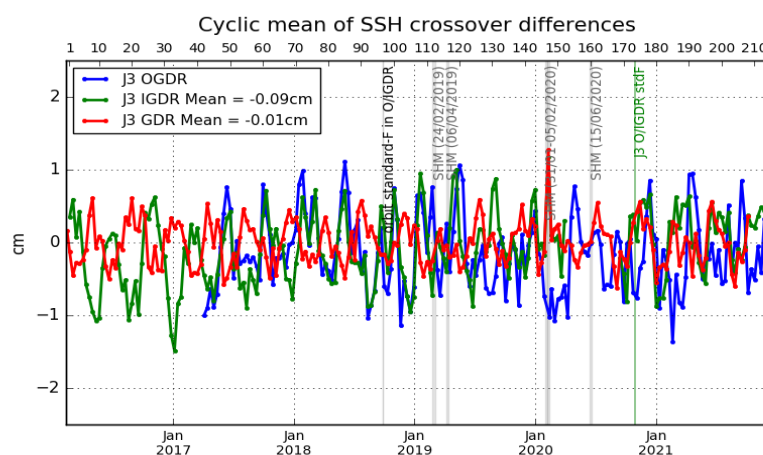


Figure 53 – Monitoring of mean of Jason-3 SSH crossover differences for OGDRs, IGDRs and GDRs. Only data with $|\text{latitude}| < 50^\circ$, bathymetry $< -1000\text{m}$ and low oceanic variability were selected. (ocean_tide_fes = FES14B is used in SSH computation)

The maps of mean SSH crossover differences on figure 54 were calculated using GDR-F products for Jason-3 (left) and Jason-2 GDR-D (right). These maps highlight reduced small geographic patterns for Jason-3 compared to Jason-2 (see [5] part 4.1).

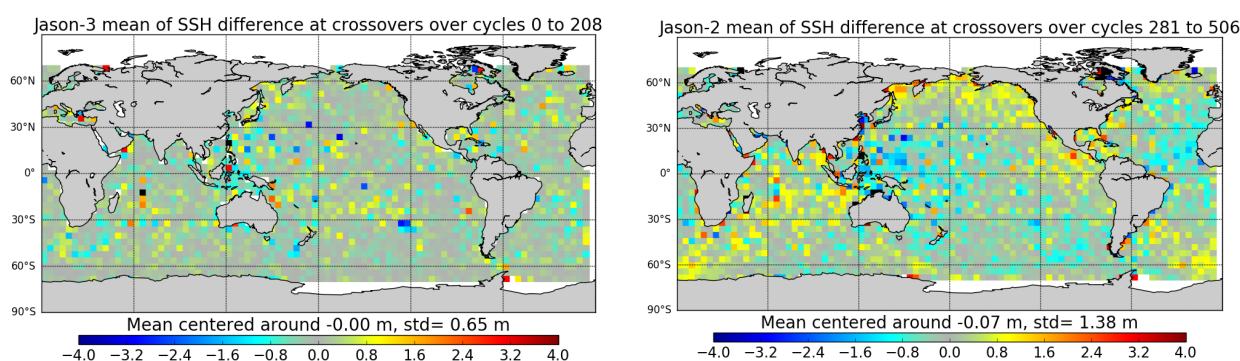


Figure 54 – Map of SSH crossovers differences mean for Jason-3 cycle 0 to 208 (left) and for Jason-2 cycle 281 to 506 (right)

Dual-mission crossover performances are computed between Jason-3 GDR-D and Jason-2 GDR-D and presented figure 55. Mean SSH differences at Jason 3/Jason 2 crossovers is quite stable and around 3 cm in average. The geographical pattern indicates some hemispheric biases, positive to the west, negative to the east. It corresponds to orbital signatures observed on sea surface height (right side of figure 55). Note that these 3 cm are due to processing differences as colocated Jason-2 minus Jason-3 non-corrected SLA (orbit - range - MSS) differences averaged over the period of tandem phase (cycle 001 to 023) shows an equivalent

bias (left side of figure 59).

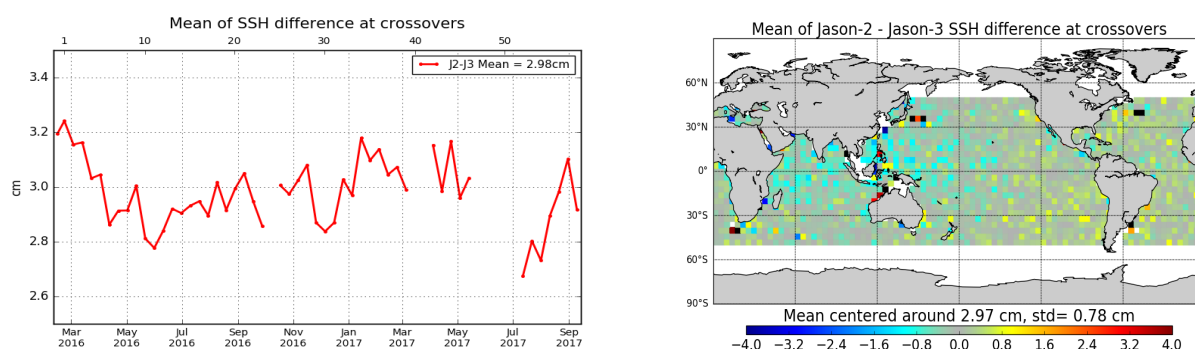


Figure 55 – Cyclic monitoring of Jason-2 - Jason-3 SSH crossover differences mean (left) and map over cycle 1 to 58 (right). Only data with $|\text{latitude}| < 50^\circ$, bathymetry $< -1000\text{m}$ and low oceanic variability were selected (for both missions, GDR-D data are used for these figures).

5.3. Standard deviation of SSH crossover differences

The cycle by cycle standard deviation of SSH crossovers differences are plotted for Jason-3 and Jason-2 in figure 56 after applying geographical criteria (bathymetry, latitude, oceanic variability). This metric allows to estimate the system noise by dividing by $\sqrt{2}$ (which leads to 3.48 cm for Jason-2 GDR-D and 3.39 cm for Jason-3 GDR-F). Both missions show very good performances, very similar and stable in time. No anomaly is detected. Thanks to GDR-F reprocessing, this indicator is significantly reduced for Jason-3 with regards to Jason-2 (and particularly the use of the filtered ionospheric correction, see part 4.1.1 of [5]).

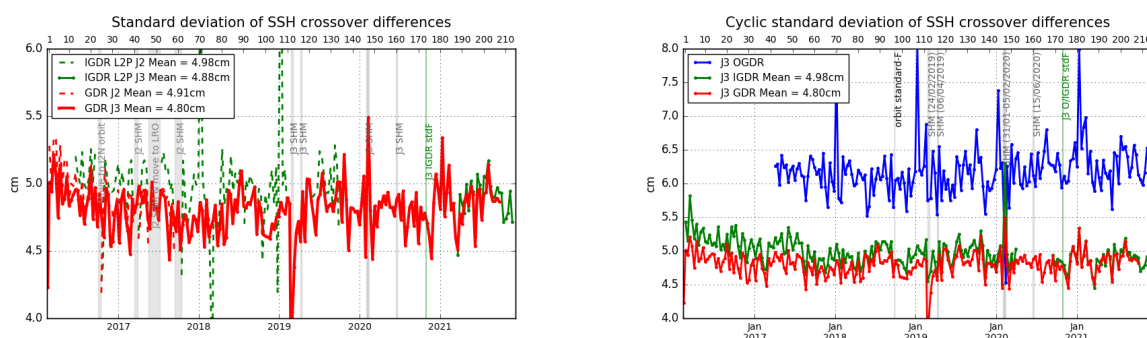


Figure 56 – Cycle by cycle standard deviation of SSH crossover differences for Jason-2 and Jason-3 (left), and for Jason-3 using OGDRs, IGDRs and GDRs (right). Only data with $|\text{latitude}| < 50^\circ$, bathymetry $< -1000\text{m}$ and low oceanic variability were selected.

5.4. Estimation of pseudo time-tag bias

The pseudo time tag bias (α) is found by computing at SSH crossovers a regression between SSH and orbital altitude rate (\dot{H}), also called satellite radial speed: $SSH = \alpha \dot{H}$.

This empirical method allows us to estimate the potential real time tag bias but it can also absorb other errors correlated with \dot{H} . Therefore it is called “pseudo” time tag bias. The monitoring of this coefficient estimated at each cycle is performed for Jason-2 and Jason-3 in figure 57. Both curves are very similar highlighting an almost 59-day signal with almost no bias (close to -0.01 ms for Jason-3). Both missions present 59 and 117 day signals. Thanks to POE-F and FES14B ocean tide, there is a significant reduction of the 59-days signal and a small reduction of the 117 days signal (compared to previous version GDRD). The 90-days signal is slightly observed with GOT ocean tide but not with FES.

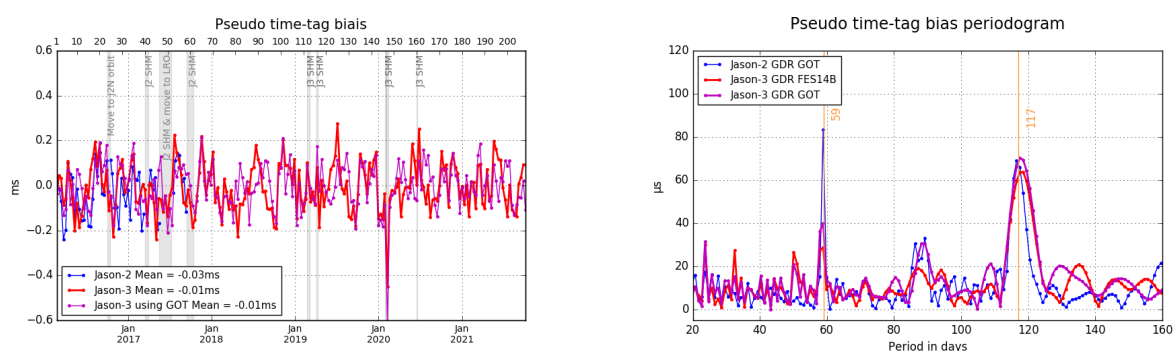


Figure 57 – Monitoring (left) and periodogram (right) of pseudo time-tag bias estimated cycle by cycle from GDR products for Jason-2 and Jason-3

6. Sea Level Anomalies (SLA) Along-track analysis

6.1. Overview

The Sea Level Anomalies (SLA) are computed along track from the subtraction of the mean sea surface to the SSH, with the SSH calculated as defined in previous section 5.1. : $SLA = SSH - MSS$. SLA analysis is a complementary indicator to estimate the altimetry system performances. It allows to study the evolution of SLA mean (detection of jump, abnormal trend or geographical correlated biases), and also the evolution of the SLA variance highlighting the long-term stability of the altimetry system performances. In order to take advantage of the Jason-3/Jason-2 tandem flight (cycles 1 to 23), we performed direct SLA comparisons between both missions during this period.

6.2. Mean of SLA differences between Jason-3 and Jason-2

The daily monitoring of mean SLA differences between Jason-2 and Jason-3 data over the tandem phase is plotted on figure 58, where this SSH bias is computed with and without the SSH corrections. During this period, both types of curves are very similar and stable in time with variations close to 1 mm rms, except that they are spaced out by a 0.75 cm bias (0.61 cm when using ECMWF model wet troposphere correction). This bias can result from differences between Jason-3 and Jason-2 sea state bias model used, and to a small amount due to ionosphere correction differences. The global average SSH bias is close to 2.98 cm using SSH corrections (2.84 cm when using ECMWF instead of radiometer wet troposphere correction) and 2.23 cm without. However, the more crucial point for scientific applications is to insure that there is no drift between both missions, since the global bias can be corrected a fortiori.

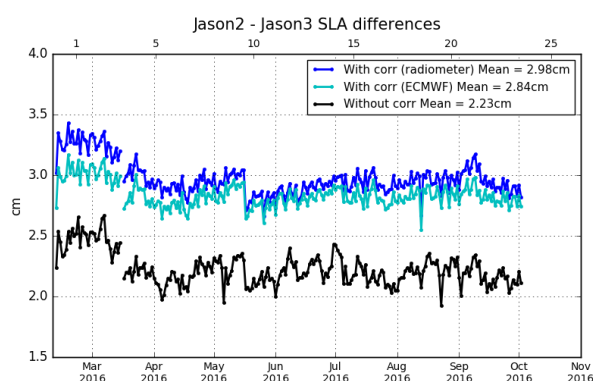


Figure 58 – Daily monitoring of SSH bias between Jason-2 and Jason-3 before Jason-2 moved to interleaved ground-track in October 2016 (using GDRD data for both missions) : SSH bias without applying geophysical corrections (**black**) and with corrections using radiometer wet troposphere correction (**blue**) or using ECMWF model wet troposphere correction (**cyan**).

Colocated Jason-2 minus Jason-3 SLA differences averaged over the period of tandem phase (cycle 001 to 023) are shown on left side of figure 59. As both satellites measure the same oceanic features only 1'20" apart, only a weak hemispheric bias is visible (likely due to differences in orbit processing). Since Jason-2 has moved to its new interleaved orbit, maps of direct Jason-2 minus Jason-3 SLA measurements are no longer available. But differences of gridded SLA for Jason-2 and Jason-3 can be made. This difference is

quite noisy for one cycle, especially as both satellites are shifted in time and sea state changes especially in regions of high ocean variability. Therefore figure 59 shows an average over SLA grid differences from Jason-3 cycles 025 to 058. High variability regions as Gulf Stream and Antarctic circumpolar current are visible.

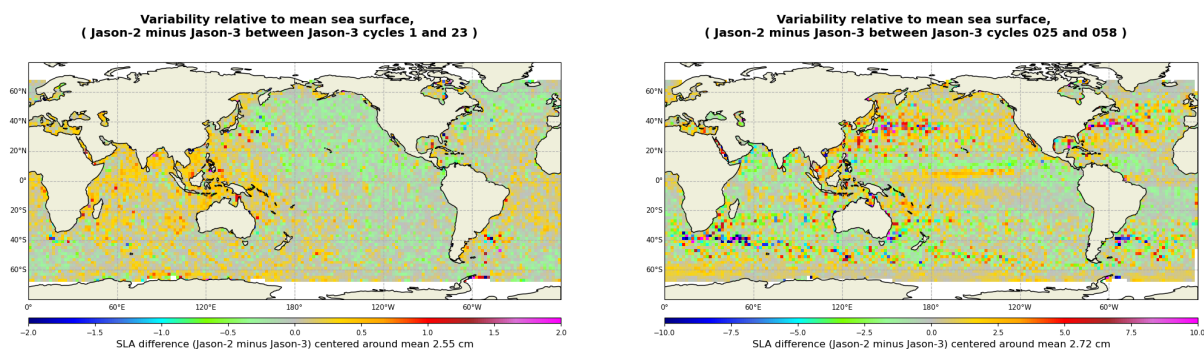


Figure 59 – GDR data. Caution: color map ranges are different between the two figures. **Left:** Map of SLA difference between Jason-2 and Jason-3 over tandem phase **Right:** Map of Jason-2 and Jason-3 SLA differences for Jason-3 cycles 025 to 058 (using Jason-3 GDR-F data and updated to GDR-F like Jason-2 data).

6.3. Standard deviation of SLA differences between Jason-3 and Jason-2

The monitoring of SLA standard deviation has been computed for both missions (figure 60).

Note that this metric is very dependant to the MSS reference solution used to compute SLA. Standard deviation of SLA from L2P products (green and black curves) are lower than with IGDR or GDR thanks to L2P updates that include a change from product MSS referenced on 7 years to a solution referenced on 20 years. In addition, Jason-2 MSS solution in GDR product (blue curve on right part of figure 60) moved from MSS CNES/CLS 2011 with a 7 years reference to MSS CNES/CLS 2015 (20 years reference) when move to LRO: that explains a better performance on Jason-2 GDR dataset from July 2017 onwards. The change of reference period from 7 years to 20 years integrates the evolution of the sea level in terms of trends, but also in terms of interannual signals at small and large scales (e.g. Niño/Niña) in the additional 13 years: changing from a 7 to 20 years reference period leads to better interannual signals and oceanic anomalies (see [18] for more details about the change on reference period).

Cartography of standard deviation of spatial Jason-3 minus Jason-2 SLA differences (not shown here) does not show any anomaly. It varies indeed in function of noise on measurements, which depends on significant wave height. Therefore, standard deviation of SLA differences is higher in regions with important significant wave heights.

Jason-3 in standard “F” is homogeneous with the CNES/CLS15 MSS and the filtered ionospheric correction, this reduces the along-track SLA std compared to standard “D” (see [5] part 4.2).

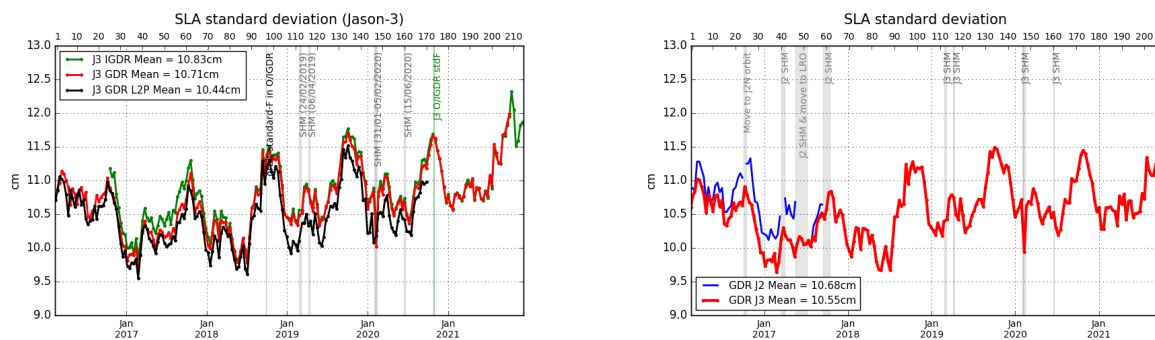
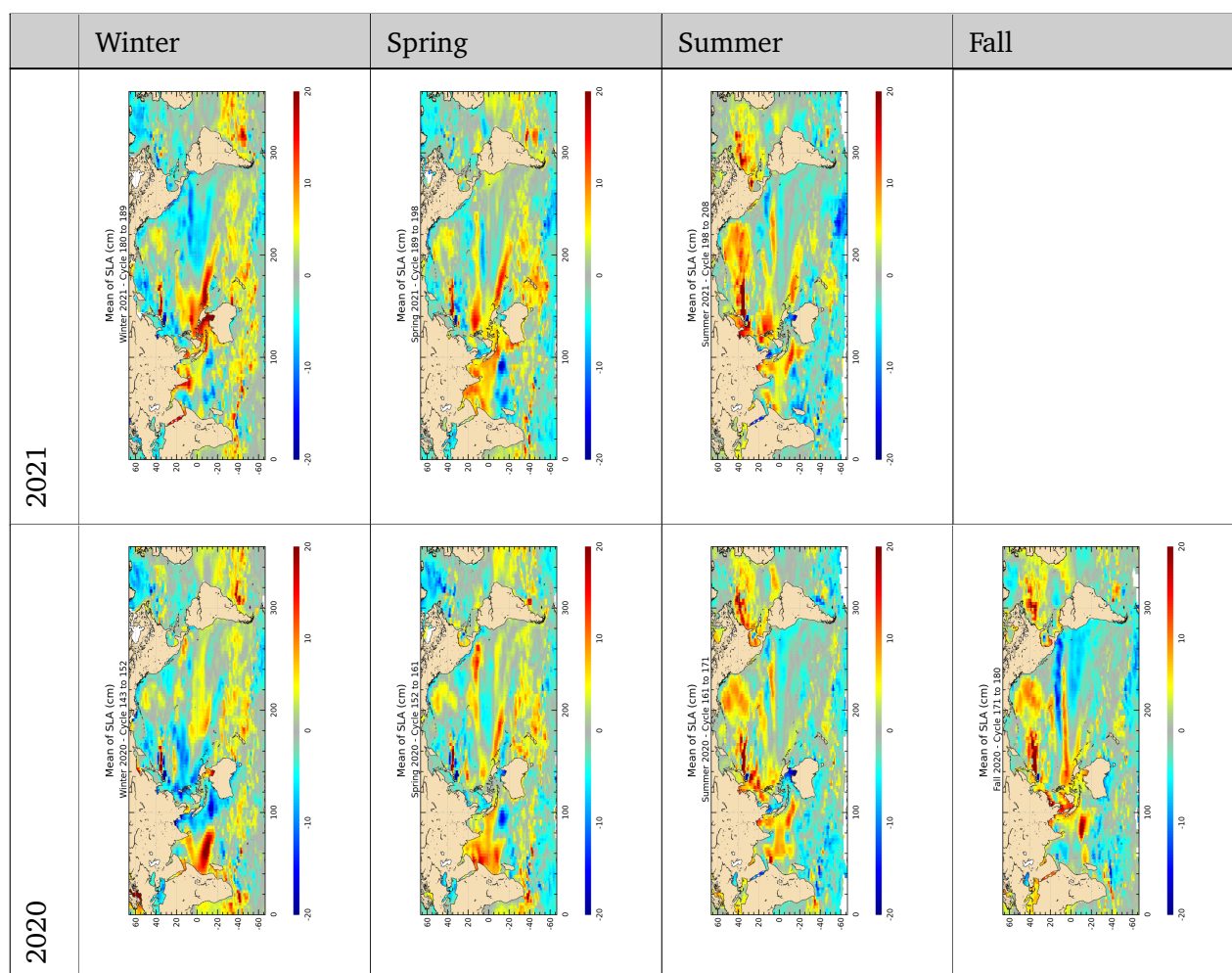


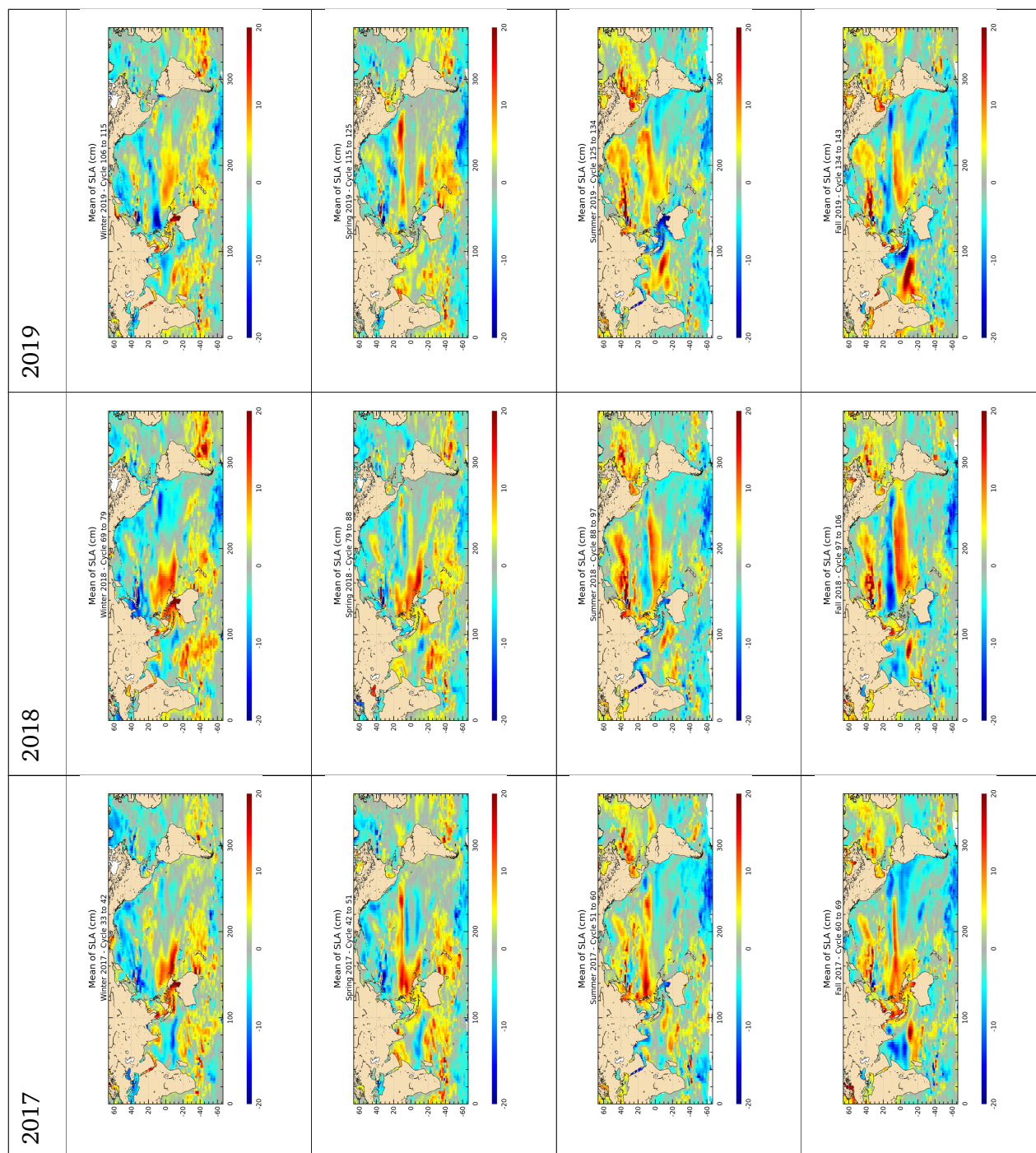
Figure 60 – Cyclic monitoring of along-track SLA standard deviation. Jason-3 OGDRs, IGDRs and GDRs (*left*). Jason-2 and Jason-3 GDRs residuals (=interpolated over theoretical ground track) (*right*)

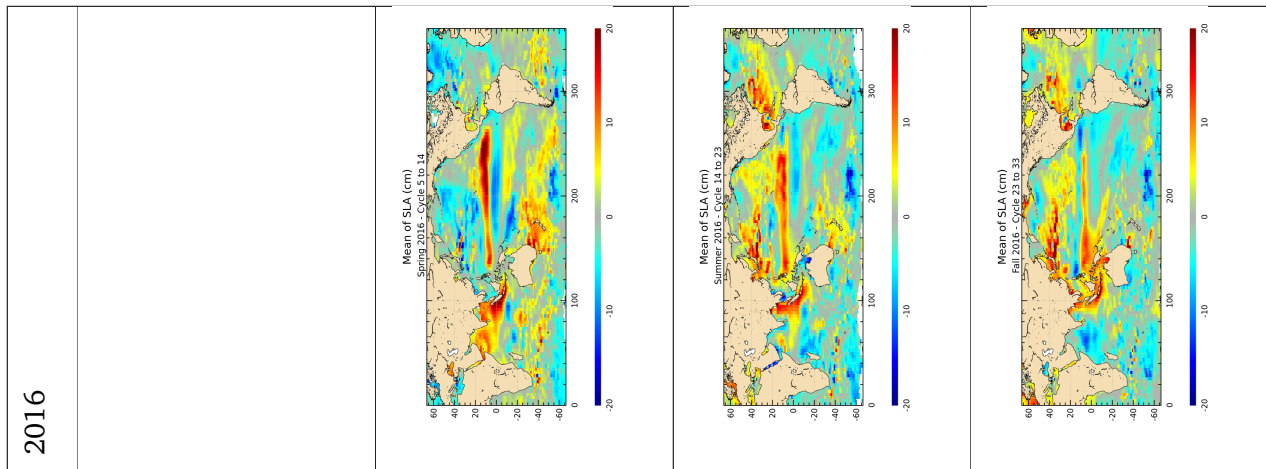
6.4. Sea level seasonal variations

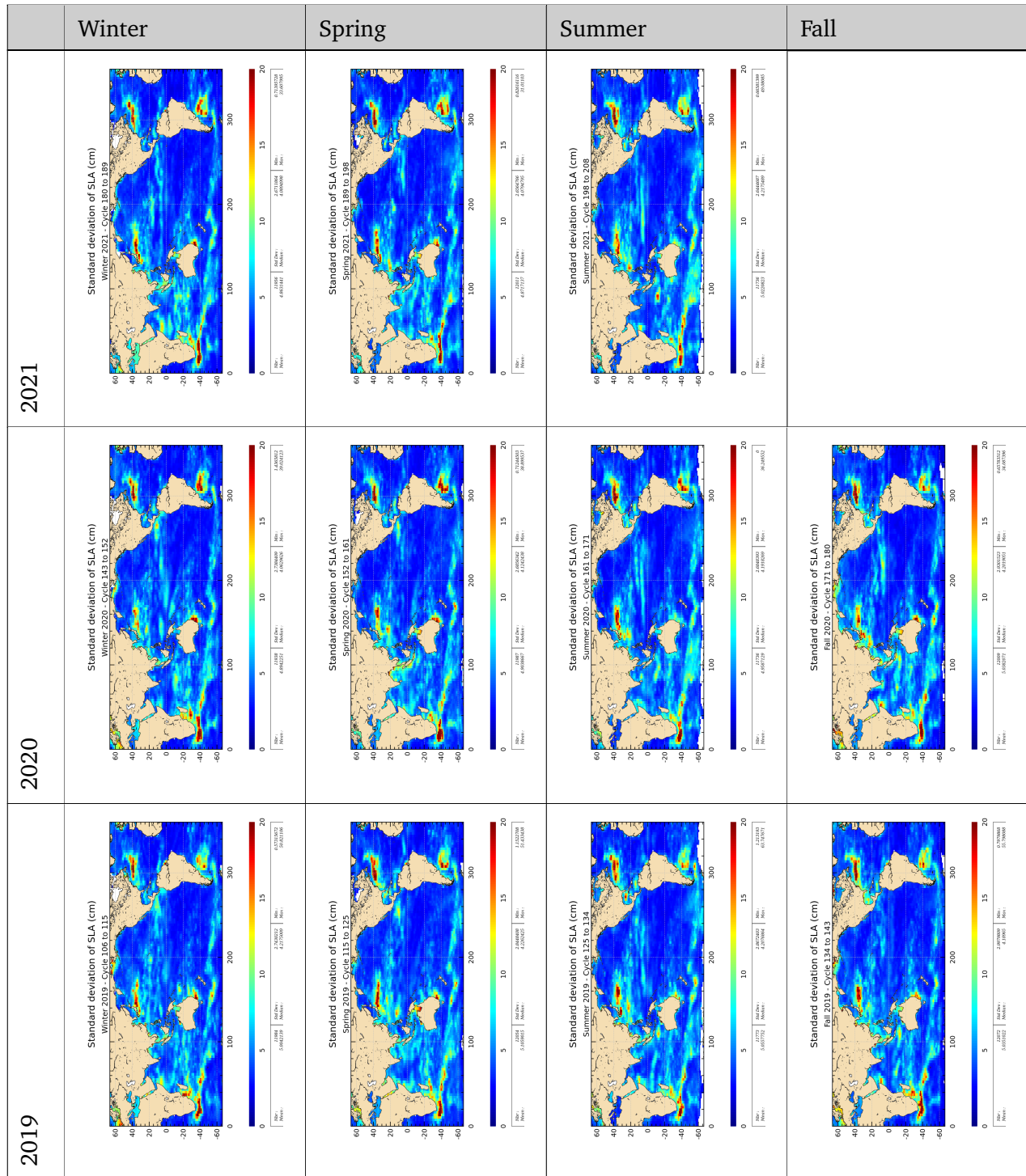
From Sea Level Anomalies computed relative to the Mean Sea Surface CNES/CLS15, the surface topography seasonal variations have been mapped in table 6 for the overall Jason-3 data set. Major oceanic signals are shown clearly by these maps: it allows us to assess the data quality for oceanographic applications.

The most important changes are observed in the equatorial band with the development of La Niña. The map of SLA over Winter 2021 echoes the one over Winter 2018 with a signature of height diminution over the Pacific Ocean (but a little bit weaker in 2021).





*Table 6 – Seasonal variations of Jason SLA (cm) for years 2016 to 2021*



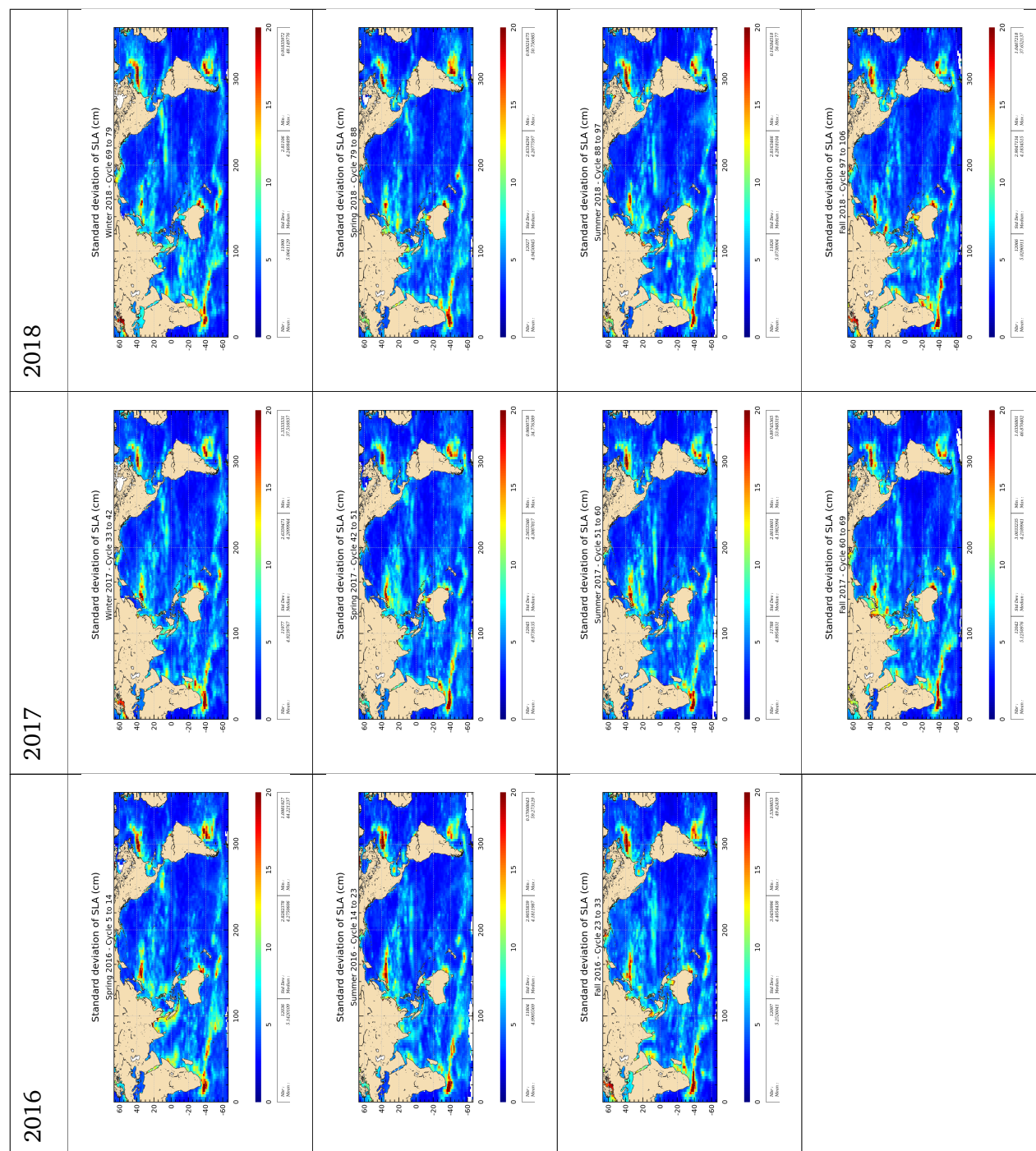


Table 7 – Seasonal variations of Jason SLA standard deviation (cm) for years 2016 to 2021

7. Mean Sea Level (MSL) trends

7.1. Computation of the Mean Sea Level

For more details about Mean Sea Level (MSL) studies method, see the dedicated annual report of activities [19] on MSL Aviso Website: <http://www.aviso.altimetry.fr/msl>. This report includes the description of the Mean Sea Level indicator, the comparisons between altimetry and tide gauges measurements, the comparisons between altimetry and *ARGO+GRACE* measurements and specific studies linked to MSL activities.

Data from Jason-3 mission were introduced in DUACS system end of September 2016 (when Jason-2 moved to its new interleaved orbit). Over the tandem phase of Jason-3 (till cycle 023), both Jason-2 and Jason-3 satellites flew on the same ground track, only 1mn20s apart. They therefore measured the same features, allowing to calibrate Jason-3. This allowed to link precisely the MSL time series of Jason-2 and Jason-3. The uncertainty of the bias value between the two time series is less than 1 mm. The evolution of the ocean MSL can therefore be precisely observed on a continual basis since 1993 thanks to the 4 reference missions: TOPEX/Poseidon, Jason-1 (from may 2002 to october 2008), Jason-2 (from october 2008 to may 2016) and now Jason-3 (since june 2016).

Wet troposphere correction, inverse barometer correction, GIA (-0.3 mm/yr) are applied to calculate the MSL and the data series are linked together accurately thanks to the tandem flying phases. The following global bias are applied: 1.16 cm between T/P&Jason-1, 0.23 cm between Jason-1/Jason-2 and -2.97 cm between Jason-2/Jason-3. An exhaustive overview over possible errors impacting the MSL evolution is given in [19]. Furthermore, annual and semi-annual signals are removed from the time serie and a 2-month filter is applied. For more details, see MSL Aviso Website: <http://www.aviso.altimetry.fr/msl>.

Though mean sea level trend is globally positive, it is inhomogeneous distributed over the ocean: locally, sea level rise or decline up to ± 10 mm/yr are observed on right panel of figure 61 (note that this map of regional MSL trends is estimated from multi-mission grids (Ssalto/DUACS products) in order to improve spatial resolution).

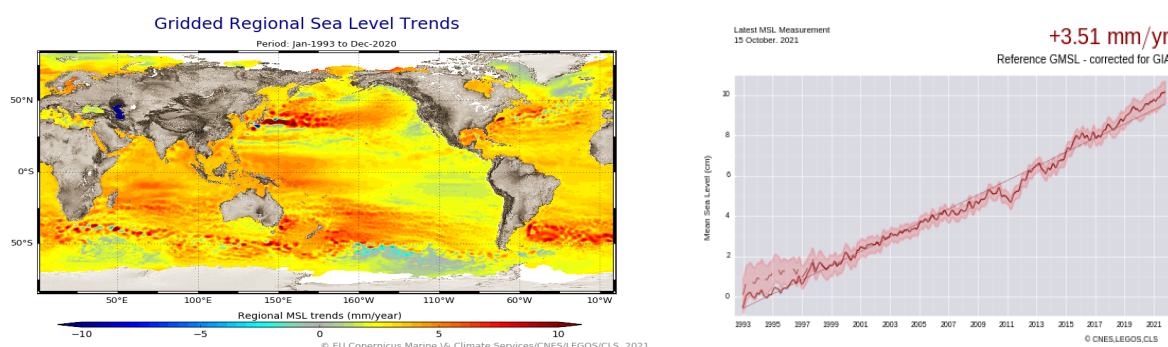


Figure 61 – Global (right) and regional (left) MSL trends from 1993 onwards.

7.2. Comparison of the MLE4 & the ADAPTIVE GDRF solutions for the GMSL computation

Part of the new GDR-F standards of the J3 data, a solution based on the adaptive retracking is distributed. Hereafter, we compare the different retracking solutions provided in the GDR-F data by computing the GMSL difference between the adaptive and the MLE4 solutions (Figure 62). A very good consistency is observed (differences are submillimeter) but a jump (about 6mm) is observed from September-2017 and June-2018. This corresponds to instrument resets (upload of the DEM at cycle 057 and BDR update at cycle 085), and differences in the echo centering between these cycles. These differences in the echo centering are visible in the difference between the two retracking solutions since the adaptive solution takes them naturally into account, whereas the MLE4 calibrations (LUT) are only based on the instrument characteristics at the beginning of the mission. It also can indicate that potential changes in the PTR have occurred and that these changes may not have been accounted for in the internal path delay (see also [8]). We recall that the LUT (only applied during MLE4 processing) have been computed only once at the beginning of the mission and never updated since then. As shown by the two panels of Figure 62, the adaptive solution does not impact the slope of the Jason-3 GMSL over the 5 years of the mission, as compared to the GDR-F MLE-4 solution. This is the case both when considering (left panel) or ignoring (right panel) the time interval where the jump is observed. As a conclusion, the adaptive solution conserves the stability of the GMSL record and allows to naturally prevent anomalies in the instrument calibrations over the lifetime of the mission. An interesting investigation to be performed in 2022 will be the estimation of the reduction/increase of the correlated noise at 2-months and 1-year (that is used in the uncertainty budget) between the MLE4 and adaptive retracking solutions. From figure 62 and the jump observed, the adaptive retracking seems to be an interesting candidate for climate studies.

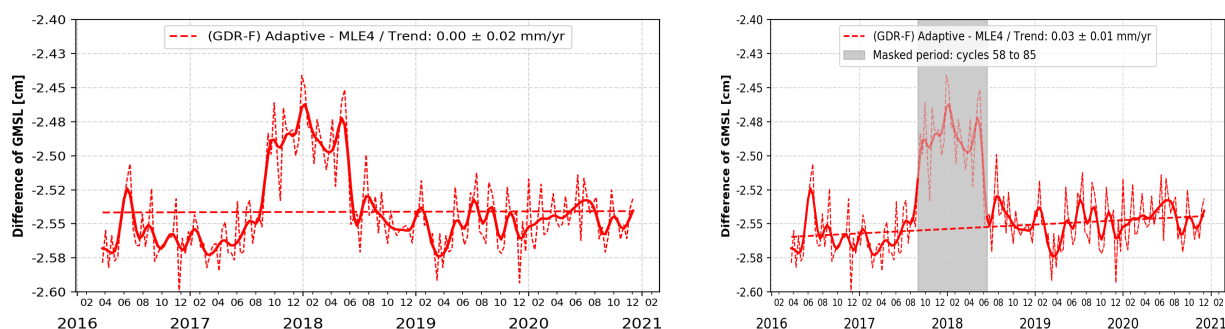


Figure 62 – J3 GMSL difference between GDR-F adaptive and MLE4 with (left) and without removal of cycles 057 to 085 (right). Figures extracted from the [19]

8. Particular points and investigations

8.1. Investigations surrounding the retracking ADAPTIVE

On the 5th of December 2020, a 3 minutes gap of filtered ionospheric correction was identified for MLE4 and ADAPTIVE retrackings. In the same period, the σ_0 , the $range_{std}$ and the ionospheric correction values exploded for the ADAPTIVE retracking.

The absence of filtered ionospheric correction only has a minor impact over the SLA measurements since these measurements are rejected over other criteria ($SWH < 11m$ & $range_{std} < 20cm$).

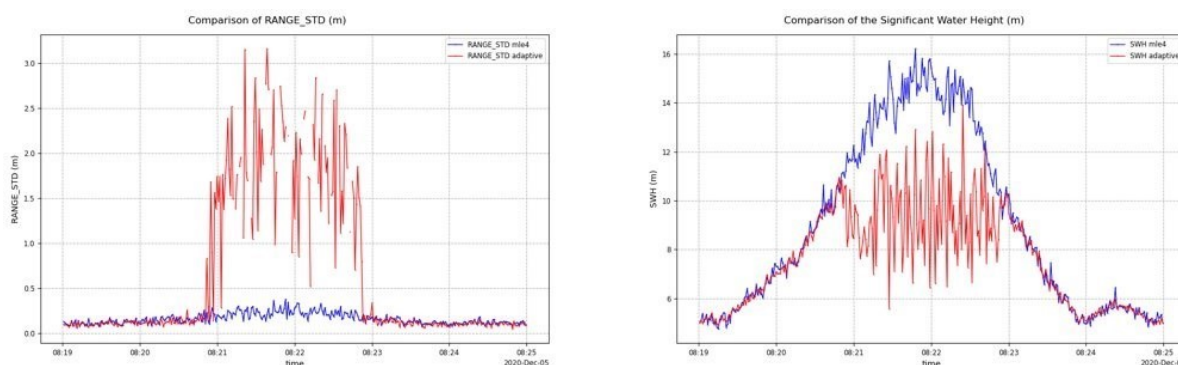


Figure 63 – $range_{std}$ and SWH for both retrackings over cycle 177 and pass 199. The SLA measurements are rejected with the SWH threshold for the MLE4 and the $range_{std}$ threshold for the ADAPTIVE.

This investigation highlighted that class 13 waveforms (representing less than 0.5% of the classes) are processed using the configuration “complicated” and not the nominal “ocean” configuration in areas of high SWH. This leads to using a dynamic window of analyse on the waveform and finally brings an erroneous computation (SWH, σ_0). To correct this anomaly, reprocessing of class 13 waveforms was done using the configuration “ocean”. An improvement of the SWH estimations and a reduction of the computation time were observed.

In conclusions, the Jason-3 ADAPTIVE products needed an update to correctly process the class 13 waveforms over high SWH area. Though this update does not change much for the valid data, it allows for a better estimation of geophysical parameters derived from the waveform.

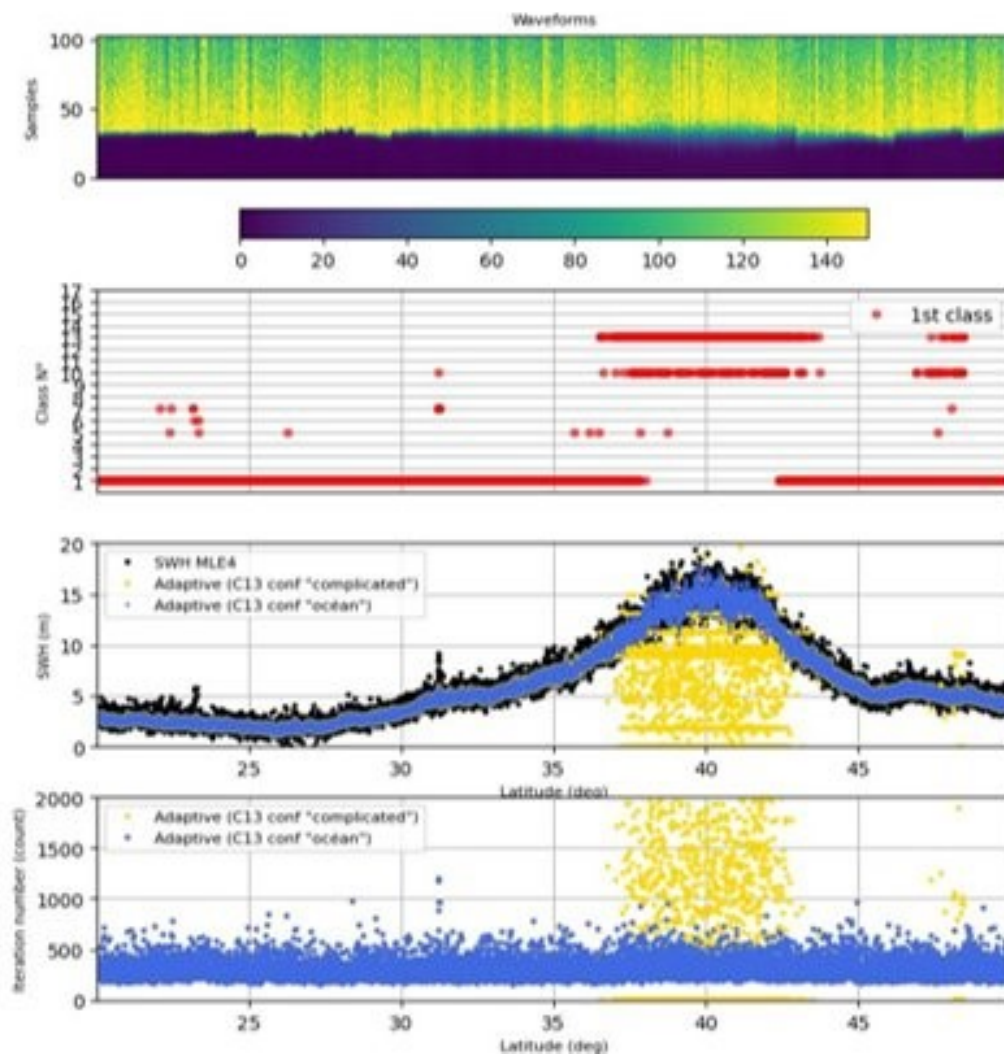


Figure 64 – Reprocessing of all class 13 waveforms using the best fitting configuration.

8.2. Waveform classification

The GDRF reprocessing changed the waveform classification process. In fact, the classification used in standard “D” was the PISTACH classification while the new J3 classification used in standard “F” data does not take into account the same classes. This new classification induces the necessity of checking the method of attribution of the 1Hz waveform classification from the 20Hz classification existing. To do so, focus was given on cycle 140 pass 199 (04/12/2019) which is a period of strong waves over the Northern hemisphere and as such contains a wide variety of waveform classes.

Over this pass was done successively :

- the extraction of the 20Hz waveform classification
- the extraction of the 1Hz waveform classification
- the computation of a 1Hz pseudo-classification from the 20 measures of the corresponding time interval in the 20Hz classification

Doing so, it was ensured that the 1Hz classification corresponds to the most represented class in the 20 measures. We can see the result of this investigation in Figure 65, green \star corresponding to the difference of classes between the 1Hz data and the equivalent derived from the most represented in 20Hz data, blue x underline all “complex” waveforms and the red line is highlighting the land areas.

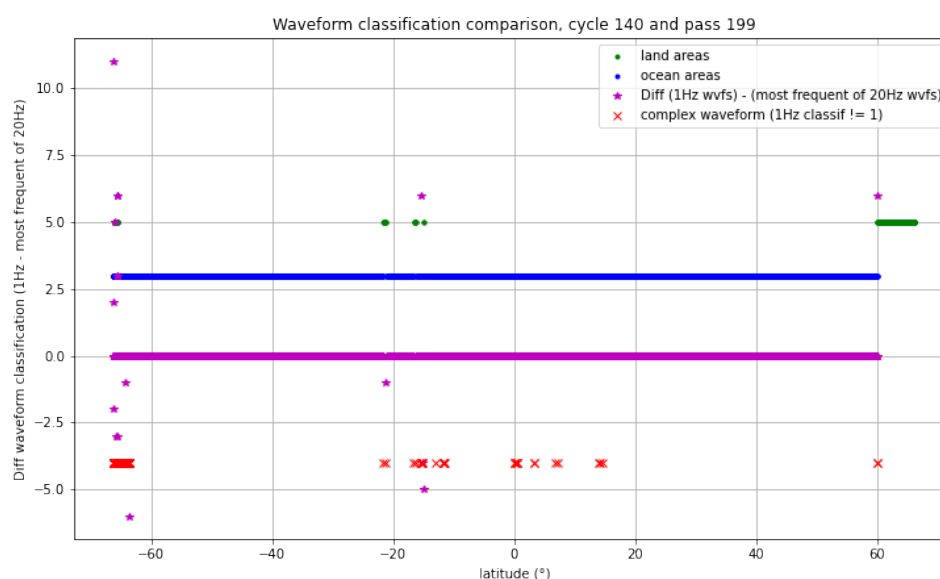


Figure 65 – Difference of classification between the 1Hz class and the most frequent class of the 20Hz measures

As a result, we can observe that the difference of classification (green \star) is almost everywhere equal to 0 which confirms the methodology of 1Hz classification used. The only differences identified correspond to land areas and sea ice as seen in Figure 66, over these specific areas the difference of classification is explained by the coastal flagging before computing the 1Hz classification.

The conclusion of this investigation is the following : the 1Hz waveform classification is deduced from the 20Hz classification attributing the main class over the period surrounding the 1Hz measure.

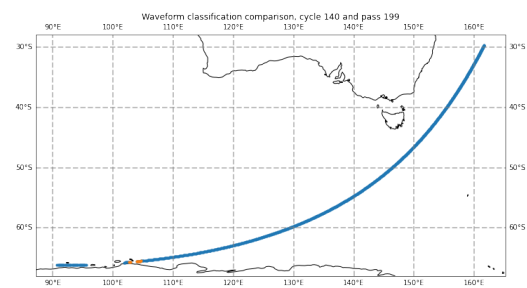
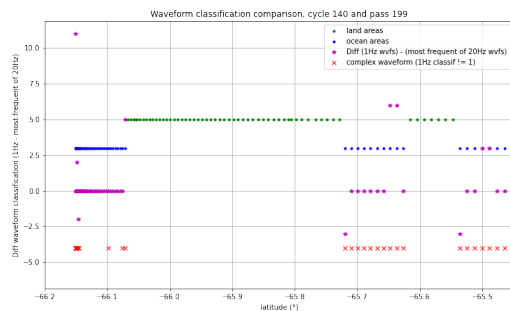


Figure 66 – Difference of classification between the 1Hz class and the most frequent class of the 20Hz measures, zoomed over low latitudes (On the right figure, the orange points correspond to a difference of classification).

8.3. Tandem Phase with Sentinel-6

During the whole year of 2021, Jason-3 had the major role to validate the performances of the Sentinel-6 mission through cross-calibration. Since both altimeters of S6 had to be verified, this tandem phase can be considered as a double tandem phase. The tandem phase was essential to prove the reliability expected from S6. At the end of this phase, S6 became the new reference mission for altimetry (April 2022).

8.3.1. Range Differences

8.3.1.1. Sea Level Anomalies

During Sentinel-6 tandem phase with Jason-3, the averaged difference of gridded SLA shows little difference between both missions as they have a very small temporal shift, similar to Jason-2/Jason-3 tandem phase.

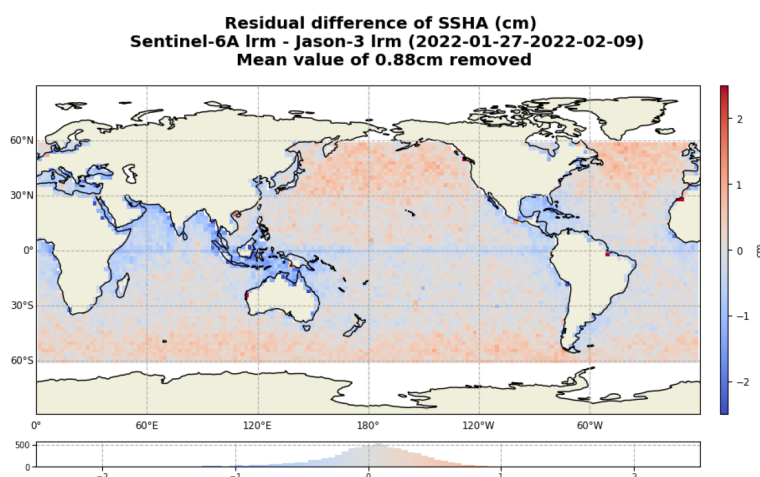


Figure 67 – GDR data. Map of Sentinel-6 and Jason-3 SLA differences for Jason-3 cycles 220 to 221

8.3.1.2. Equatorial Band

An equatorial band is observed in SSHA differences, this geographical pattern is only observed on range retracking parameters (range, SSH, SSHA). It seems to come from Jason-3 and is currently under investigation (see [1]). This pattern is seen on figure 67.

8.3.1.3. Noise Level

When looking at the range noise, Sentinel-6 is slightly lower in LR for the Ku-Band altimeter than Jason-3, this is due to a better sampling and a higher PRF. In HR (SAR mode) and Ku-Band, the noise level is considerably reduced compared to Jason-3.

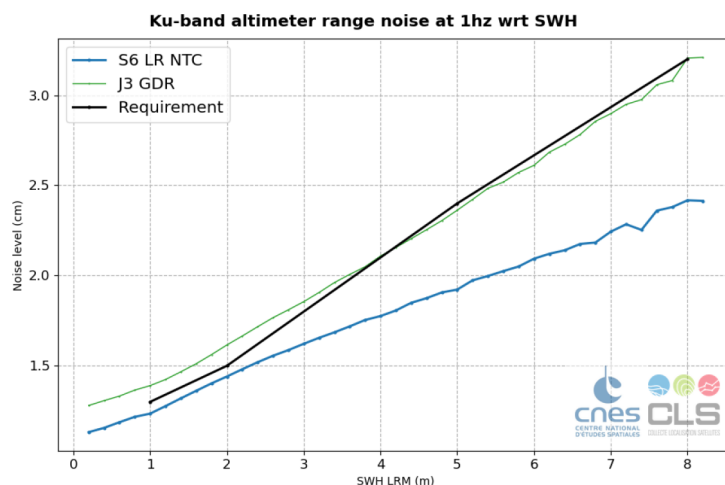


Figure 68 – GDR data. Plot of Sentinel-6 and Jason-3 noise level with regard to LRM SWH.

8.3.2. SWH Differences

The residual difference of SWH between Jason-3 and Sentinel-6 is weak and shows almost no difference between both missions.

When comparing both modes of Sentinel-6 (HR / SAR v.s. LR mode), a bias is observed on SWH due to the motion impact of vertical waves. This will also lead to a signature in the SSHA via the SSB (Sea State Bias) when comparing Jason-3 with Sentinel-6 in SAR mode.

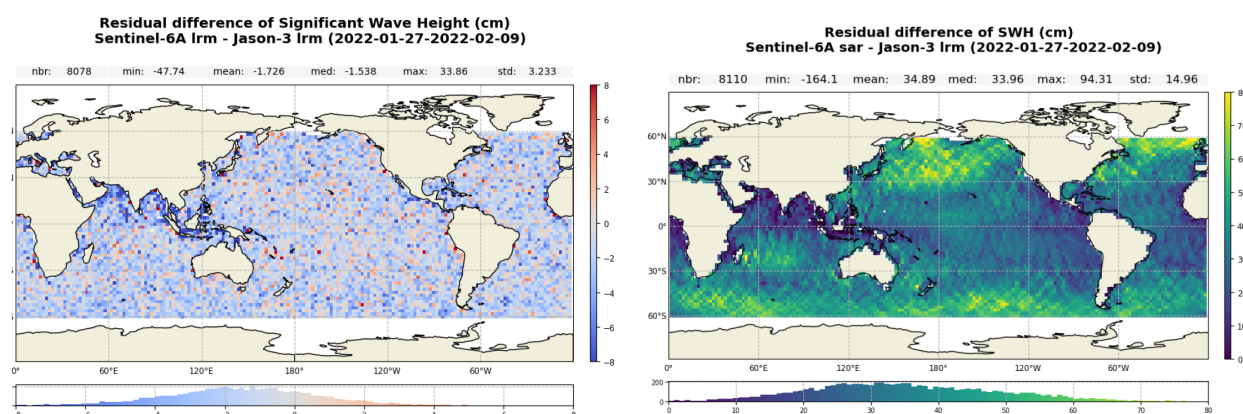


Figure 69 – GDR data. Map of Sentinel-6 and Jason-3 SWH differences for Jason-3 cycles 220 to 221

8.3.3. Crossover differences

The difference at crossover points is a key indicator of the mission performance. Comparing Sentinel-6 and Jason-3 with this criteria shows a slight reduction of the standard deviation of the SSH crossover differences for Sentinel-6 and thus an excellent performance.

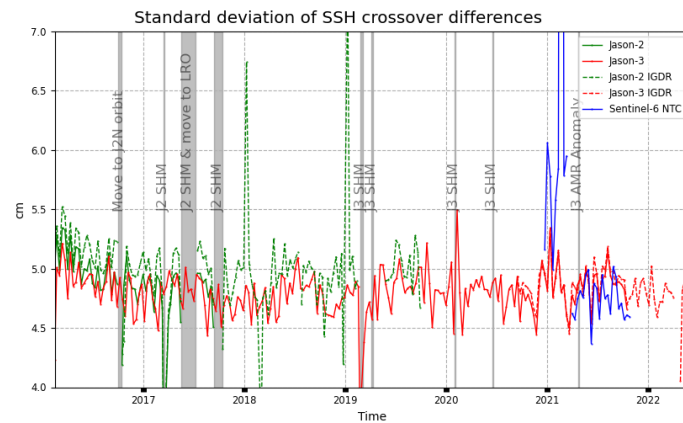


Figure 70 – GDR data. Plot of Sentinel-6 and Jason-3 SSH differences at crossover points.

8.4. Caution about qual_inst_corr_1hz_sig0_ku

The Jason-3 O/I/GDR products provide a quality flag, `qual_inst_corr_1hz_sig0_ku`, for the Ku-band sigma-0 instrument correction, `net_instr_corr_sig0_ku`.

This flag was set when `net_instr_corr_sig0_ku` values exceed a threshold of 1 dB, which was specified at the beginning of the mission. Due to the nominal evolution (aging) of the altimeter's point target response (PTR), the instrument correction values have increased, and can exceed the threshold. On Jason-3 it happened over ocean from cycle 160 onwards over C-band and from cycles 72 to 99 over Ku-band (see [7]), so that it was decided to change the threshold value and put it to 2 dB for GDR-F reprocessing. When the 2 dB threshold is exceeded the `qual_inst_corr_1hz_sig0_ku` flag is activated (in red on left of the figure 71). It happened again on GDR-F from cycle 206 over Ku-band (in red on top of the figure 71). The ageing of both bands for Jason-3 is monitored through the evolution of the total PTR power of the bottom of the figure 71.

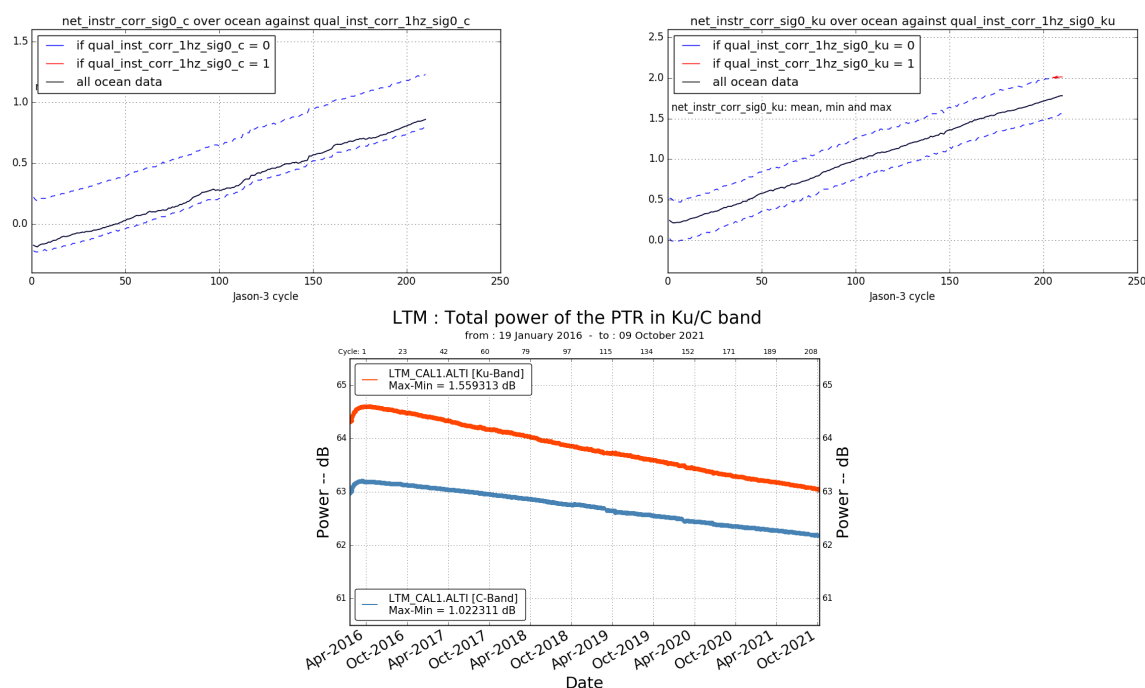


Figure 71 – **Top left:** Jason-3 `net_instr_corr_sig0_C` flag. **Top right:** Jason-3 `net_instr_corr_sig0_Ku` flag. **Bottom:** Evolution of PTR power.

Until cycle 206, only few ocean points were flagged with this `qual_inst_corr_1hz_sig0_C` flag (see cycle 205 on left part of figure 72). From cycle 206 until change in the processing chain, the number of flagged data is increasing over ocean, especially near Antarctic Ocean (see cycle 208 on right part of figure 72).

Users are advised to ignore this flag during their processing of the Jason-3 products. The quality flag for the Ku-band sigma-0 itself, `qual_alt_1hz_sig0_ku`, is a sufficient editing criterion. The threshold in the processing chain will be adjusted from april onwards for IGDR-F product, so the flag won't constantly be set.

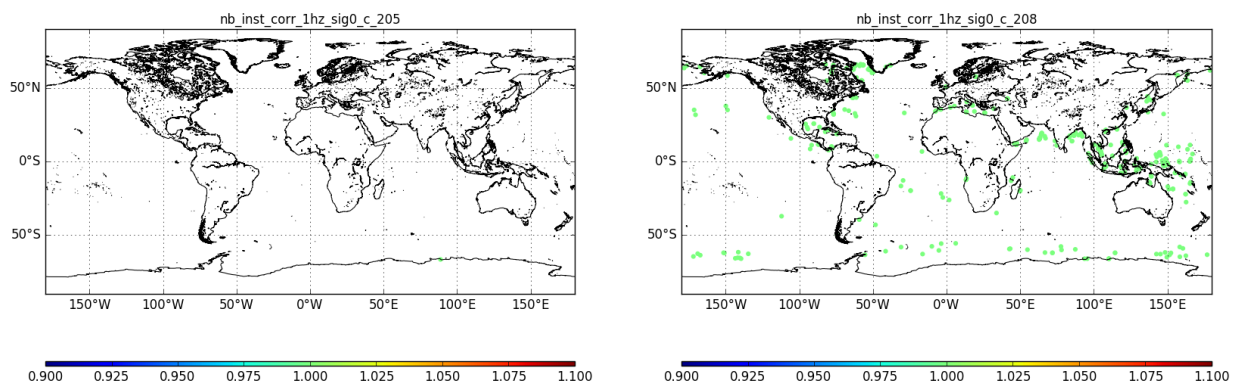


Figure 72 – Jason-3 net_instr_corr_sig0_C flag over ocean. **Left:** Jason-3 cycle 205. **Right:** Jason-3 cycle 208.

8.5. Dry tropospheric correction solutions

Two dry tropospheric correction solutions are available in Jason-3 GDR-F, both computed from ECMWF atmospheric pressures:

- `model_dry_tropo_cor_zero_altitude`, from pressure at sea level
- `model_dry_tropo_cor_measurement_altitude`, from 3d meteorological fields at measurement altitude

The comparison of the both available corrections over one Jason-3 cycle highlights few geographically correlated patterns of 2 to 3 mm (see Figure 73). These patterns are correlated to the known impact of S1S2 climatology from 6hours pressure grids, that is corrected and then re-estimated from atmospheric tide model by Ray and Ponte ([21]) during dry tropospheric correction computation. Those two available models, computed from a 6 hours resolution grids, are compared over ocean to a dry tropospheric correction computed from ERA5 reanalysis grids with a 1hour resolution (see Figure 74): this allows to avoid the necessity to correct the atmospheric tide effects. These comparisons clearly indicate that the geographically correlated patterns that were identified between the two L2 variables are now only visible in the comparison map with `model_dry_tropo_cor_measurement_altitude`: the impact of the S1S2 climatology in atmospheric pressures is not correctly considered during the correction computation at measurement altitude (figure 75).

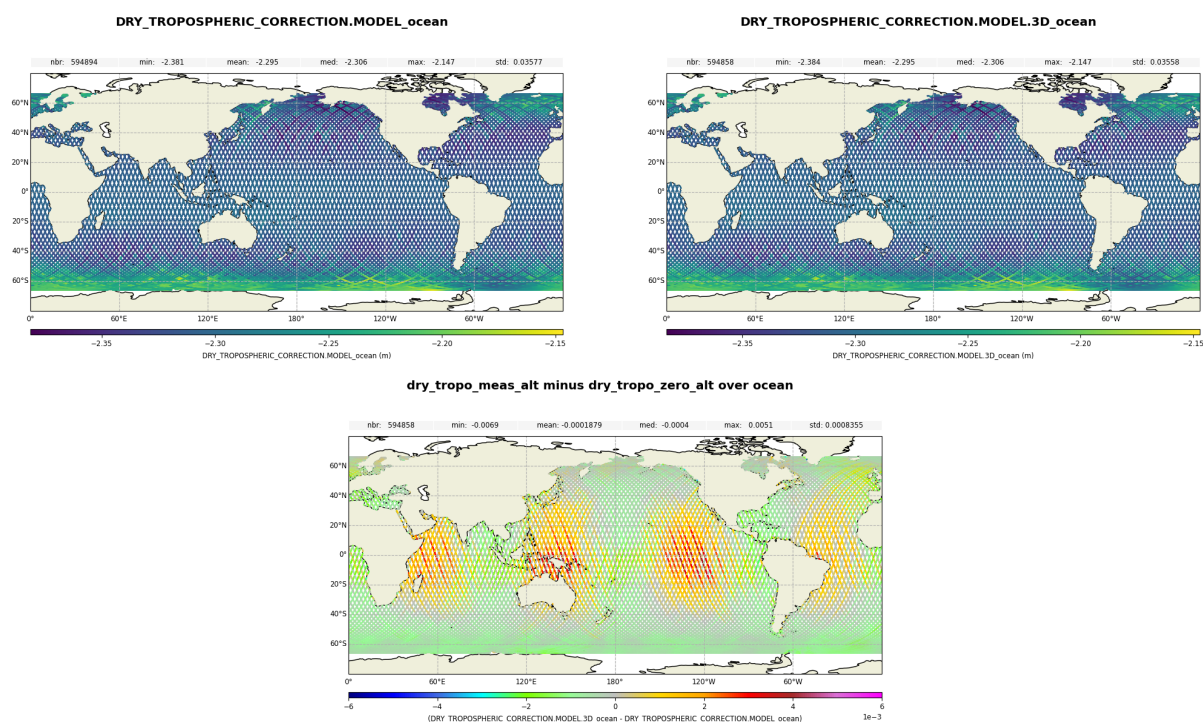
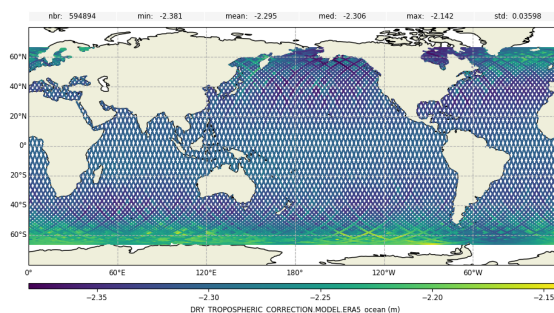
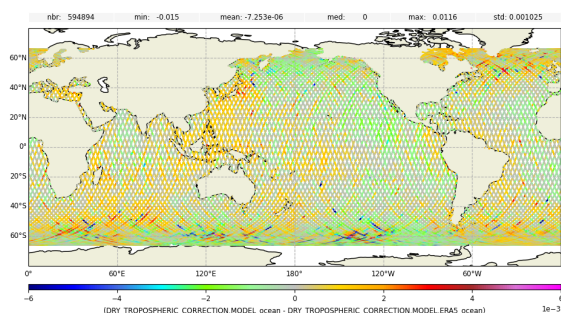


Figure 73 – Dry tropospheric correction over ocean for Jason-3 cycle 150. `model_dry_tropo_cor_zero_altitude` (top left), `model_dry_tropo_cor_measurement_altitude` (top right), and `model_dry_tropo_cor_measurement_altitude` minus `model_dry_tropo_cor_zero_altitude` point to point difference (bottom)

DRY_TROPOSPHERIC_CORRECTION.MODEL.ERA5_ocean



dry_tropo_zero_alt minus dry_tropo_era5 over ocean



dry_tropo_meas_alt minus dry_tropo_era5 over ocean

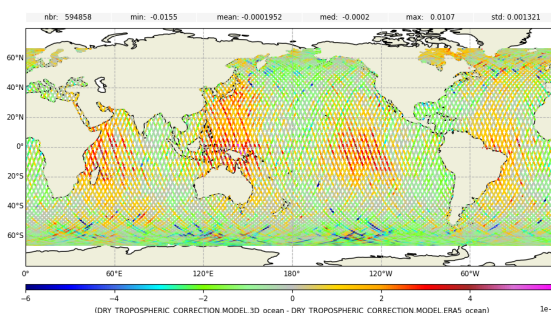


Figure 74 – Dry tropospheric correction over ocean for Jason-3 cycle 150. Dry tropospheric correction from ERA5 pressures at sea level (**top**), model_dry_tropo_cor_zero_altitude minus $DTC_{fromERA5}$ point to point difference (**bottom left**), and model_dry_tropo_cor_measurement.altitude minus $DTC_{fromERA5}$ point to point difference (**bottom right**)

In conclusions, the use of model_dry_tropo_cor_zero_altitude is recommended for sea surface height estimations for studies over ocean.

Ground segment processing of L2 product will be modified to take into account these S1S2 effects on the correction for model_dry_tropo_cor_measurement.altitude.

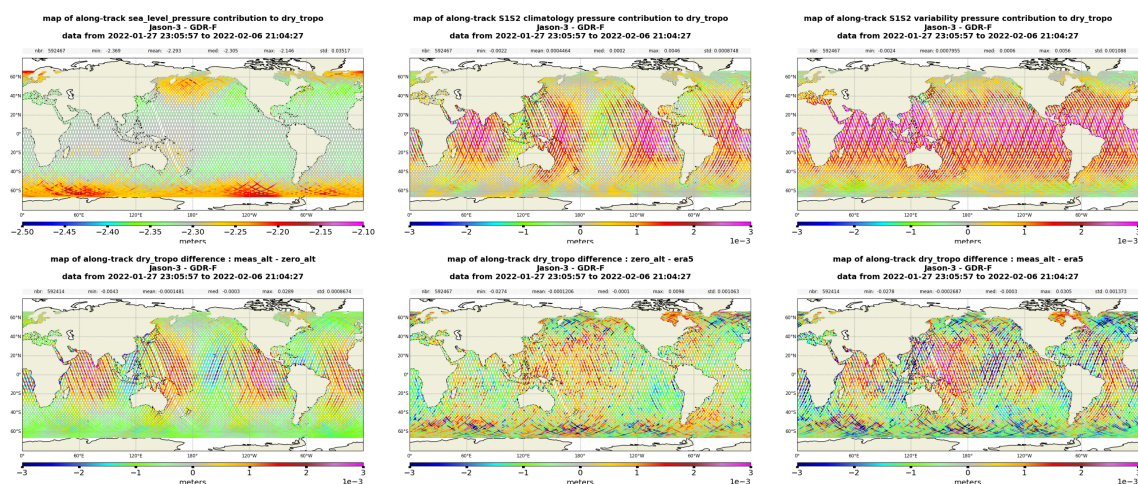


Figure 75 – Dry tropospheric correction over ocean for Jason-3 cycle 150. Contribution of sea level pressure, S1S2 pressures climatology and atmospheric tide (top) with regard to model_dry_tropo_cor_measurement_altitud minus model_dry_tropo_cor_zero_altitude point to point difference (**bottom left**) model_dry_tropo_cor_zero_altitude minus $DTC_{fromERA5}$ point to point difference (**bottom middle**), and model_dry_tropo_cor_measurement_altitude minus $DTC_{fromERA5}$ point to point difference (**bottom right**)

9. Conclusion

Jason-3 was launched on January 17th, 2016. Since February 12th, Jason-3 was on its operational orbit following Jason-2 with 80 seconds delay on the same ground track. OGDR/IGDR products were opened to users end of June 2016, whereas the GDR products were available from November 2016 onwards.

The verification phase allowed extensive analysis and validation of the data, as both satellites observed the same geophysical phenomena until October 2nd 2016 when Jason-2 was moved to its interleaved ground track. This tandem flight phase has shown that Jason-3 data quality is excellent, at least of the same order as the Jason-2 one.

The main points of the performance assessment are summarized below:

- Ocean data availability is excellent and similar between Jason-3 and Jason-2 with a percentage greater than 99.9% after removing specific events.
- Data quality is also very good with less than 4% of measurements not consistent with altimeter and radiometer parameters threshold criterion. Jason-2 presents an equivalent percentage of edited data.
- The altimetry parameters analysis highlights a similar behaviour compared to Jason-2. Some biases exist as between dual-frequency ionosphere correction, but they are stable.
- At crossovers, Jason-3 shows performance similar to Jason-2 with a standard deviation lower than 5 cm. However mean difference analysis highlights a 120-days signal, which is present for both missions but was reduced for Jason-3 using new standard "F".
- At crossovers between Jason-3 and Jason-2, SSH performance presents excellent results with an SLA bias of about 3 cm. The consistency between both SLA is good with a small geographically correlated signal (lower than 0.5 cm in GDR) due to orbit quality.

Thanks to these good results, Jason-3 became the reference mission to ensure the continuity of Global Mean Sea Level monitoring on September 2016.

This reference role will be transmitted to Sentinel-6 during the year 2022 after the end of Jason-3/Sentinel-6 tandem phase.

Data production has followed standards F for OGDR and IGDR from cycle 174 onwards, and has been entirely reprocessed in this new standard for GDR. The reprocessing in GDR-F, including the update of mean sea surface, pole tide, internal tides, ocean tides and sea state bias allowed to significantly improve the quality of Jason-3 products over all the mission data.

10. References

References

- [1] Analysis of the Sentinel-6A SLA bias correction at https://www.aviso.altimetry.fr/fileadmin/documents/data/tools/bias_S6ASAR_L2PL3_forORR.pdf
- [2] Jason-3 cyclic reports available at <https://www.aviso.altimetry.fr/en/data/calval/systematic-calval/validation-reports/jason-3-gdr.html>
- [3] Jason-3 product description available at https://www.aviso.altimetry.fr/fileadmin/documents/data/tools/product_description_j3.pdf
- [4] Jason-3 handbook available at https://www.aviso.altimetry.fr/fileadmin/documents/data/tools/hdbk_j3.pdf
- [5] Jason-3 validation of GDR-F data over ocean https://www.aviso.altimetry.fr/fileadmin/documents/calval/validation_report/J3/SALP-RP-MA-EA-23480-CLS_Jason3_Reprocessing_Report_v1-2.pdf
- [6] Mean Sea Level informations in AVISO. <https://www.aviso.altimetry.fr/en/data/products/ocean-indicators-products/mean-sea-level.html>
- [7] Roinard H. Jason-3 validation and cross calibration activities (Annual report 2020). https://www.aviso.altimetry.fr/fileadmin/documents/calval/validation_report/J3/SALP-RP-MA-EA-23473-CLS_Jason-3_AnnualReport2020_v1-1.pdf
- [8] P. Thibaut et al., "Benefits of the "Adaptive Retracking Solution" for the JASON-3 GDR-F Reprocessing Campaign," 2021 IEEE International Geoscience and Remote Sensing Symposium IGARSS, 2021, pp. 7422-7425, doi: 10.1109/IGARSS47720.2021.9553647. Available at https://www.aviso.altimetry.fr/fileadmin/documents/data/tools/NT-Thibaut_AdaptiveRetrackingForJason3GDRF.pdf
- [9] Benefits of the Adaptive Algorithm for Retracking Altimeter Nadir Echoes: Results From Simulations and CFOSAT/SWIM Observations. IEEE Transactions on Geoscience and Remote Sensing. 2021-journal-article. DOI: 10.1109/TGRS.2021.3064236
- [10] Ngan Tran (CLS, France), Gerald Dibarboure (CNES, France), Nicolas Picot (CNES, France). Improving the continuity of the Jason SSB time-series. https://meetings.aviso.altimetry.fr/fileadmin/user_upload/tx_ausyclsseminar/files/Poster_OSTST18_SSB_tran.pdf
- [11] Nencioli Francesco, Roinard Hélène, Bignalet-Cazalet Francois. 2021. Filtering ionospheric correction from altimetry dual-frequencies solution. DOI 10.24400/527896/a02- 2021.001. Available at https://www.aviso.altimetry.fr/fileadmin/documents/data/tools/NT-Nencioli_FilteredIonosphericCorrection.pdf
- [12] Roinard H.. Jason-3 validation and cross calibration activities (Annual report 2017). SALP-RP-MA-EA-23187-CLS. https://www.aviso.altimetry.fr/fileadmin/documents/calval/validation_report/J3/SALP-RP-MA-EA-23187-CLS_Jason-3_AnnualReport2017_v1-2.pdf
- [13] Brown G.S., "The average impulse response of a rough surface and its application", *IEEE Transactions on Antenna and Propagation*, Vol. AP 25, N1, pp. 67-74, Jan. 1977.

-
- [14] Thibaut, P. O.Z. Zanifé, J.P. Dumont, J. Dorandeu, N. Picot, and P. Vincent, 2002. Data editing: The MQE criterion. *Paper presented at the Jason-1 and TOPEX/Poseidon Science Working Team Meeting, New-Orleans (USA), 21-23 October.*
 - [15] Obligis, E., L. Eymard, M. Ablain, B. Picard, J.F. Legeais, Y. Faugere and N. Picot, 2010. The wet tropospheric correction for altimetry missions: A mean sea level issue. *Oral presentation at OSTST meeting, Lisbon, Portugal.* Available at http://www.aviso.oceanobs.com/fileadmin/documents/OSTST/2010/oral/19_Tuesday/OBLIGIS.pdf.
 - [16] H. Roinard, E. Cadier. Jason-2 validation and cross calibration activities (Annual report 2017). Reference: SALP-RP-MA-EA-23186-CLS. Available at https://www.aviso.altimetry.fr/fileadmin/documents/calval/validation_report/J2/SALP-RP-MA-EA-23186-CLS_Jason-2_AnnualReport2017_v1-2.pdf.
 - [17] Roinard H.. Jason-3 validation and cross calibration activities (Annual report 2019). SALP-RP-MA-EA-23399-CLS.
 - [18] DUACS/Aviso team 'A new version of SSALTO/Duacs products available in April 2014' <http://www.aviso.altimetry.fr/fileadmin/documents/data/duacs/Duacs2014.pdf>
 - [19] A. Guerou. SALP annual report (2021) of Mean Sea Level Activities. Reference: SALP-RP-MA-EA-23541-CLS.
 - [20] Updates available for DUACS products. <https://www.aviso.altimetry.fr/en/data/product-information/updates-and-reprocessing/ssalto/duacs-product-changes-and-updates.html>
 - [21] Ray, R. D. and Ponte, R. M.: Barometric tides from ECMWF operational analyses, *Ann. Geophys.*, 21, 1897–1910, <https://doi.org/10.5194/angeo-21-1897-2003>, 2003.